DONALDSONVILLE SITE

Ciel Facility
Ascension Parish, LA
CO_2 Injection Facility

BKVerde, LLC
1200 17th St, Suite 2100, Denver, CO 80202

December 2023

CLASS VI PERMIT APPLICATION NARRATIVE
40 CFR 146.82(a)

DONALDSONVILLE SITE

Project Background and Contact Information

Large-scale capture and sequestration of anthropogenic carbon dioxide (CO_2) is increasingly viewed as critical for the United States and the global community to meet greenhouse gas reduction goals established by companies, states, and national governments. To meet these climate goals, tangible projects and investments are required in the field of carbon capture and sequestration.

BKVerde, LLC (BKVerde) is planning to develop an integrated carbon capture and storage (CCS) project in Ascension Parish, Louisiana. This project is designed to accommodate geologic sequestration for owners of industrial facilities seeking to transition to low carbon products and address environmental, safety, and governance (ESG) goals. BKVerde is a CCS project management company that develops, designs, builds, owns, and operates carbon capture, transport, and storage projects in multiple states within the United States. The BKVerde team members have extensive experience in the diverse skills required to develop and operate a full-scale CCS project, including wellbore management, drilling operations, midstream operations, site design, monitoring and reporting, regulatory approvals, gathering and processing, fluid transportation, and geologic injection of various waste streams.

The Donaldsonville sequestration site is being developed to accommodate and sequester anthropogenic CO_2 within secure geologic storage. The CO_2 will be sourced from a variety of emitters within the Baton Rouge, Louisiana area. The extensive screening process undertaken for the Donaldsonville sequestration site resulted in an optimal location that meets Underground Injection Control (UIC) requirements with minimal existing wellbores, an injection interval with excellent injectability properties, and substantial confining zones. The storage site is also within close proximity to existing CO_2 emissions, allowing for the economic delivery of sourced volumes for the project.

This permit application is for drilling, completing, operating, and monitoring one Class VI CCS well, Ciel No.1, located in Ascension Parish, Louisiana. The Ciel No.1 CO_2 injection well is designed to meet the requirements of American Petroleum Institute (API) 1171 [Title 40, U.S. Code of Federal Regulations (40 CFR) **§146.86**].

Ciel No.1 will target the Miocene sand formations for CO_2 injection. These sand beds comprise alternating sands and clays/shales that offer an advantageous compartmentalization of the targeted injection horizons. These Miocene-age sand and shale sequences are well understood and are commonly found throughout the Gulf Coast of Texas, Louisiana, and Mississippi. The wellsite was selected, in part, because of the favorable geologic properties associated with the Gulf Coast depositional environment of south Louisiana.

The Ciel No.1 CO_2 plume and area of review (AoR) contains one landowner group. BKVerde has secured a definitive pore space lease agreement from this group and has full access to develop the site as described within this application. A map and list of the landowners associated with the AoR are provided herein.

The Ciel No.1 is a planned CO_2 sequestration well intended to inject within the Ciel sequestration site. This well is designed to accommodate an injection rate of 1,000,000 metric tons per year of CO_2 for over 11 years.

This permit application includes a detailed assessment of the overall geologic environment (Site Characterization section) and the resulting plume model and results (Plume Model section) used to determine the aerial extent of the plume and the resulting AoR. As detailed in the Area of Review Delineation and Corrective Action Plan section, the AoR for Ciel No.1 has one existing artificial penetration that will require corrective action. Well design and construction plans that take into consideration the needs of the project, modeling results, and requirements to ensure the protection of the underground sources of drinking water (USDWs) are detailed in the Engineering Design and Operating Strategy section.

To ensure that the CO_2 plume is being monitored during the life of the project, a detailed Testing and Monitoring Plan is provided. The plan consists of (1) an above-confining-zone monitoring well, (2) an in-zone monitoring (IZM) well, (3) USDW monitoring wells, (4) soil-gas monitoring stations, and (5) the use of fiber optic cable in conjunction with vertical seismic profile (VSP) technology to monitor the growth of the CO_2 plume during the life of the project.

The proposed Ciel No.1 project addresses all the requirements for a Class VI sequestration well. This well is ideally located to sequester significant amounts of CO_2 with a positive impact to the environment and surrounding communities.

1. Site Characterization

1.1 Regional Geology, Hydrogeology, and Local Structural Geology [40 CFR 146.82(a)(3)(vi)]

1.1.1 Regional Geology

The Donaldsonville sequestration site and the proposed Ciel No.1 injection well are in Central Louisiana within the Gulf of Mexico sedimentary basin. **Figure 1-1** depicts the Gulf of Mexico basin with a red star indicating the approximate proposed injection site. The proposed Ciel No.1 well lies within the lower coastal plain to the northeast of Atchafalaya Bay.

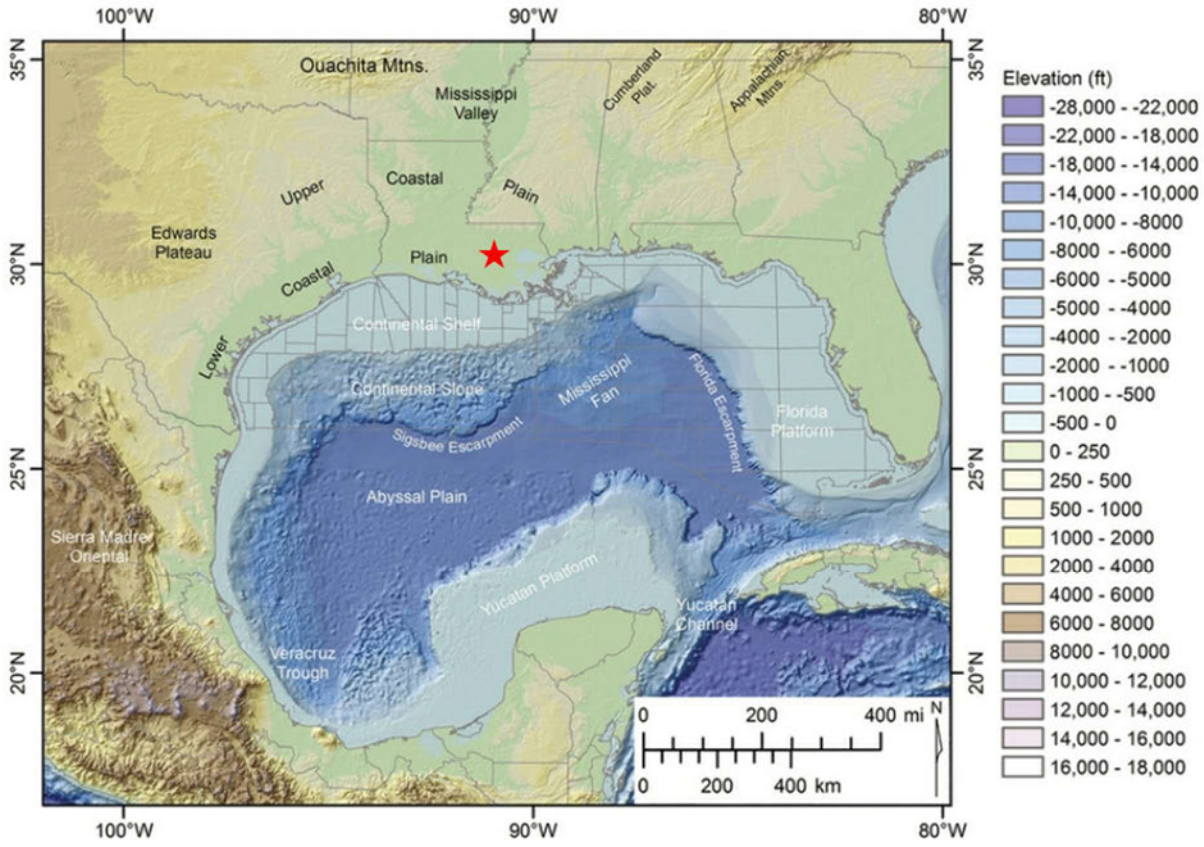

Figure 1-1. Location of Ciel No.1 within the northern Gulf of Mexico Basin (Snedden and Galloway, 2019).

Much of the present lower coastal plain, shelf, and continental slope is underlain by relatively homogenous thin transitional crust (Snedden and Galloway, 2019) that was stretched and attenuated during the Middle to Late Jurassic rifting of the Gulf of Mexico.

The structural opening of the Gulf of Mexico basin was accompanied by the northwest-to-southeast trending transfer faults that influenced distribution of the Louann Salt and basin subsidence rates. The current landscape of the Gulf of Mexico basin is primarily influenced by sediment loading and salt mobilization. These processes are typically expressed by structures such as growth faults, allochthonous salt bodies, salt welds, salt-based detachment faults, salt diapirs, and basin-floor compressional fold belts (Snedden and Galloway, 2019).

1.1.2 Depositional History

The Oligocene was a time of massive sediment influx to the Gulf of Mexico that began with extensive crustal heating, uplift, and volcanism of source areas in northern Mexico and the southwestern United States. Uplift impinged directly on the western margin of the Gulf of Mexico basin. The northwest margin, now the western edge of the Burgos basin, was similarly elevated in the Middle Oligocene. Further west, explosive volcanism and caldera collapse combined with the uplift to create a long-lived outpouring of recycled sedimentary rocks, volcaniclastics, and reworked devitrified ash that peaked by the mid-Oligocene and continued into the Early Miocene. The response in the Gulf of Mexico was the sediment-supply-dominated

Frio depositional episode (Snedden and Galloway, 2019). A decreasing rate of sediment supply and accumulation in the Late Oligocene (Galloway and Williams, 1991, as cited in Snedden and Galloway, 2019) terminated the Frio depositional episode. Long-term backstepping of delta and shore-zone systems culminated in regional transgressive flooding and deposition of the Anahuac shale across the breadth of the Gulf of Mexico margin (Snedden and Galloway, 2019). **Figure 1-2** depicts these depositional features.

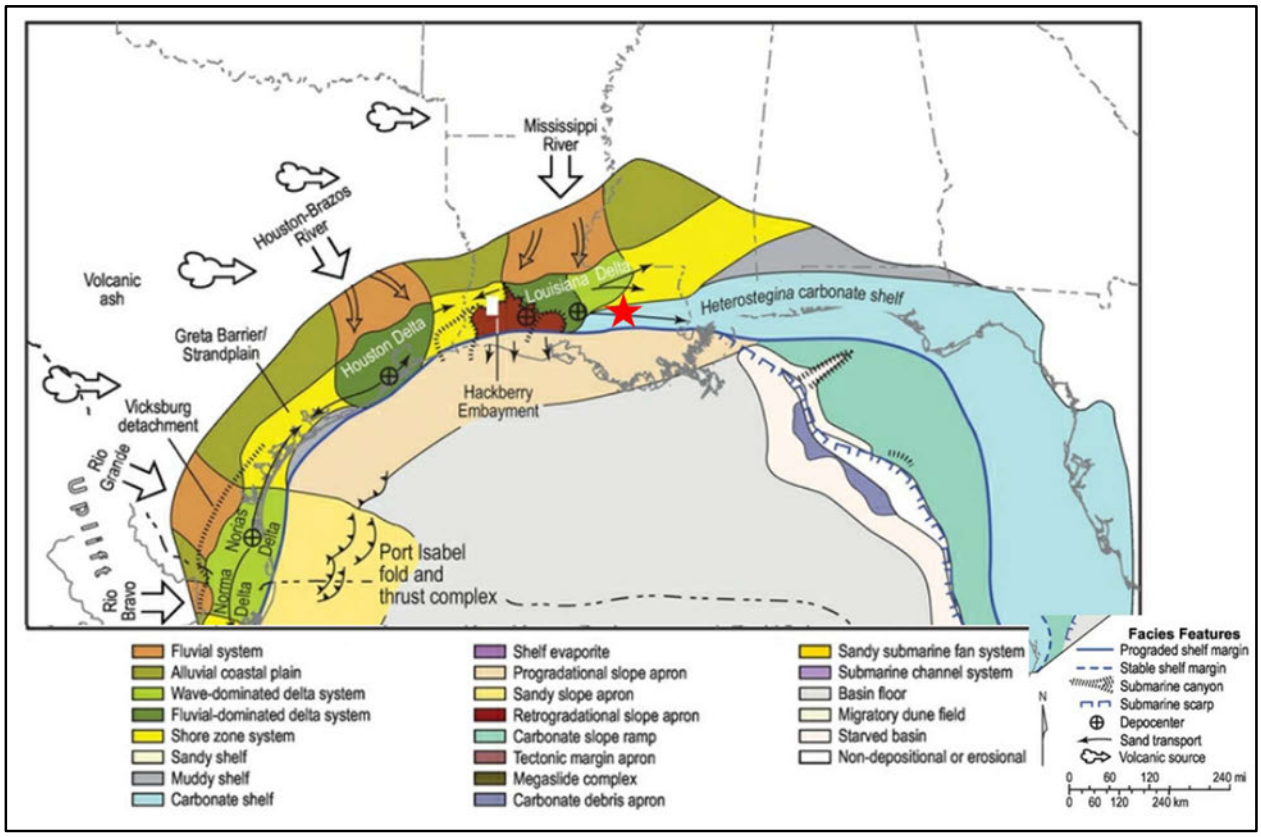

Figure 1-2. Paleogeography and principal depositional systems of the Oligocene Frio depositional episode (Snedden and Galloway, 2019).

Miocene strata of the central Louisiana coast were sediments associated with regressive cycles, and typically expressed in the geologic section by an increased presence of deltaic sands, silts, and clays. Periods of transgressive coastal onlaps are represented by marine shales that divide Miocene strata into Lower, Middle, and Upper units. Index fossils associated with the Miocene section breaks, listed from oldest to youngest, include *Heterostegina* sp., *Amphistegina* B (Amph B), *Textularia* W/*T. stapperi*, and *Bigenerina* A/*Robulus* E (Rob E) (Galloway, 2008; Hulsey, 2016) **Figure 1-3**. These benthic faunal markers are associated with first-order maximum flooding surfaces that correspond to global eustatic highs and are interpreted by the United States Geological Survey (USGS) to "serve as fine-grained sealing units" (Roberts-Ashby et al., 2014).

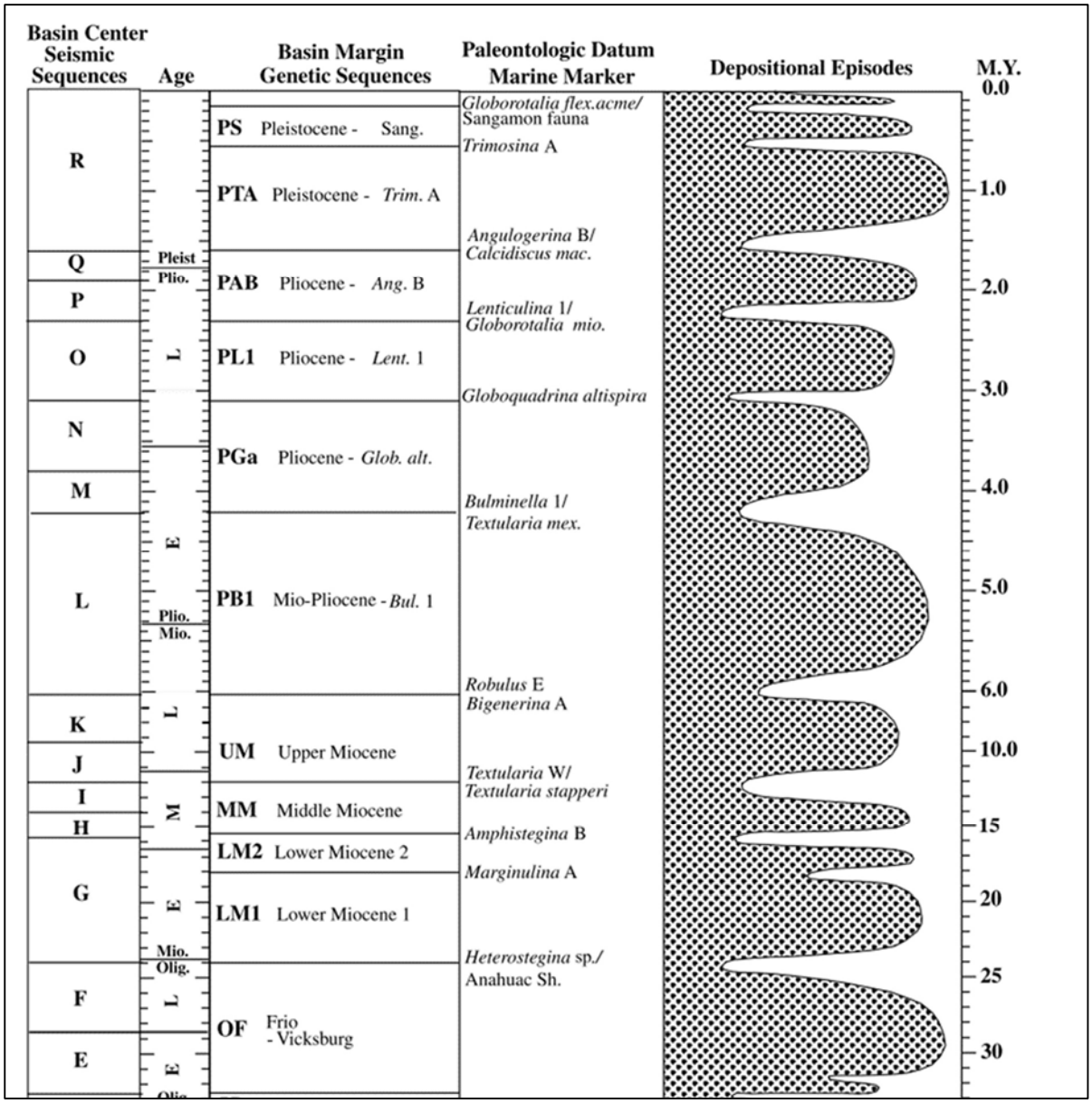

Figure 1-3. Chronology of Gulf of Mexico Cenozoic genetic sequences and their bounding marine shale units and paleontological markers. Genetic sequences record the principal basin-filling depositional episodes seen in amplitude of the episode curve. Note scale change at 6 m.y. Galloway etal. 2000.

Figure 1-4 and **Figure 1-5** illustrate the depositional features of the Lower and Middle Miocene units, respectively.

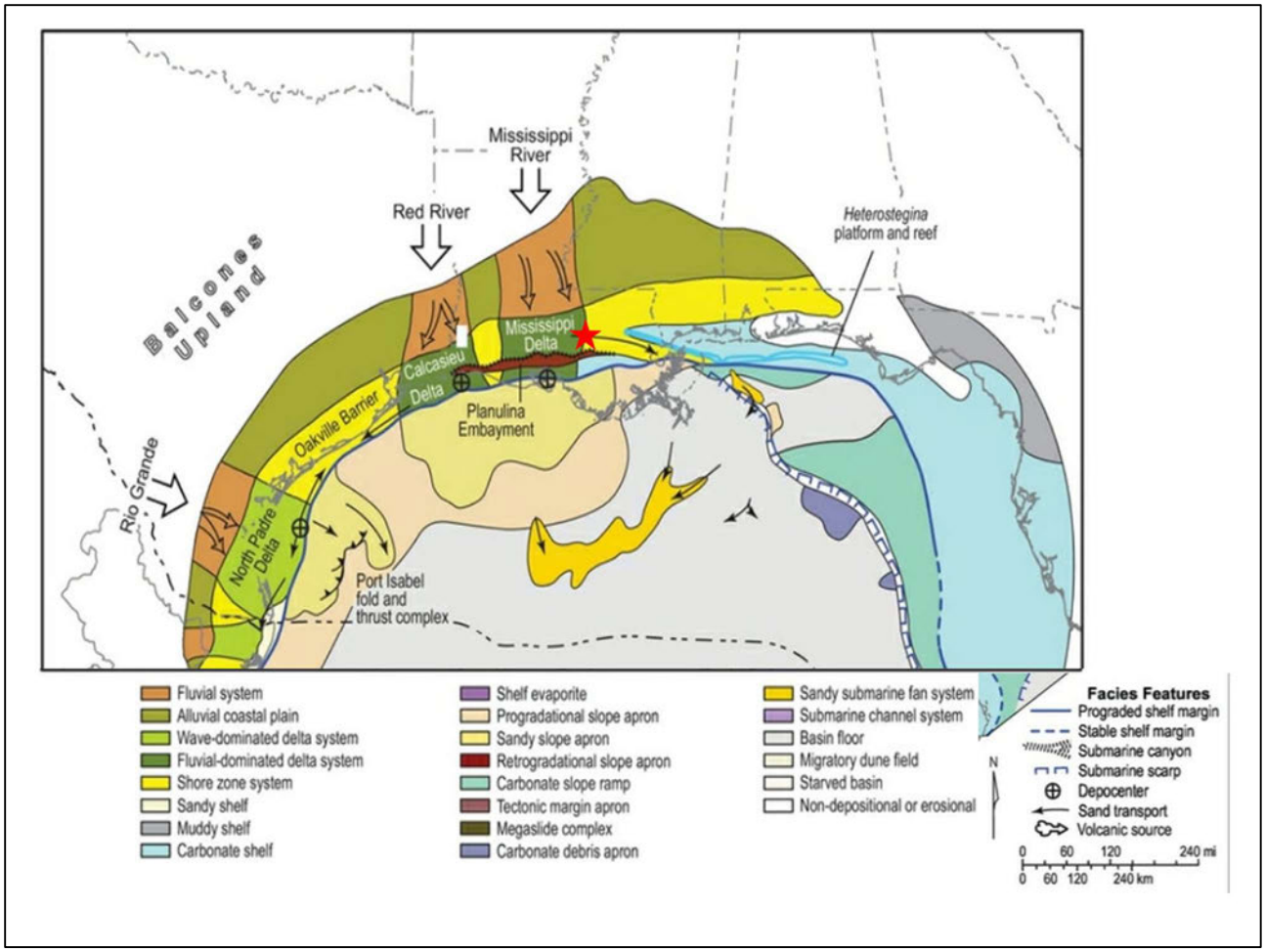

Figure 1-4. Paleogeography and principal depositional systems of the Lower Miocene depositional episode (Snedden and Galloway, 2019).

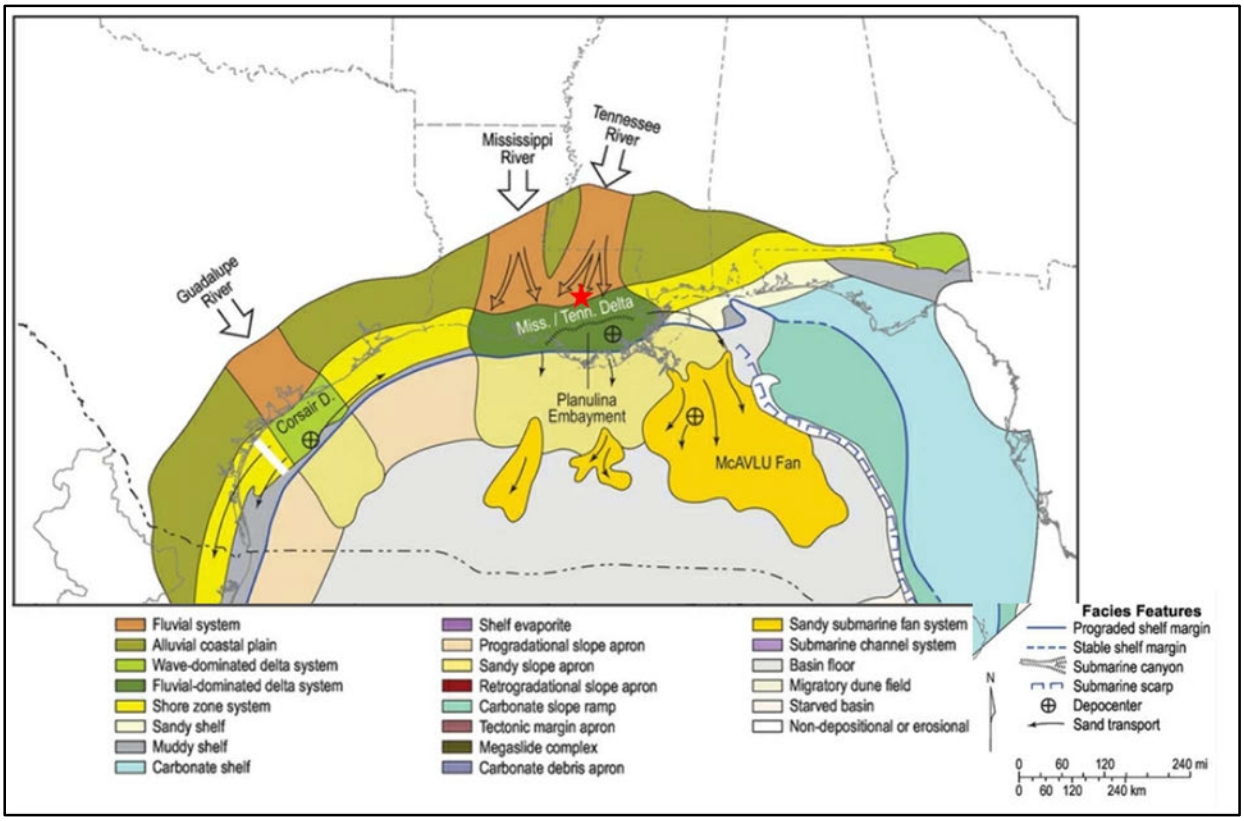

Figure 1-5. Paleogeography and principal depositional systems of the Middle Miocene depositional episode (Snedden and Galloway, 2019).

1.1.3 Stratigraphy

Figure 1-6 shows a generalized stratigraphic column of Cenozoic geologic units of Louisiana. Red shading indicates a reservoir; blue shading indicates a regional seal. The target injection interval for the proposed Ciel No.1 is the Miocene Formation sand packages. The highest gross and net thicknesses correspond to the major deltaic axes, specifically the Mississippi Delta. Due to a location adjacent to the Mississippi depocenter, net-sandstone thickness averages for the Miocene sandstone formations are as follows: 1,500 feet for the Lower Miocene I, 1,600 feet for the Lower Miocene II, 3,200 feet for the Middle Miocene, and 5,400 feet for the Upper Miocene (Roberts-Ashby et al., 2014).

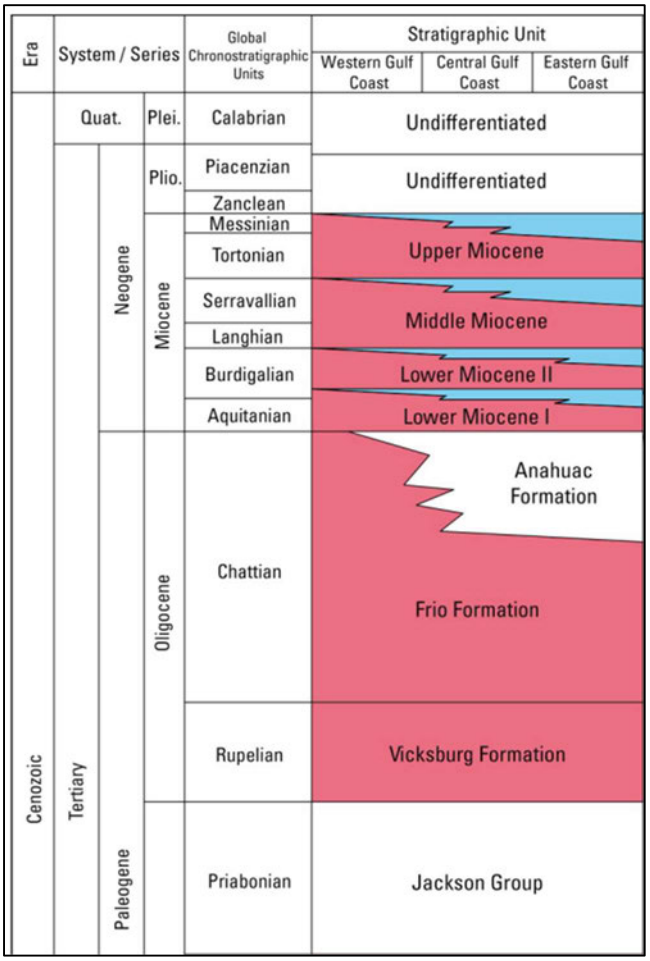

Figure 1-6. Stratigraphic column displaying the east-west distribution of the Tertiary rocks within the USGS Gulf Coast Carbon Dioxide Storage Resources Study Area (adapted from Dubiel et al., 2007; Warwick et al., 2007; and Mancini et al., 2008, as cited in Roberts-Ashby et al., 2014).

The stratigraphic column depicted in **Figure 1-6** is consistent with Gulf of Mexico basin deposits expected to be encountered at the proposed Ciel No.1 injection site. This figure expands on the information in **Figure 1-7**, which plots individual Miocene and Oligocene units relative to key biostratigraphic markers and a coastal-onlap curve to provide context to regional transgressive flooding surfaces. For this permit application's purpose, the proposed injection interval is the Miocene. The gross geologic section contains both shale and sand sections. Only clean, sandy zones with injection potential were modeled to sequester CO_2.

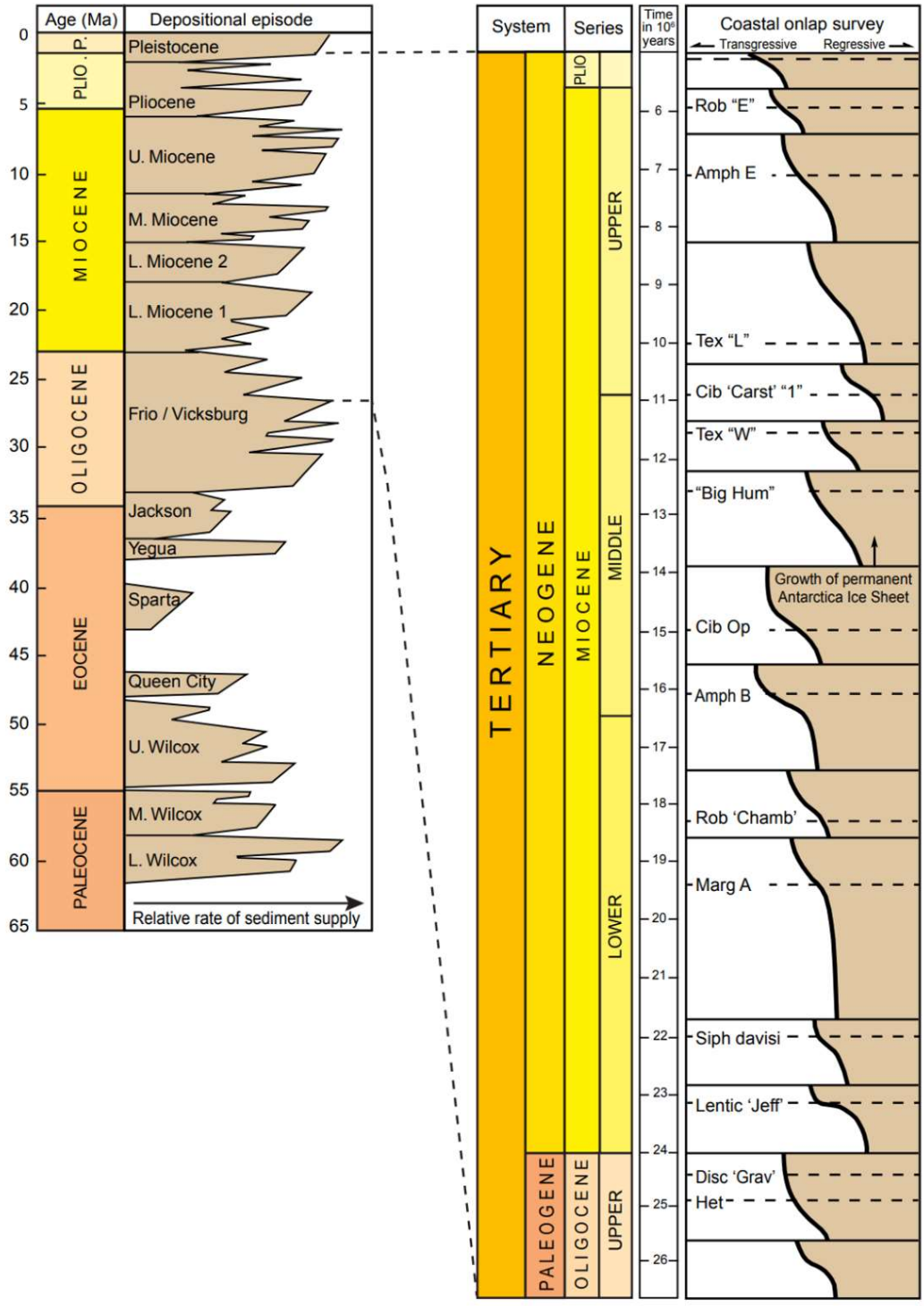

Figure 1-7. Stratigraphic column of major Tertiary depositional episodes (Fillon et al., 1997, as cited in Treviño and Rhatigan, 2017).

The Miocene section is divided into four storage assessment units (SAUs) as shown in **Figure 1-6** (Roberts-Ashby et al., 2014).

For the Lower Miocene I SAU, gross thickness averages 1,500 feet ± 500 feet (**Figure 1-8**).

For the Lower Miocene II SAU, gross-thickness estimates average 1,600 feet ± 300 feet, with thicknesses of more than 6,000 feet in the Mississippi Delta (**Figure 1-9**). Net-sandstone thicknesses for this SAU are 550 ± 200 feet. The updip portion of the Mississippi Delta area may have aggregate sandstone thickness >1,000 feet (Roberts-Ashby et al., 2014).

The Middle Miocene SAU averages 3,200 ± 900 feet in thickness, exceeding 6,000 feet at the Mississippi Delta (**Figure 1-10**). Average net-sandstone thickness estimates are 480 ± 140 feet, with thicknesses approaching 1,000 feet in the Mississippi Delta,

The Upper Miocene SAU averages 5,400 ± 1,000 ft in gross thickness, exceeding 10,000 feet at the Mississippi Delta (**Figure 1-11**). The average net-sandstone thickness for this SAU is 1,500 ± 400 feet, with thicknesses of more than 3,000 feet at the Mississippi Delta.

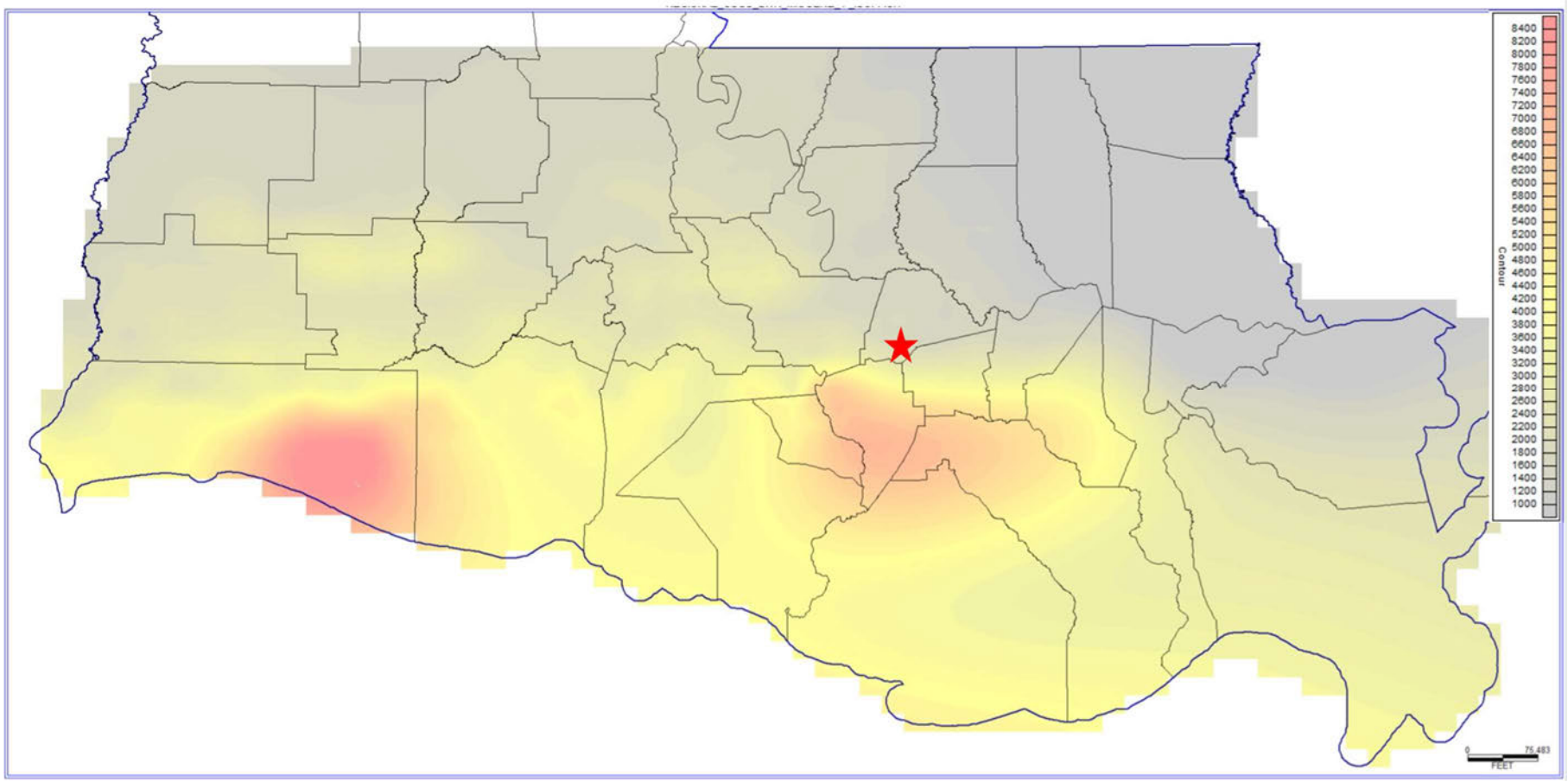

Figure 1-8. Isopach map of Lower Miocene 1 (USGS, 2004a).

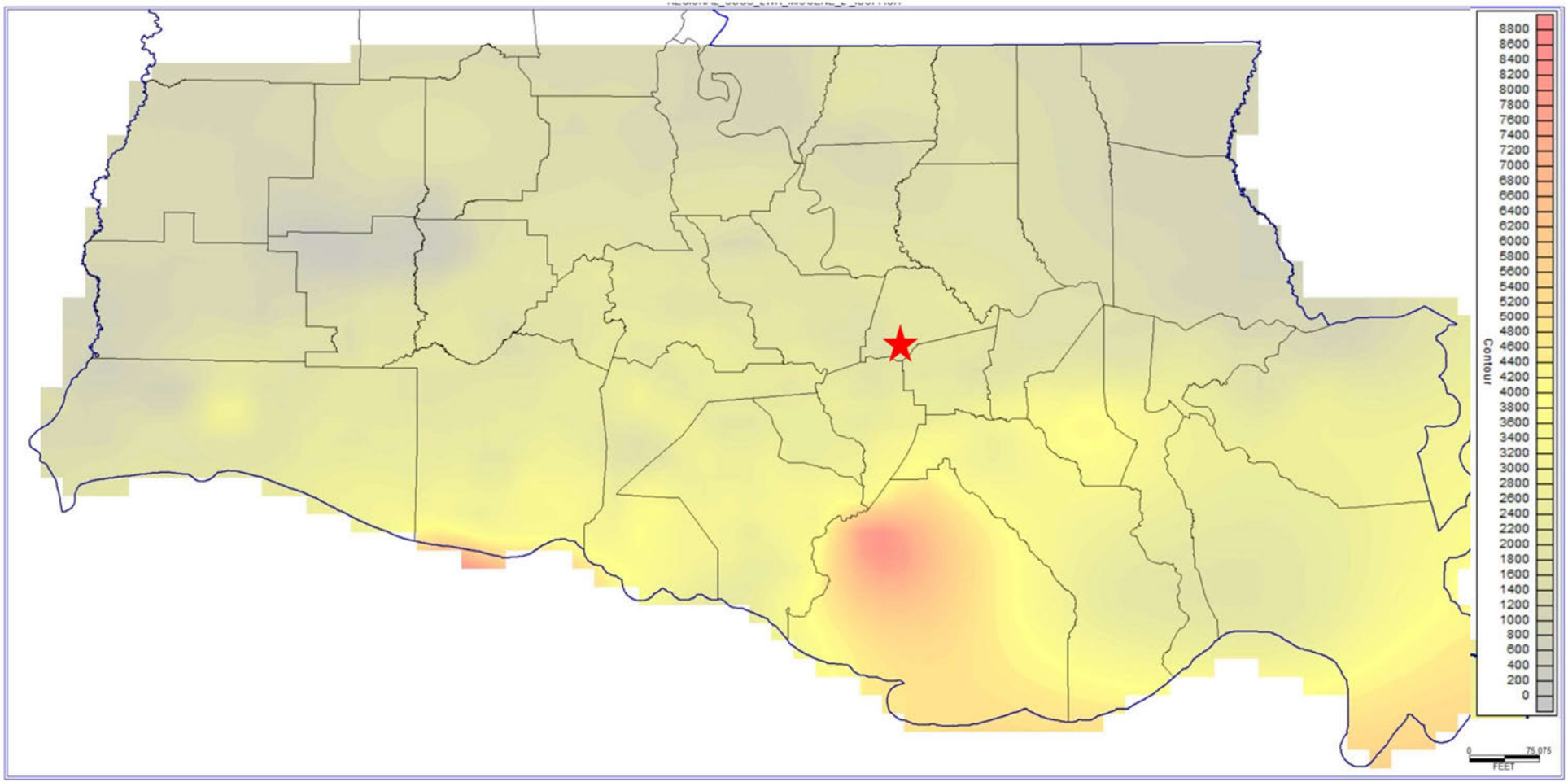

Figure 1-9. Isopach map of Lower Miocene II (USGS, 2004b).

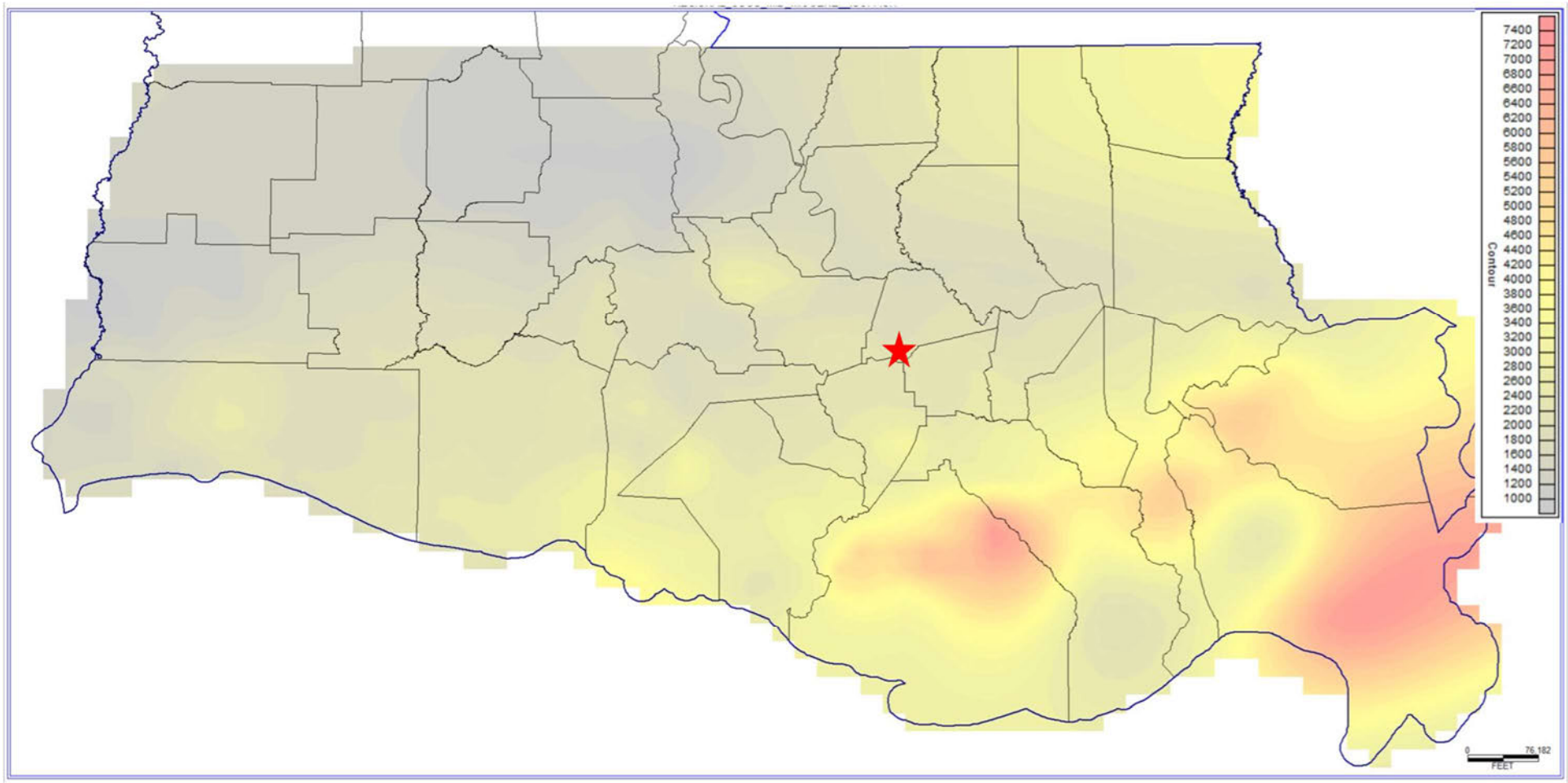

Figure 1-10. Isopach map of Middle Miocene (USGS, 2004c).

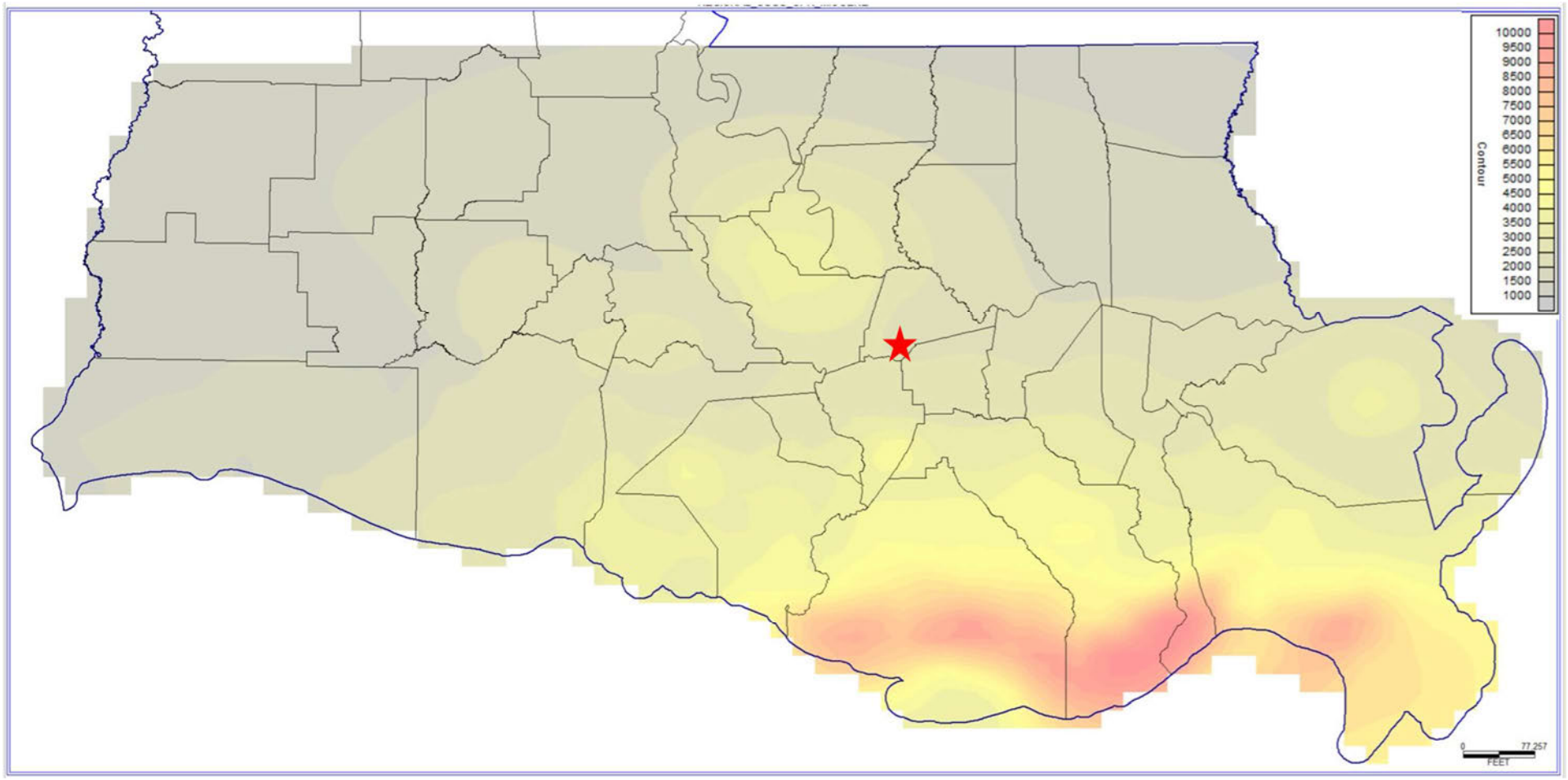

Figure 1-11: Isopach map of Upper Miocene (USGS, 2004d).

1.1.4 Structure

During the Mesozoic Era breakup of the supercontinent Pangea, crustal extension and seafloor spreading created the Gulf of Mexico basin as it exists today (Salvador, 1987, as cited in Snedden and Galloway, 2019). Most of the structural basin is underlain by transitional crust that was stretched and attenuated by Middle to Late Jurassic rifting. The deformation caused areas of thick transitional crust along the basin margin to be separated by areas of stretched crust that subsided more deeply. This resulted in a chain of arches, embayments, and salt domes within the northern part of the basin. Much of the present lower coastal plain, shelf, and continental slope is underlain by homogenous thin transitional crust (Snedden and Galloway, 2019).

Figure 1-12 shows that this thin transitional crust comprises the basement beneath the proposed Ciel No.1 well (Sawyer et al., 1991, as cited in Snedden and Galloway, 2019).

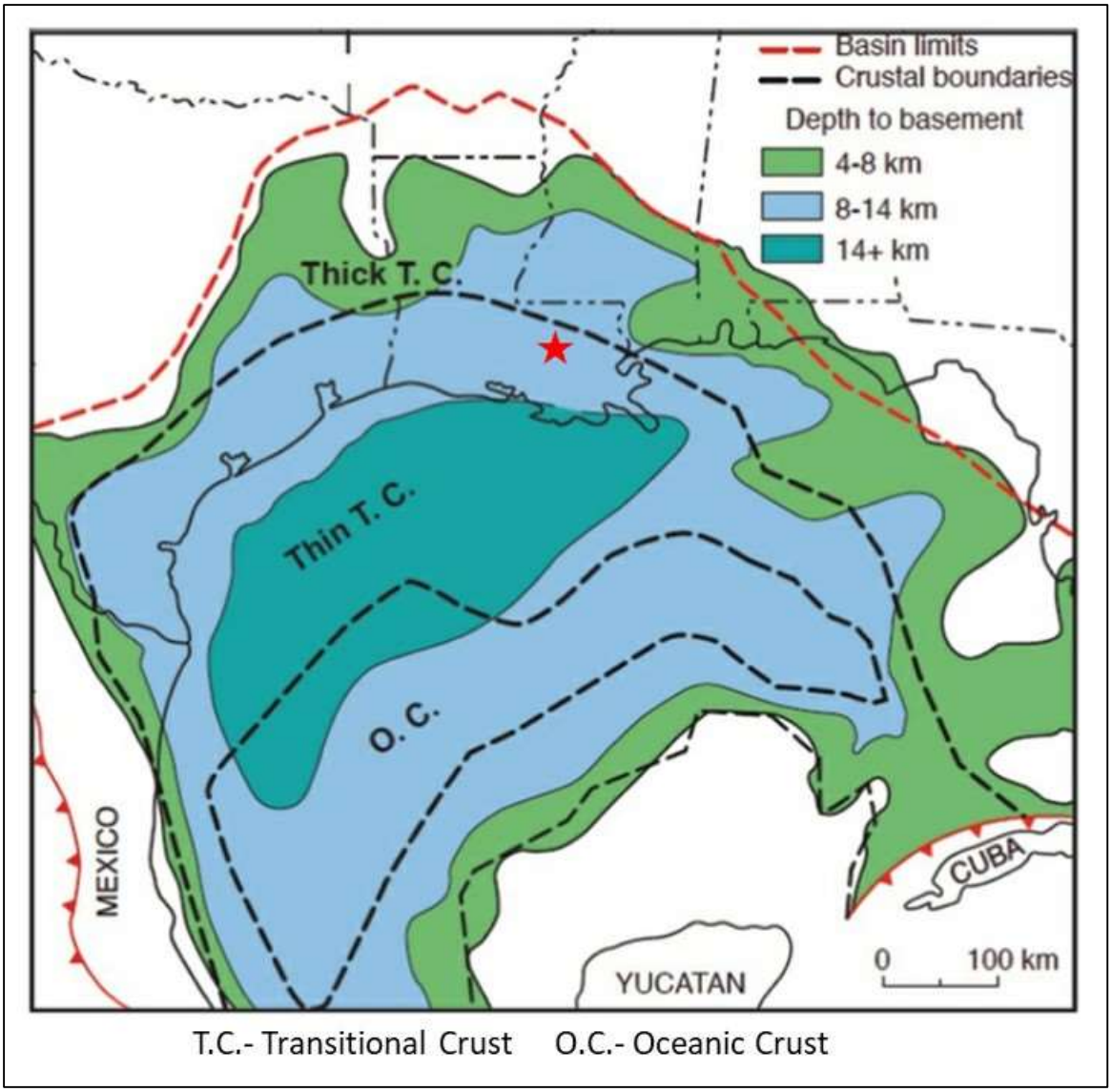

Figure 1-12. Crustal types and depth to basement in kilometers (Sawyer et al., 1991, as cited in Snedden and Galloway, 2019).

The structural opening of the Gulf of Mexico basin was also accompanied by the northwest-to-southeast-trending transfer faults that influenced the distribution of the Louann Salt and basin subsidence rates. Basement structures associated with the Ouachita range, Appalachian range, and Llano uplift contributed to Louann Salt placement and affected subsequent sediment distributions. Regional salt tectonics were also influenced by structural flexures such as the Balcones, Luling-Mexia-Talco, State Line, and Pickins-Gilberton fault zones (Snedden and Galloway, 2019). The current landscape of the Gulf of Mexico basin is primarily influenced by sediment loading and salt mobilization. These processes are typically expressed by structures such as growth faults, allochthonous salt bodies, salt welds, salt-based detachment faults, salt diapirs, and basin-floor compressional fold belts (Snedden and Galloway, 2019). **Figure 1-13** shows the structure contours of the top of the Miocene Formation, with regional faults and locations of salt domes. Depth to the top of the Miocene is approximately –2,500 feet measured depth and the thickness is approximately 6,000 feet at the proposed location. Site-specific depth to top of formation, total injection interval thickness, and net sand thickness values will be discussed in more detail in the Injection and Confining Zone Details section.

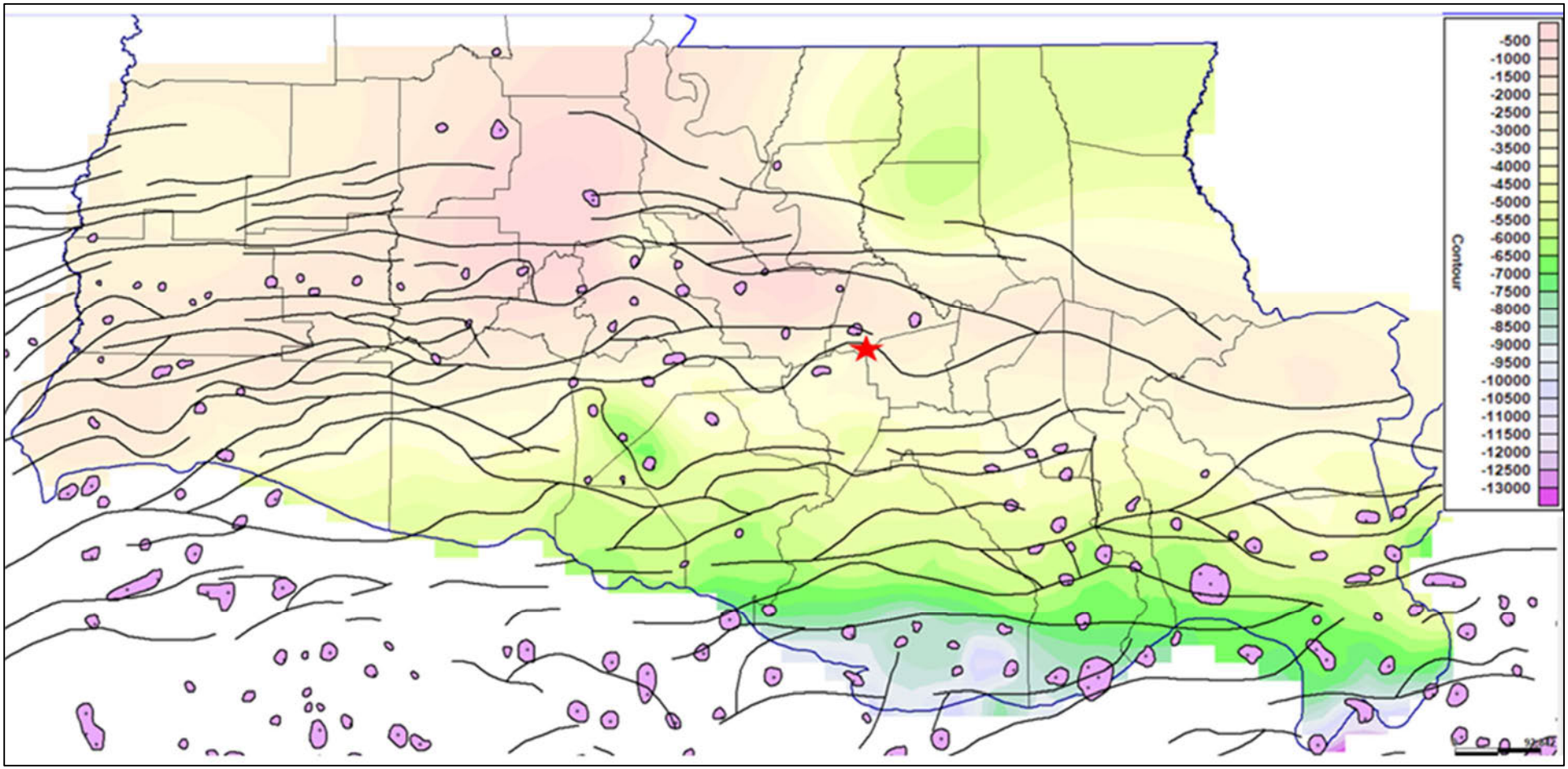

Figure 1-13. USGS (2004e) of the regional top of the Miocene, showing major faults and salt domes of Louisiana. Red star is the approximate location of the Ciel No.1 well.

1.2 Maps and Cross Sections of the AoR [40 CFR 146.82(a)(2), 146.82(a)(3)(i)]

The Donaldsonville storage site is located approximately 2.4 miles to the southeast of Donaldsonville, Louisiana, and approximately 30 miles south of Baton Rouge, Louisiana, as shown in

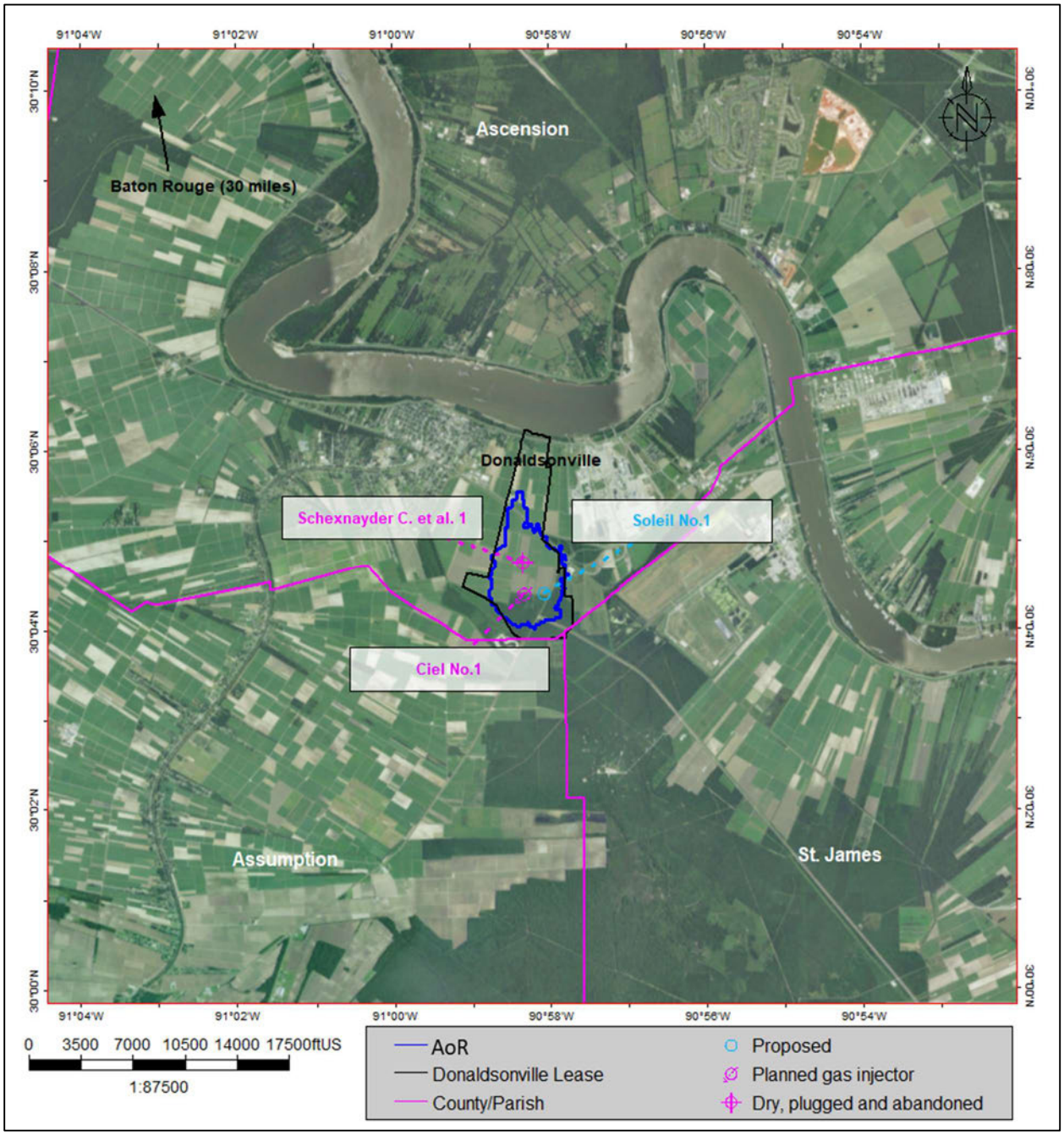

Figure 1-14.

The cross sections through the AoR are shown as follows: **Figure 1-15** through **Figure 1-18** are south-north and east-west sections in the upper confining zones, and **Figure 1-19** through **Figure 1-22** are south-north and west-east sections through the lower confining zones.

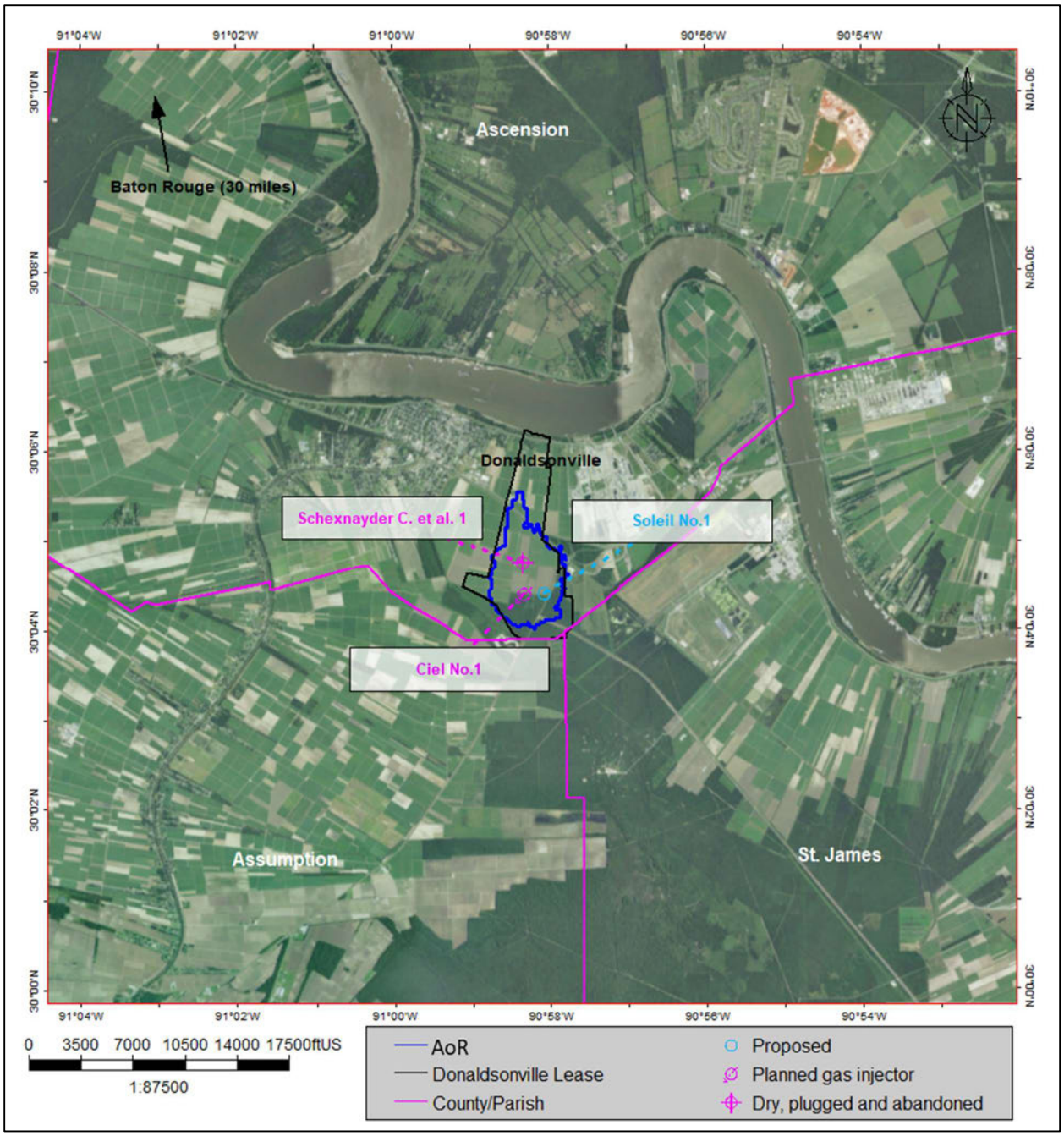

Figure 1-14. Map of proposed injection well location in relation to stratigraphic test well. CO_2 and pressure plumes are indicated with the blue polygon.

Figure 1-15. Structural cross section in south-north orientation of the upper confining zone, showing the local dip of the strata. Red vertical line is the location of the proposed Ciel No.1.

Figure 1-16. South-north stratigraphic section in the AoR, showing the continuity of the injection and confining zones. Red vertical line is the location of the. proposed Ciel No 1.

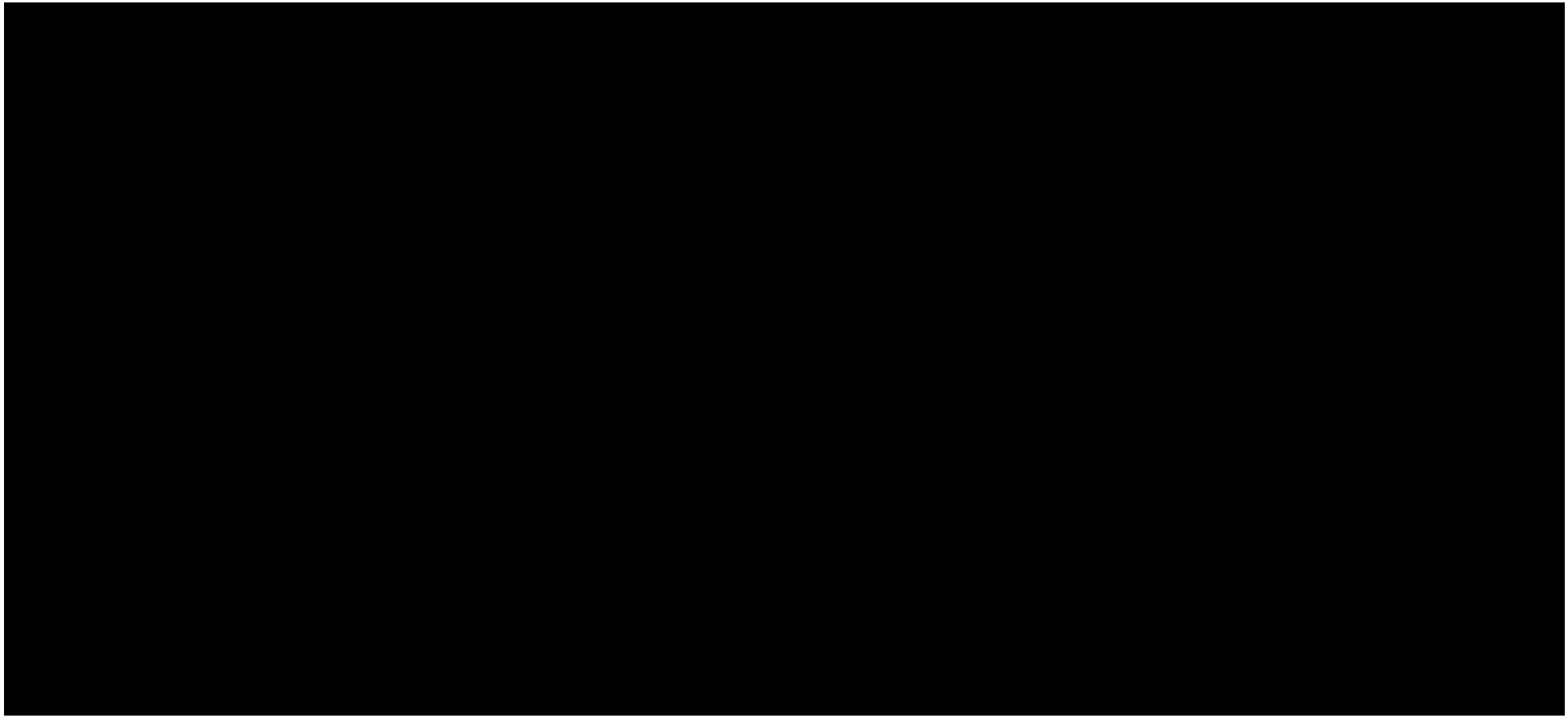

Figure 1-17. West-east stratigraphic section of the upper confining zone within the AoR, showing continuity of the strata. Red vertical line is the location of the proposed Ciel No.1.

:

Figure 1-18. Structural cross section in west-east orientation of the upper confining zone. Red vertical line is the location of the proposed Ciel No.1.

Figure 1-19. Structural cross section in south-north orientation of the lower confining zone. The red vertical line marks the location of the proposed Ciel No.1 injection well.

Figure 1-20. Stratigraphic cross section in south-north orientation of the lower confining zone. The red vertical line marks the location of the proposed Ciel No.1 injection well.

Figure 1-21. Structural cross section in west-east orientation of the lower confining zone. The red vertical line marks the location of the proposed Ciel No.1 injection well.

Figure 1-22. Stratigraphic cross section in a west-east orientation of the lower confining zone. The red vertical line marks the location of the proposed Ciel No.1 injection well.

1.3 Faults and Fractures [40 CFR 146.82(a)(3)(ii)]

Three faults exist within the 35-square-mile area mapped from the 3D seismic data. The faults are normal faults with an average dip of 45 degrees. Average displacement along fault planes is less than 100 feet. Two faults penetrate the lower confining zone (shale mrk 11, shown in **Figure 1-23,** and none penetrates the upper confining zone (shale mrk 2) Figure 1-24. The two faults extend radially from the Lapice Field.

The fault closest to the proposed injection well location is approximately 1 mile away and strikes north-northwest and south-southeast (**Figure 1-23**). It is a normal fault downthrown to the west. The seismic data show that the fault is traceable throughout the lower injection zone and does not reach the upper confining zone (**Figure 1-24**) and is therefore not a concern for the plume, as demonstrated by the initial dynamic modeling (Section 1.11 of this document).

Figure 1-23. 3D seismic map in time, showing location of the normal faults (colored plus signs) at the top of the lower confining zone (top of Shale Mrk 11).

Figure 1-24: 3D seismic map in time of top of Shale Mkr 2 (upper confining zone), illustrating the absence of faulting.

The dip within the proposed injection outline at the Miocene level ranges from 1 to 2 degrees, with the primary direction updip to the north and downdip to the south. Little dip rotation occurs at the Miocene level.

1.4 Seismic

Approximately 35 square miles of 3D surface and 2D seismic data were licensed and interpreted by BKVerde (**Figure 1-25**).

Figure 1-25. Red dashed polygon is acquired 3D seismic data; blue line represents the 2D line. Yellow-filled black polygon is the lease outline.

The interpreted seismic data are a combination of two merged 3D surveys and one 2D line. The 2D line was acquired in 1985 (**Figure 1-25** blue line). It was acquired with dynamite as the energy source, a group interval of 220 feet, and a shotpoint interval of 440 feet, resulting in nominal 24-fold data. The 2D data were reprocessed in 2015.

The first 3D survey was shot in May 2005 (Lapice 3D). The legacy survey was acquired using Dynoseis as the energy source with a 110 × 110 feet bin size and a 29,920 × 31,460 feet patch, resulting in nominal 81-fold data. The second 3D survey was shot in June 2005 (Romeville 3D). The legacy survey was acquired using dynamite as an energy source with a 110 × 110 feet bin size and a 19,360 × 31,460 feet patch, resulting in nominal 54-fold data. The 3D surveys were merged and reprocessed in 2012 using pre-stack time migration.

The 3D reflection profiles, which image the subsurface based on density and velocity contrasts, were combined with subsurface well control (geologic formation tops) to map the proposed injection and confining zones. **Figure 1-26** shows the location of the seismic lines that are represented in **Figure 1-27**. **Figure 1-28**, and Figure 1-29. The interpreted seismic sections contain horizons and any discontinuities, such as faults. The 3D seismic volume was used to map the Miocene-age rocks, which are approximately 6,500 feet thick. The seismic data are of good quality with sufficient offset information to image the target section between 4,000 feet and 11,500 feet measured depth. The 3D seismic data recorded and interpreted across the proposed CO_2 storage area does not indicate large-scale changes in thickness of the injection or confining

zones (**Figure 1-29**). Interpreted faults in the modeled plume area are limited to the southern periphery, more than 1.5 miles away from the deepest section of the injection interval.

Figure 1-26. Map showing the location of the interpreted lines in Figures 1-15, 1-16, and 1-17.

Figure 1-27. North-south 2D seismic line in time with projected injection well (Ciel No.1) in red. Line does not indicate the presence of obvious faults or large changes in thickness of the injection or confining zones.

Figure 1-28. West-to-east 3D seismic crossline, crossing the proposed CO_2 storage area, which does not indicate the presence of obvious faults or large changes in thickness of the injection or confining zones at the proposed site.

Figure 1-29. Northwest-southeast inline of 3D seismic survey intersecting the proposed injection well, which does not indicate the presence of obvious faults or large changes in thickness of the injection or confining zones at the proposed site.

For velocity control, three time-to-depth relationships were available near the 3D data. These were used for the initial velocity model and seismic interpretation (

Figure 1-30). Sonic data will be acquired in the stratigraphic test well (Soliel No.1), and we will make a synthetic seismogram and update the data.

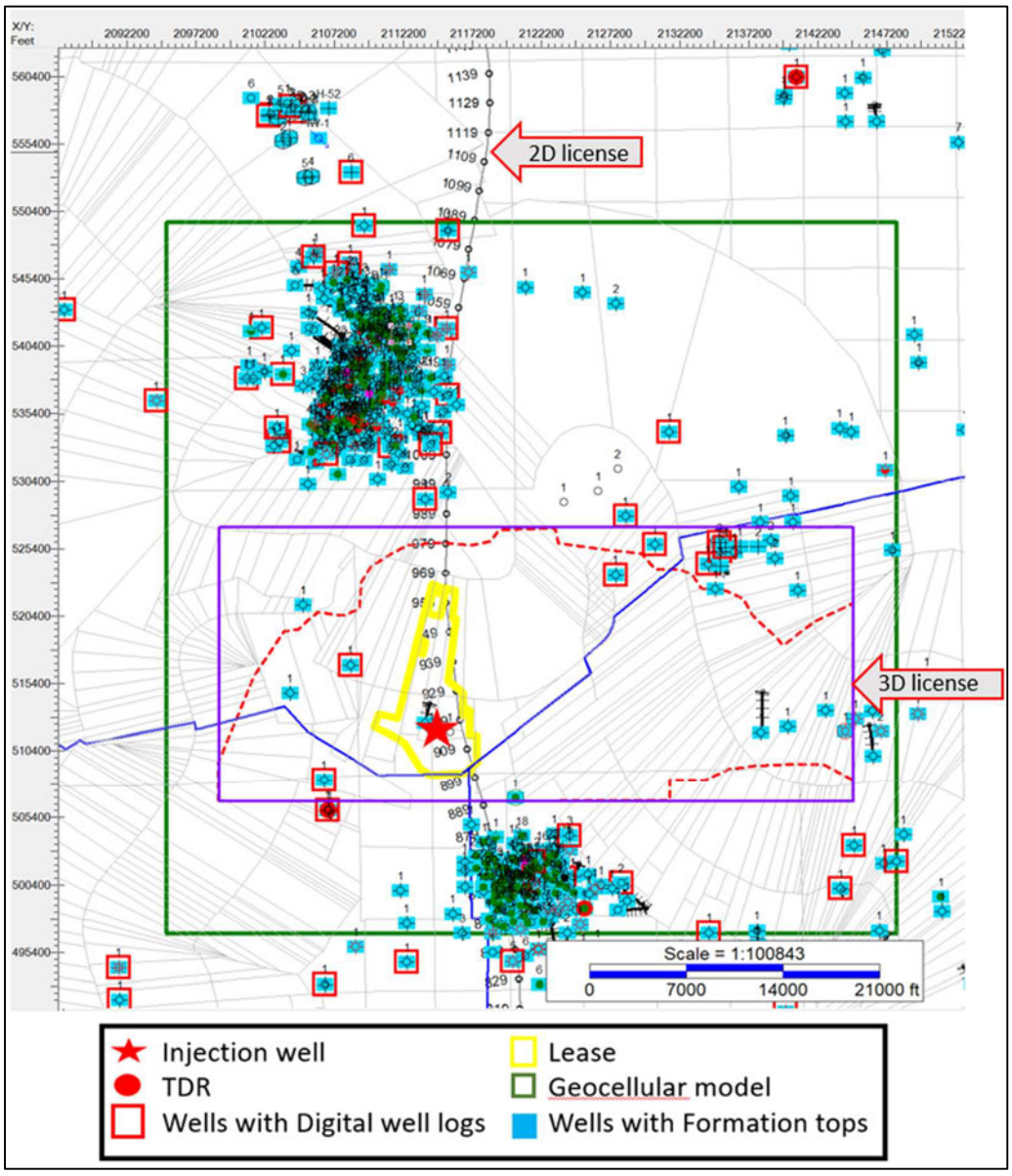

Figure 1-30. Locations of time-to-depth relationship data (red dots) near the 3D and 2D seismic data (red dashed area).

1.5 Injection and Confining Zone Details [40 CFR 146.82(a)(3)(iii)]

1.5.1 Characteristics of the Injection and Confining Zones

The depths and thicknesses of the injection and confining zones are summarized in

Table 1-1.

Table 1-1. Injection and confining zones identified in Ciel No.1 with shale statistics reported for confining zones and sand statistics reported for the injection zones.

Group/ Formation Name	Injection/ Confining Zone	Formation Top (ft) Formation Bottom (feet)	Thickness (feet)	Average Effective Porosity (%)	Average Permeability (mD)
Upper Miocene	Upper Confining	3644 – 4250	606		0.48
Upper Miocene to Lower Miocene 1	Injection	4250 – 10957	6707	31	660.9
Lower Miocene 1	Lower Confining	10957 –11611	654	12	0.28

Primary Lower Confining Zone: Anahuac Shale

The Oligocene Anahuac Shale is the lower confining zone at the Ciel No.1 location. It is a shale-dominated, offshore, prodelta deposit that hydrologically isolates the Lower Miocene from the underlying Frio strata (Hovorka, et al., 2003). In the project area, the Anahuac ranges in thickness from 100 to 1000 feet (**Figure 1-31**).

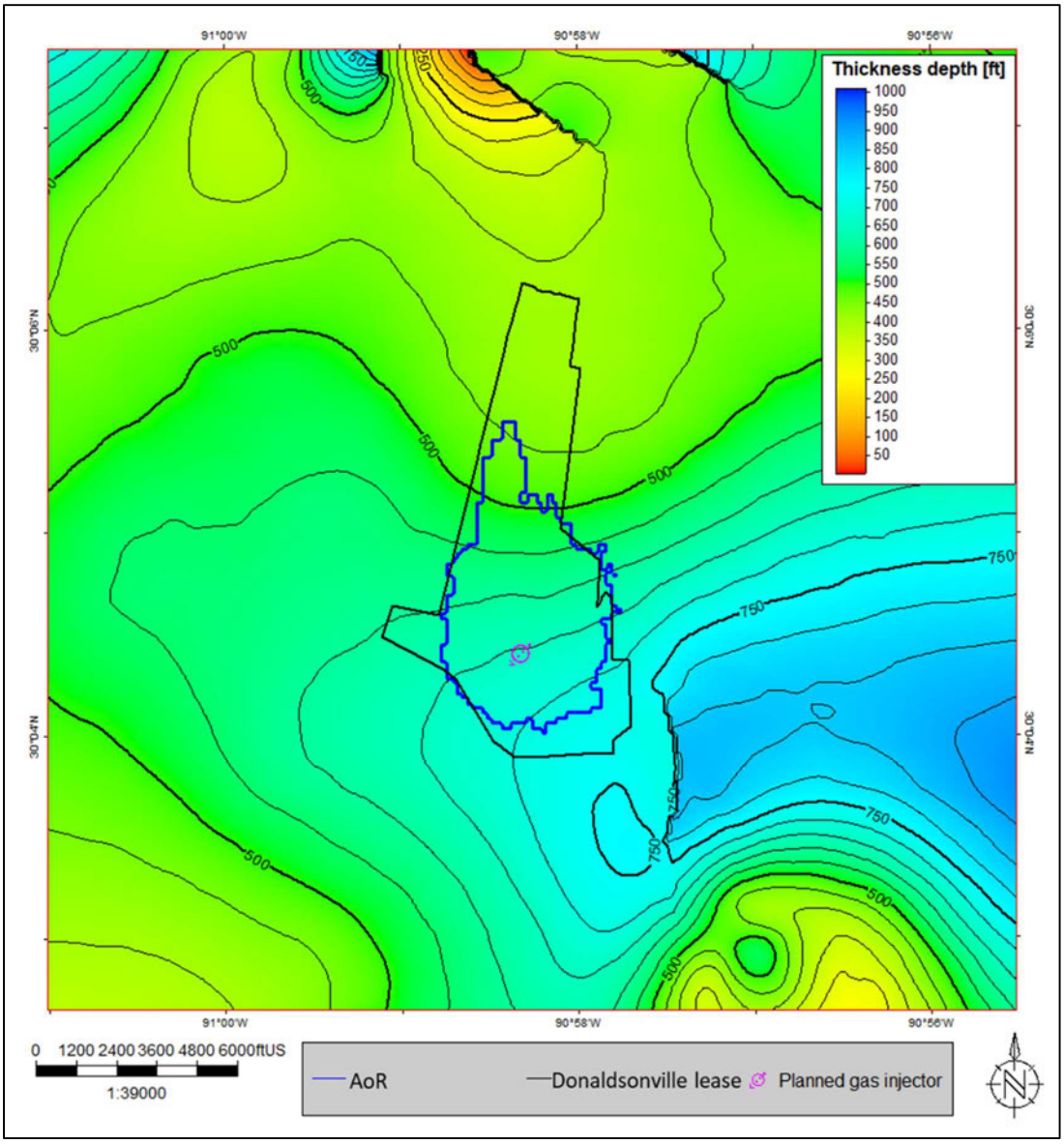

Figure 1-31. Isopach map of the lower confining zone.

As displayed in **Figure 1-32**, a thick marine shale sequence can be identified by the color-filled SP curve directly below the lowest injection zone. This sequence acts as a lower confining seal for the proposed permitted injection interval. The seal is blanketed over the area of interest, as depicted in the cross section in **Figure 1-20**. Because of the high shale composition and the lateral continuity, this confining seal will impede any fluid migration below the injection interval. **Figure 1-32** is an openhole log of the Southdown Sugars 6 (API 170932011600), with estimated effective porosity and permeability. The log clearly depicts the low porosity and permeability found within the Anahuac confining unit.

The shale facies in the lower confining zone have a porosity range of 4% to 30%, with an average effective porosity of 12%. The permeability ranges from 0.003 mD to 506.1 mD with an

average permeability of 0.28 mD. These higher ranges reflect very thin, localized sand stringers that will not affect transmissibility.

The buoyancy of the supercritical CO_2 is greater than the brine despite the density increases due to the reduction in reservoir volume (Chen et al., 2023.) Low porosity and permeability within the shale suggest the strong confining nature of the Anahuac shale.

Core is not available in the Anahuac at the site. It will be collected as part of the site characterization well and provide measurements to calibrate the current petrophysical evaluation (porosity and permeability), mineralogy, and confining capacity from mercury injection capillary pressure (MICP) testing.

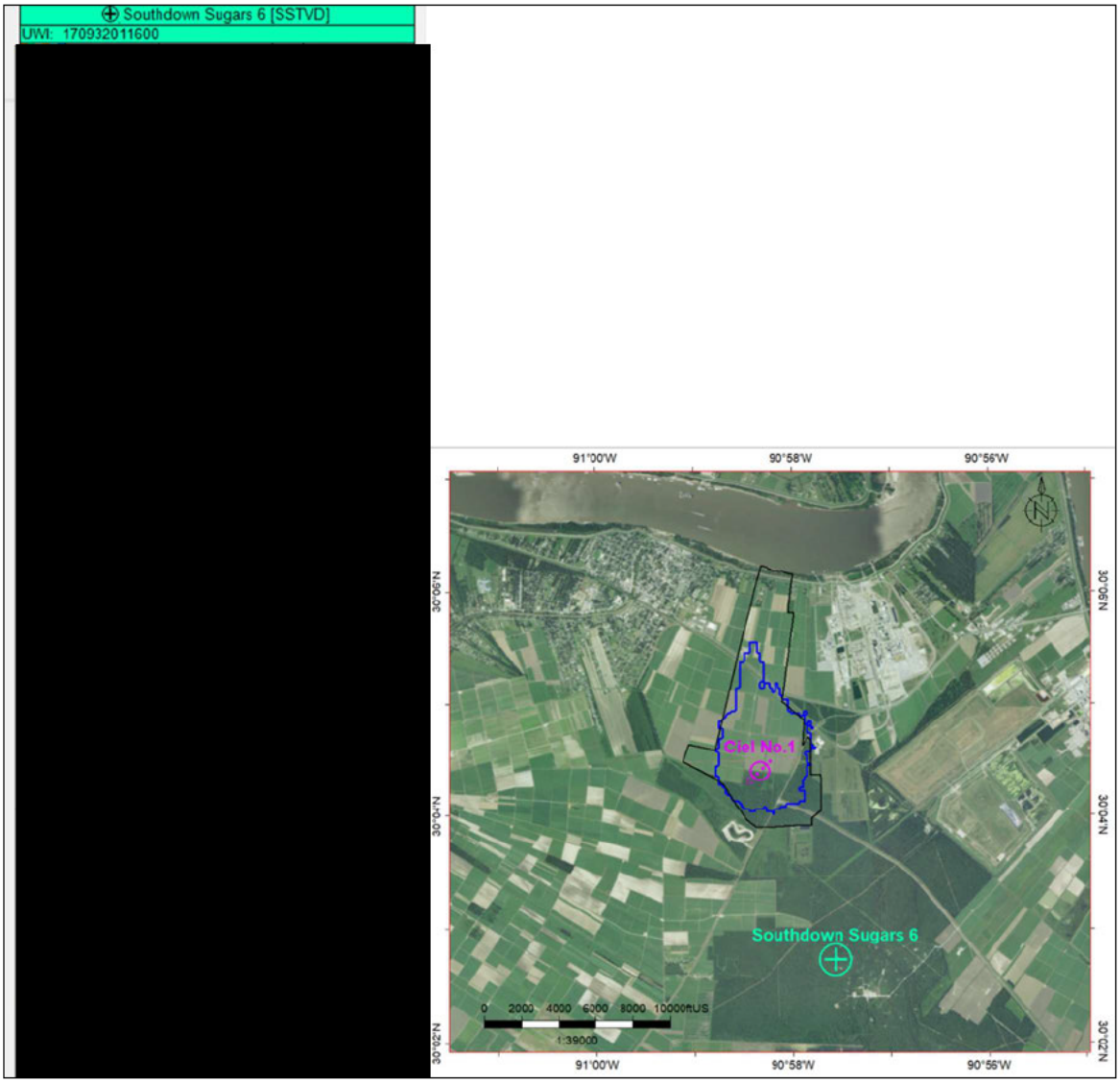

Figure 1-32. Openhole log of offset well Southdown Sugars 6 (170932011600) depicting the lower confining zone.

Injection Interval: Miocene

The Miocene injection interval was deposited as a south-dipping package of siliciclastic sediments along the Gulf of Mexico continental margin. The nearest primary depocenter to the proposed Ciel No.1 well is the Mississippi Delta. Miocene sandstone and shales were deposited in a wide variety of depositional environments, including distributary channels, delta plains, deltas, interdeltaic embayments, and continental shelf (Galloway et al., 2000, as cited in Roberts-Ashby, 2014).

Figure 1-33 is a structure map on top of the Miocene injection interval and **Figure 1-34** is an isopach map of the Miocene injection interval. Depth to the top of the Miocene is approximately

4,250 feet subsea true vertical depth (SSTVD) measured depth, and the thickness is 7,350 feet at the proposed location (**Figure 1-34**).

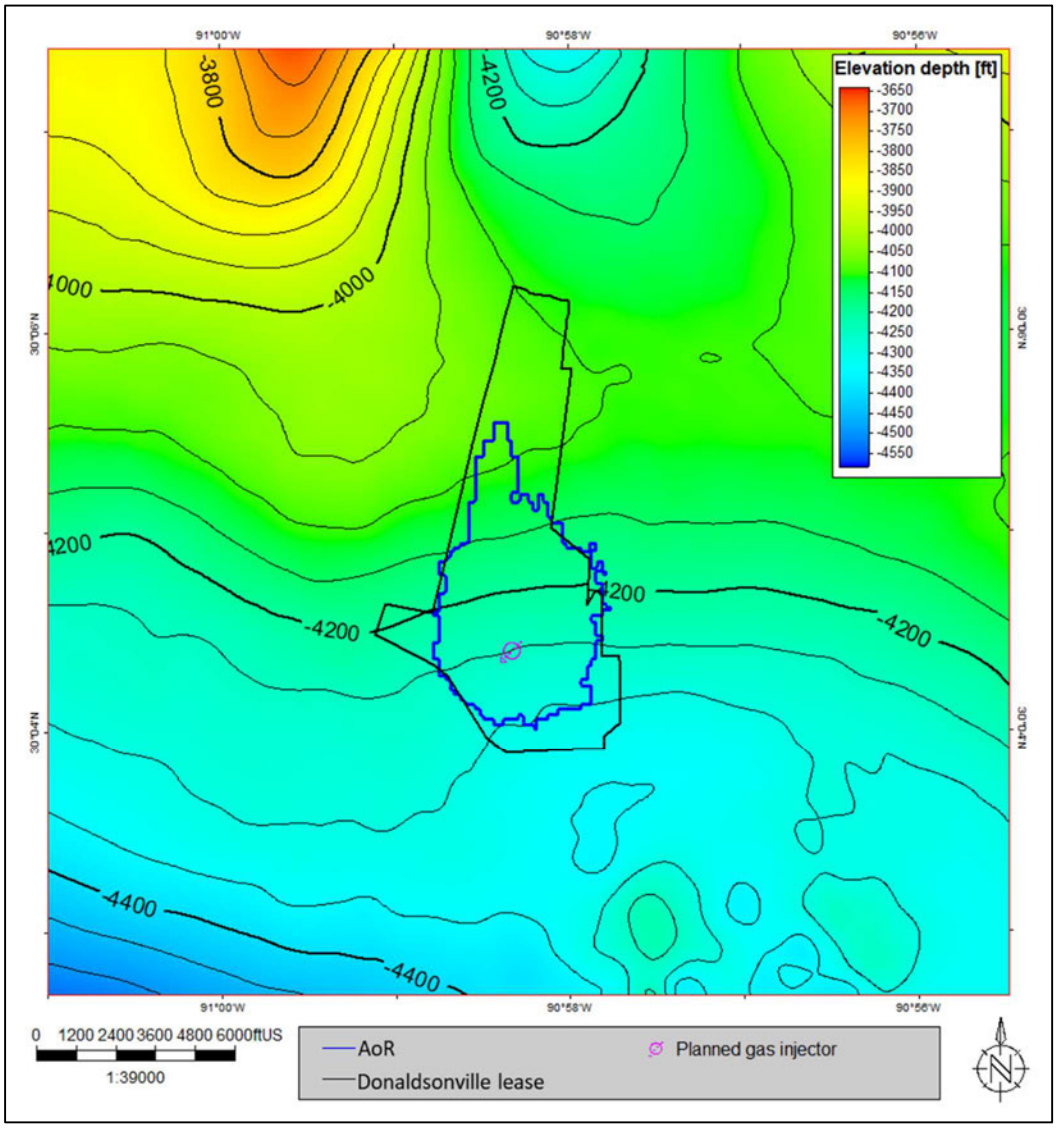

Figure 1-33. Structure map of the top of the Miocene.

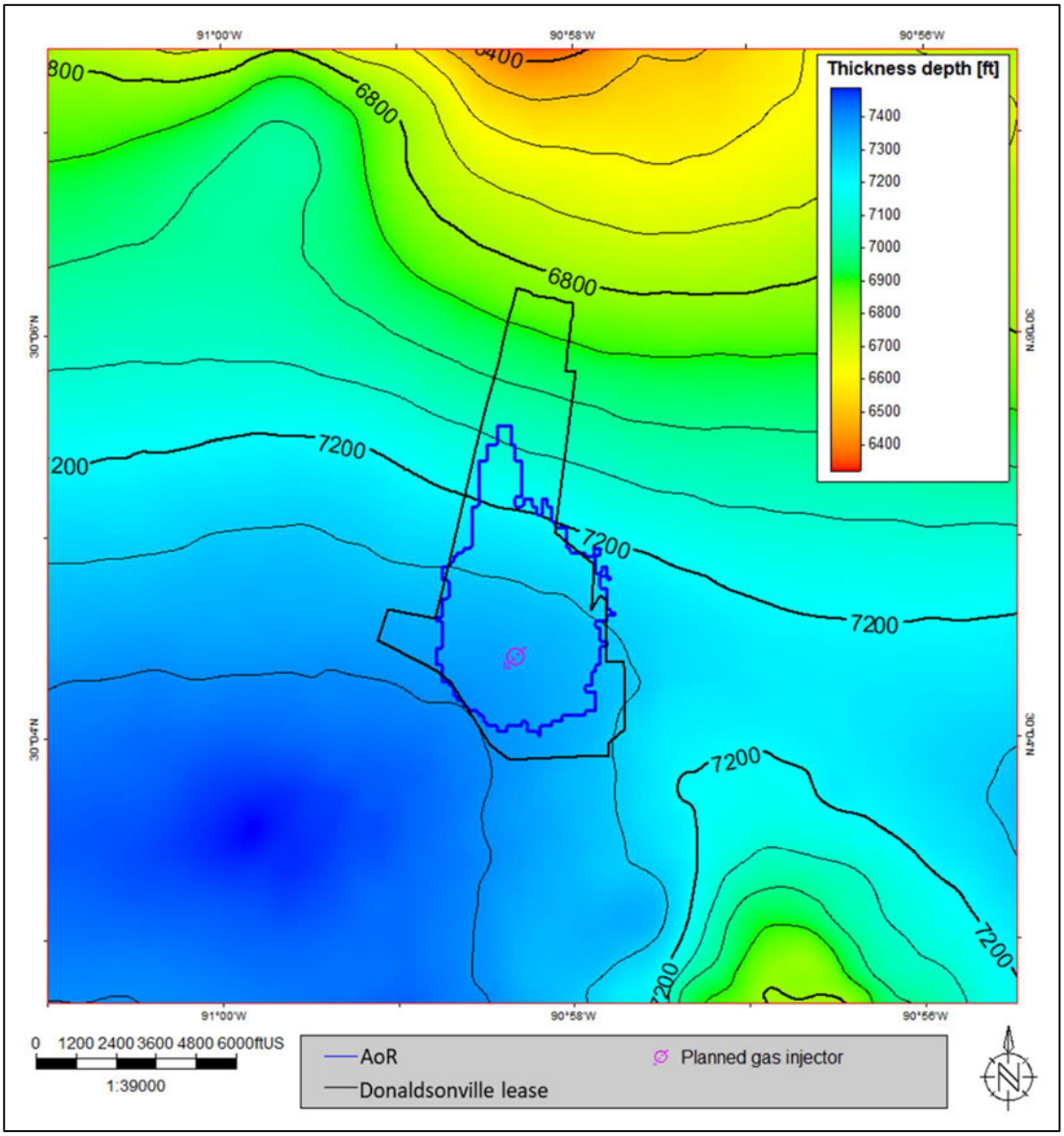

Figure 1-34. Isopach map of the entire injection zone.

Within the injection interval, fluvial-deltaic sands with higher effective porosities and permeabilities will be the targets for injection, with the interbedded shales acting as seals. Nineteen injection zones were chosen based on petrophysical properties of the zones that are predominantly sand. These injection zones are separated by shaly to silty sections (**Figure 1-35**). Details of these injection zones are provided in **Table 1-2**.

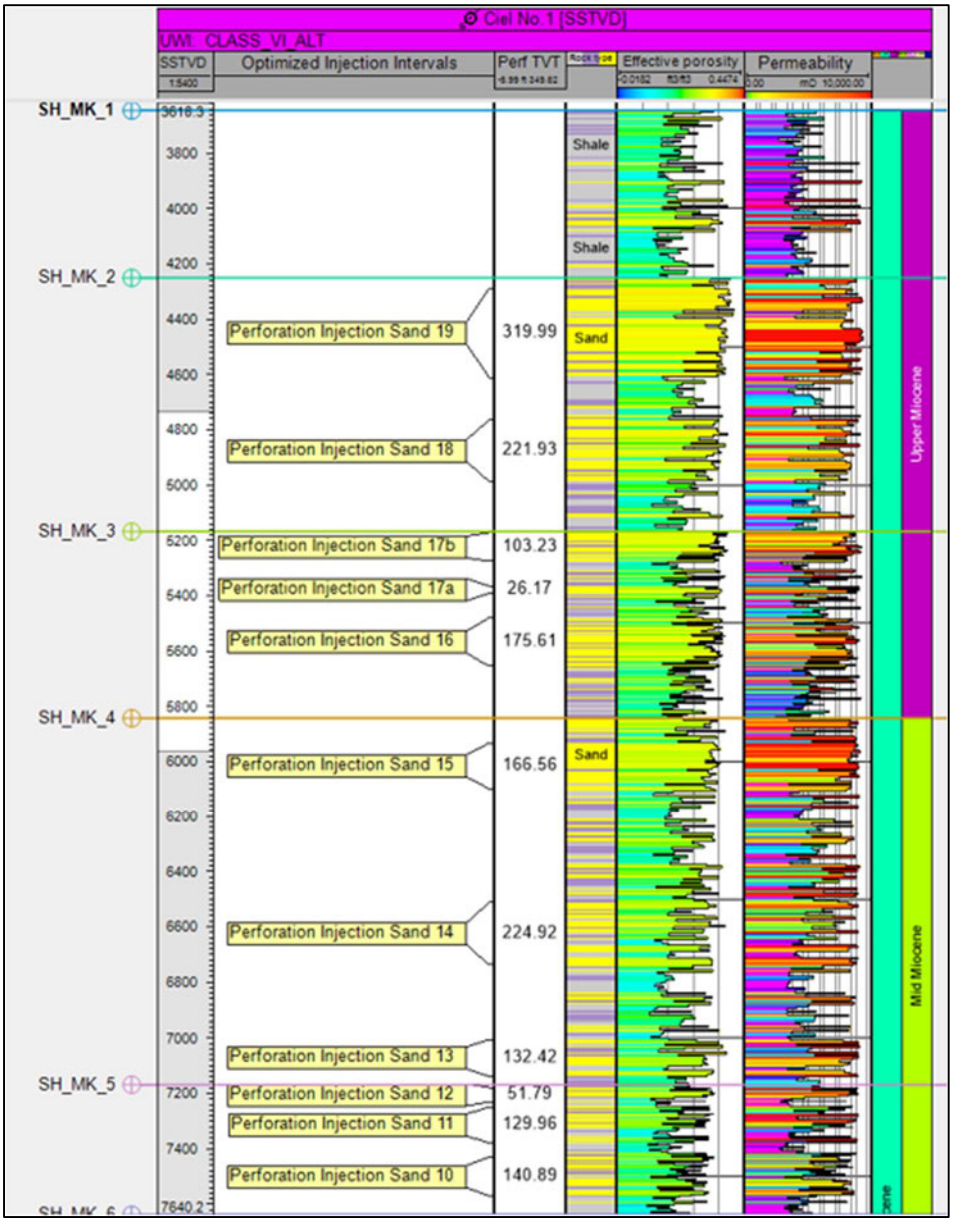
Ciel No.1 [SSTVD]
UWI: CLASS_VI_ALT
SSTVD
Optimized Injection Intervals
Perf TVT
Effective porosity
Permeability
SH_MK_1
SH_MK_2
SH_MK_3
SH_MK_4
SH_MK_5
Perforation Injection Sand 19
319.99
Perforation Injection Sand 18
221.93
Perforation Injection Sand 17b
103.23
Perforation Injection Sand 17a
26.17
Perforation Injection Sand 16
175.61
Perforation Injection Sand 15
166.56
Perforation Injection Sand 14
224.92
Perforation Injection Sand 13
132.42
Perforation Injection Sand 12
51.79
Perforation Injection Sand 11
129.96
Perforation Injection Sand 10
140.89
Shale
Sand
Upper Miocene
Mid Miocene

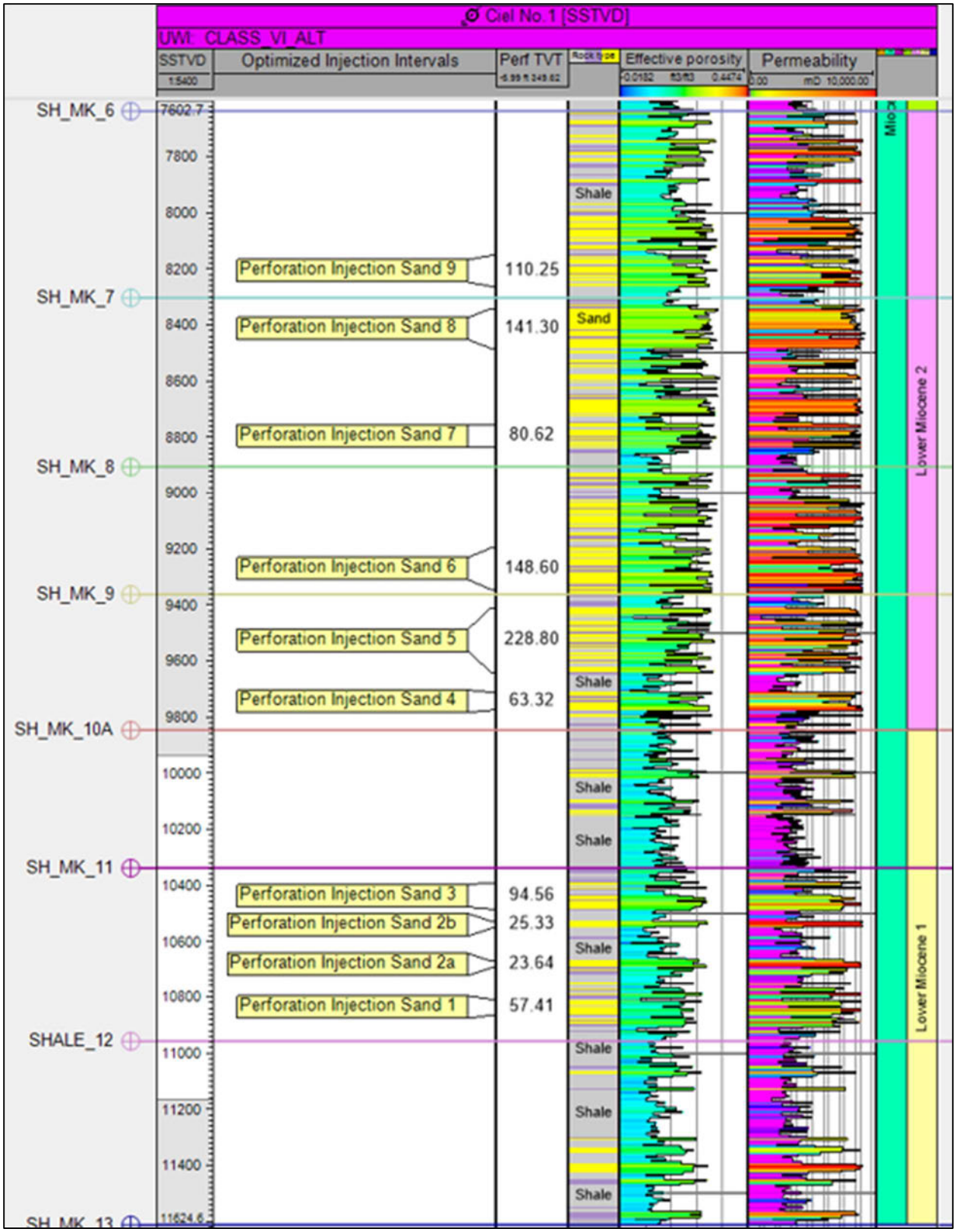

Figure 1-35. Injection well Ciel No.1, showing the 19 injection zones that were selected based on porosity and permeability values, displayed in the adjacent tracks.

Table 1-2. Petrophysical properties of the individual injection zones.

Injection Interval	Top Perforation in Feet	Base Perforation in Feet	Thickness in Feet	Average Effective Porosity	Average Permeability
Sand 19	4,331	4,651	320	35%	822
Sand 18	4,806	5,027	222	31%	361
Sand 17b	5,213	5,317	103	33%	571
Sand 17a	5,406	5,432	26	33%	735
Sand 16	5,521	5,696	176	32%	398
Sand 15	5,984	6,140	167	32%	716
Sand 14	6,554	6,779	225	26%	319
Sand 13	7,047	7,179	132	27%	496
Sand 12	7,220	7,272	52	26%	479
Sand 11	7,290	7,420	130	23%	356
Sand 10	7,471	7,612	141	24%	181
Sand 9	8,194	8,304	110	26%	376
Sand 8	8,383	8,525	141	29%	589
Sand 7	8,795	8,876	81	24%	447
Sand 6	9,265	9,387	149	26%	601
Sand 5	9,453	9,681	229	23%	341
Sand 4	9,753	9,817	63	25%	454
Sand 3	10,431	10,526	95	22%	227
Sand 2b	10,569	10,594	25	25%	815
Sand 2a	10,711	10,735	24	25%	781
Sand 1	10,849	10,907	57	20%	283

To better reflect the porosities within the targeted injection zones, the values shown in **Figure 1-36** are extracted from the facies within the geocellular model deemed sand facies. Within the gross injection interval, porosities range from 0% to 43%, with an average effective porosity of 23%. The lower-porosity zones within this range are likely shales within the model. **Figure 1-36** presents the histogram displaying these distributions. These high values reflect low cementation and compaction that correlate with the lack of depth, pressure, and temperature.

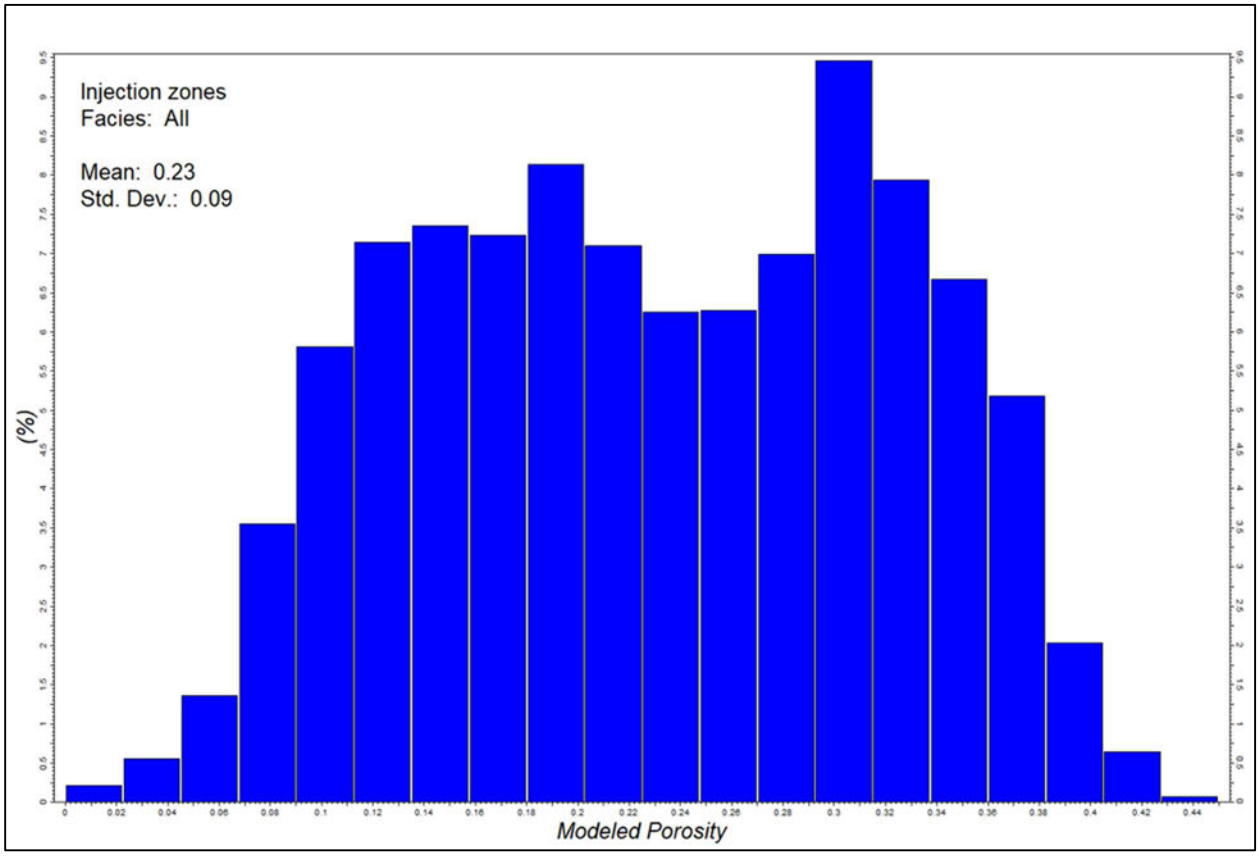

Figure 1-36. Histogram of porosity distribution within the injection interval.

Within the injection interval, permeabilities range from 0.0005 to 4,510.74 mD, and the average for the sand facies is 328.28 mD. **Figure 1-37** presents the histograms displaying these distributions. With the wide-ranging permeabilities within the injection interval, vertical permeability/horizontal permeability (Kv/Kh) will also vary. The ratio trend correlates directly with porosity (as does permeability) and increases with increasing porosity. A geocellular model was built on the relationship between the porosity/permeability distribution within offset wells and 3D seismic acquired over the project area.

The models will be updated with the newly acquired porosity and permeability data when the stratigraphic test well (Soliel No.1) and injection well (Ciel No.1) are drilled.

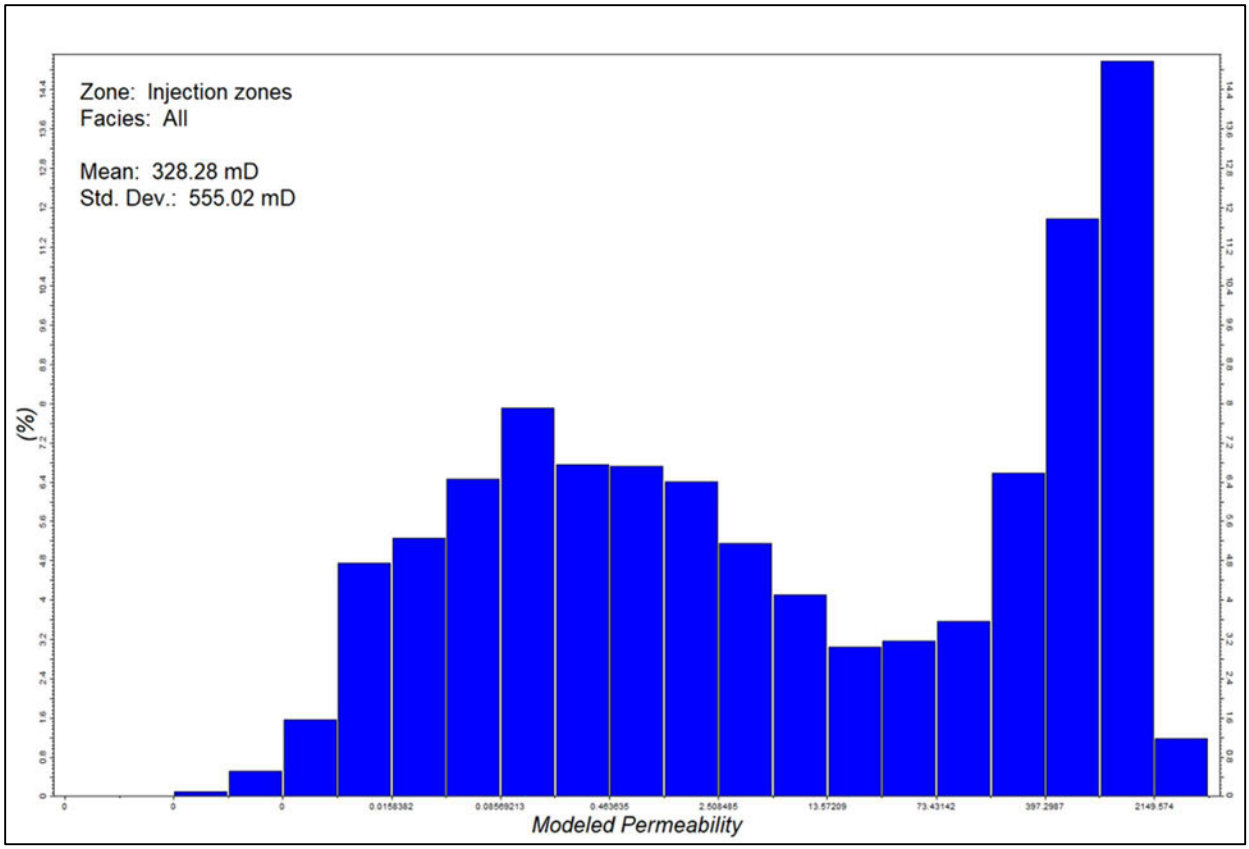

Figure 1-37. Histogram of permeability distribution within the injection interval.

Within the injection interval, the average effective porosity for sand facies is 32%. **Figure 1-38** presents the histograms displaying the porosity distributions in the sand facies.

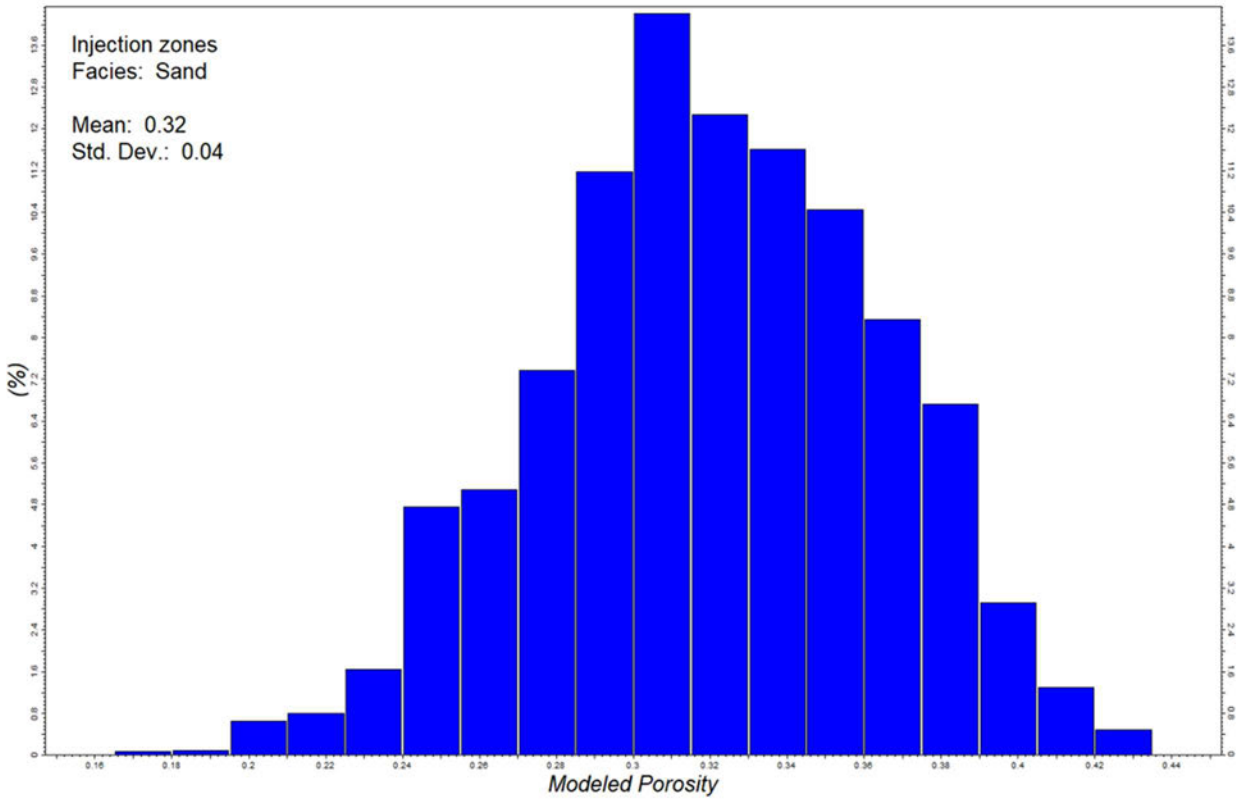

Figure 1-38. Histogram of sand facies porosity distribution within the injection interval.

Within the injection interval, the average permeability for sand facies is 814.65 mD. **Figure 1-39** presents the histograms displaying the distribution of permeability in the sand facies.

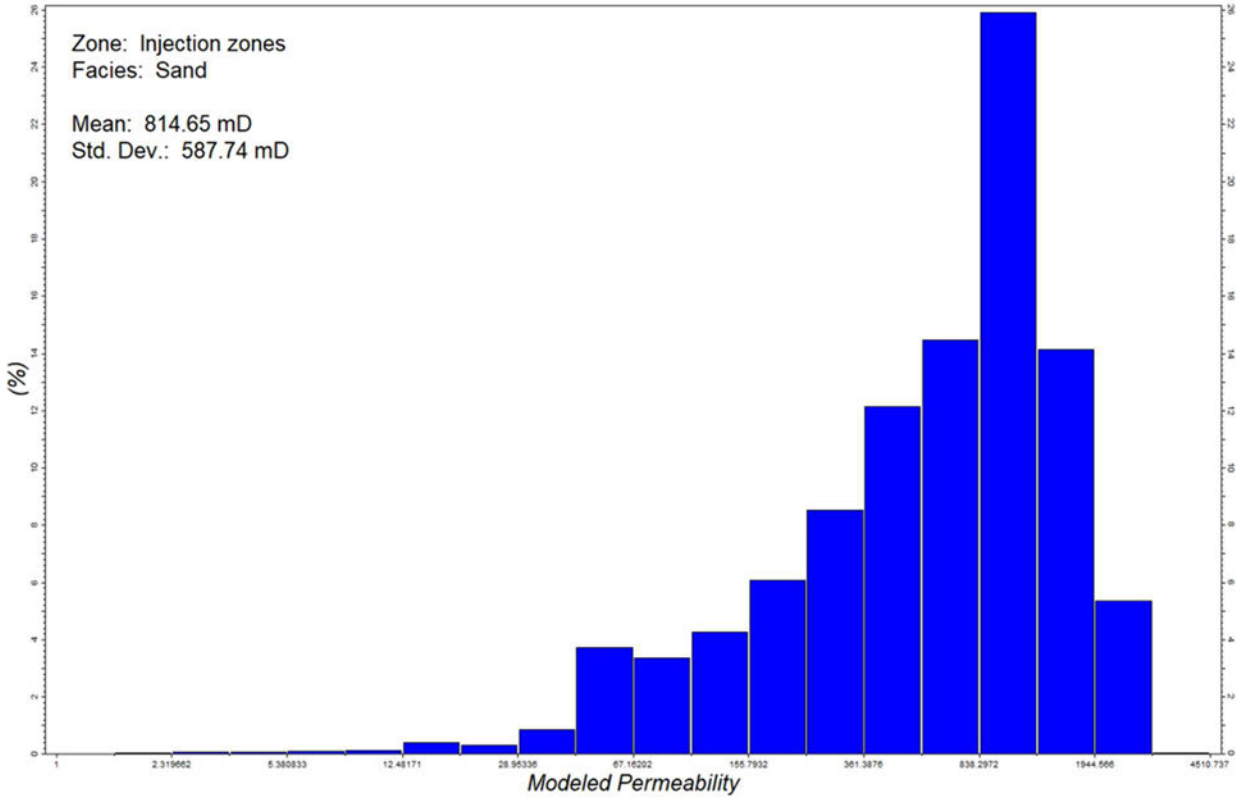

Figure 1-39. Histogram of sand facies permeability distribution within the injection interval

Core does not currently exist in the Miocene at the site. It will be collected as part of the site characterization well and provide measurements to calibrate the current petrophysical evaluation (porosity and permeability), and mineralogy.

Primary Upper Confining Zone: Upper Miocene

The Upper Miocene upper confining unit consists primarily of silt and clay with a few interbedded sands that were deposited on an alluvial coastal plain. **Figure 1-40** is an openhole log showing the upper confining zone in the Dugas & LeBlanc No. 1 (API 170072027500) and C. Schexnayder etal No. 1 (API 17005202650) wells. At the uppermost portion of the Miocene is a shale that is the primary confining unit, with the overlying shales in the Pliocene acting as additional baffles. The clay content found in these units agrees with a study that determined the clay-rich Miocene mudrocks have adequate capacity for CO_2 confinement because the clay-rich mudstone has small pore throats (Lu et al., 2011). High silt and clay content can also be seen above the upper confining unit in the offset log, which acts as a secondary source of confinement above the primary confining zone. These qualities support the upper Miocene as the optimal

confining zone for the injection interval. **Figure 1-41** is an openhole log image of the Schexnayder; J RC SU well (17-005-2031600), showing effective porosity and permeability. Shale Mrk 2 represents the top shale layer directly above the first injection zone. This layer displays very low effective porosity and permeability and will act as the primary confining layer within the upper confining unit. Two highly porous and permeable channel sands above SH_MK_2 are in the gross confining zone. Low permeability and porosity shale layers above and below the sands will isolate them from the injection zone.

Figure 1-40. Openhole logs of offset wells Dugas & LeBlanc 1 (API 170072027500) and C. Schexnayder etal. No.1 (API 17005202650) depicting the upper primary and secondary confining zones. Ciel No.1 is located between the other two wells.

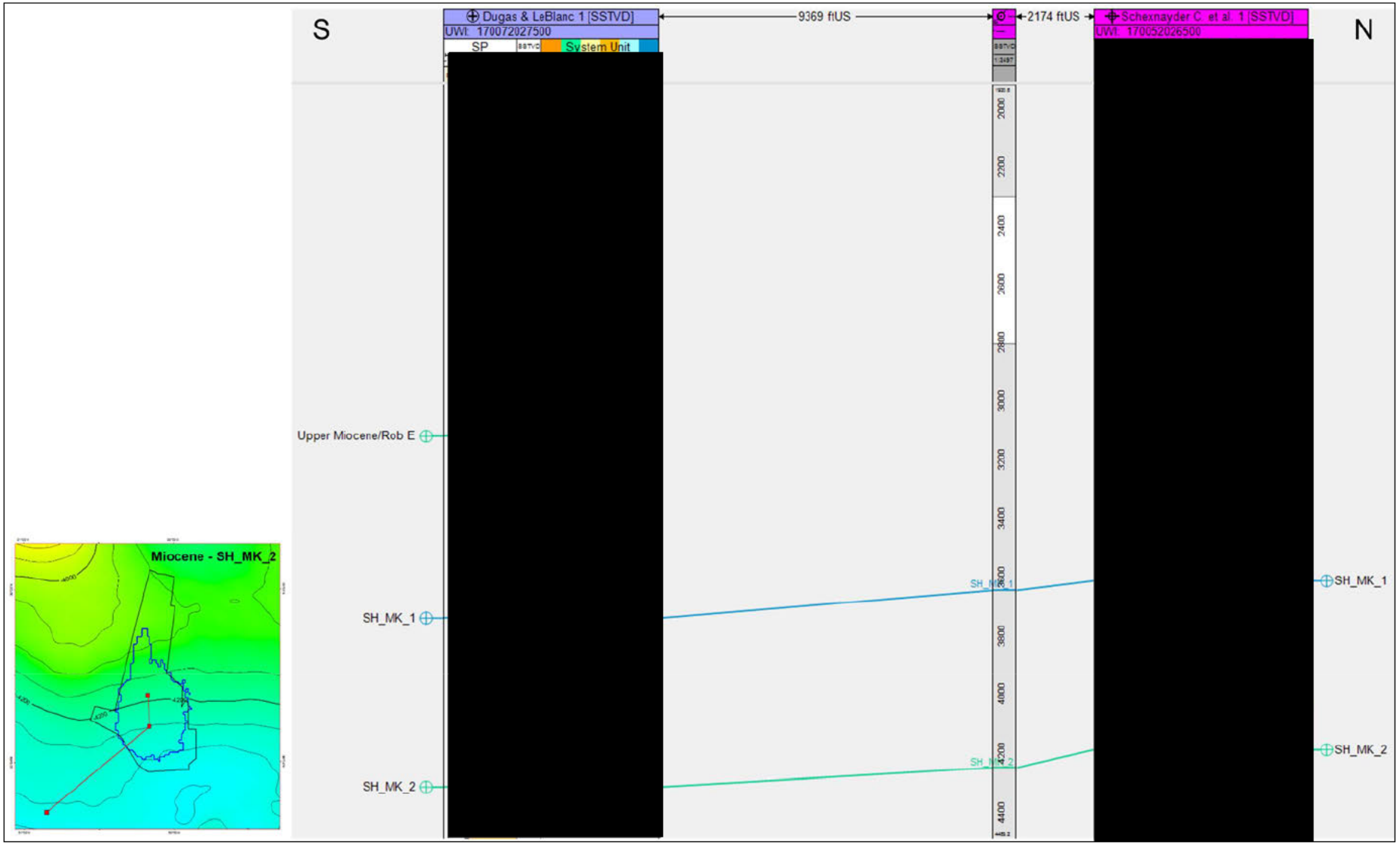

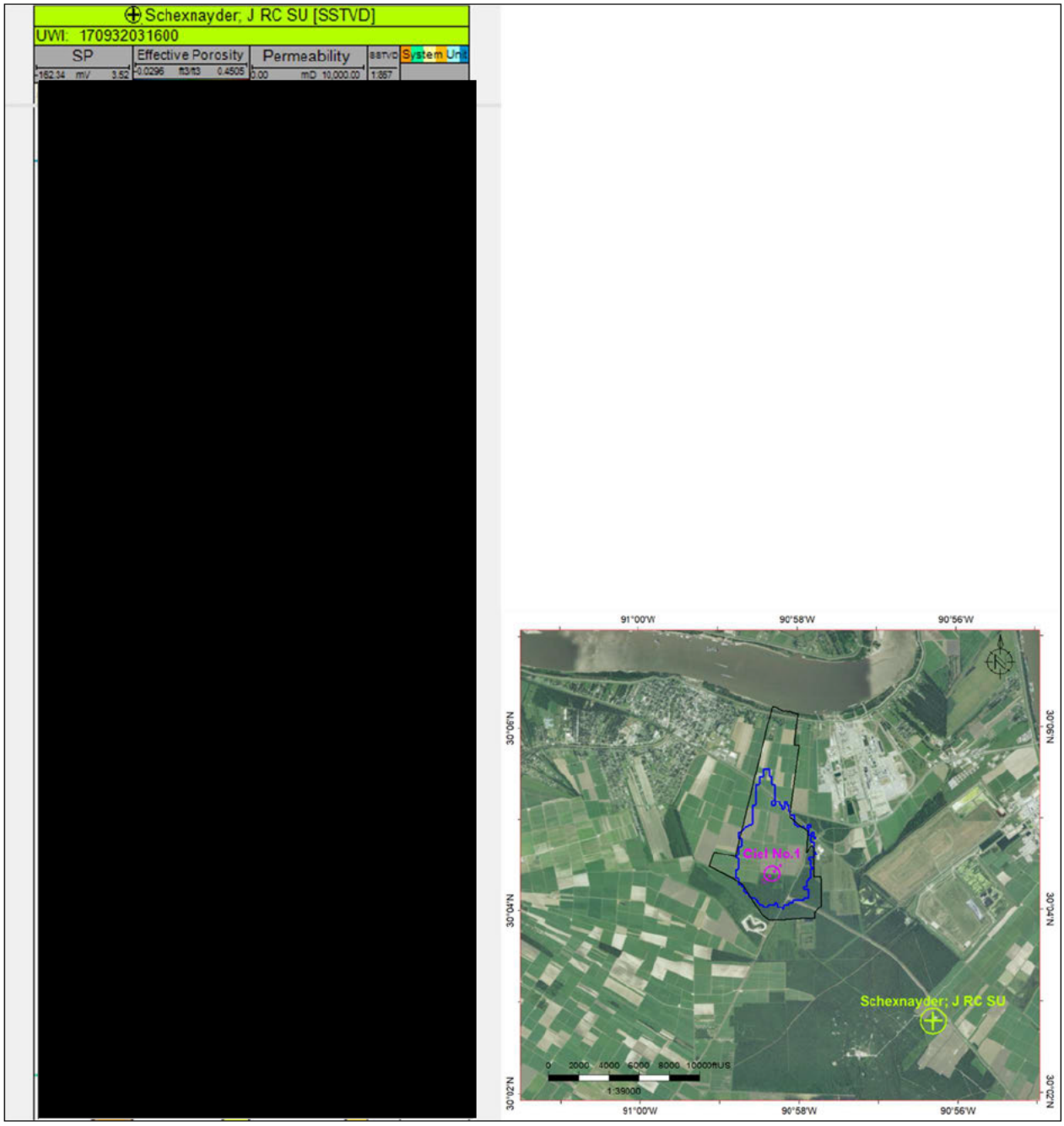

Figure 1-41. C. Schexnayder, etal No.1; J RC SU well (170932031600) showing effective porosity and permeability for the upper confining zone.

The confining features described previously were recently validated in a study by Bump et al. (2023), demonstrating the advantages of having a "composite confining system" for optimal CO_2 sequestration. This study, conducted in a similar depositional environment to the Donaldsonville

sequestration site in southern Louisiana, concluded, "permanent storage may be better served by composite confinement than by classic petroleum seals" (Bump et al., 2023). Even without a continuous seal, the CO_2 spreads laterally beneath the capillary barriers, leading to significant residual trapping that attenuates and ultimately immobilizes the CO_2 (Bump et al., 2023). This study identifies very similar features in the upper confining unit along with strata above the upper confining unit, further validating the confining nature of this zone.

The primary confining layer above SH_MK_2 has a range of porosity from 7% to 42% with an average effective porosity of 21% in the shale. These higher ranges most likely reflect thin sandy layers within this shale unit. As seen in **Figure 1-41** there will be approximately 585 feet of net shale with less than 15% porosity at the proposed Ciel No.1. The effective porosity distribution within the upper confining zone is shown in the histogram in **Figure 1-42**.

The permeability range is from 0 mD to 3,972 mD with an average permeability of 324 mD and an average of 1.75 mD within the shales. These higher ranges represent very thin layers of discontinuous sand within the unit that will not affect confinement. **Figure 1-43** presents the histograms displaying modeled permeability distribution within this upper confining zone.

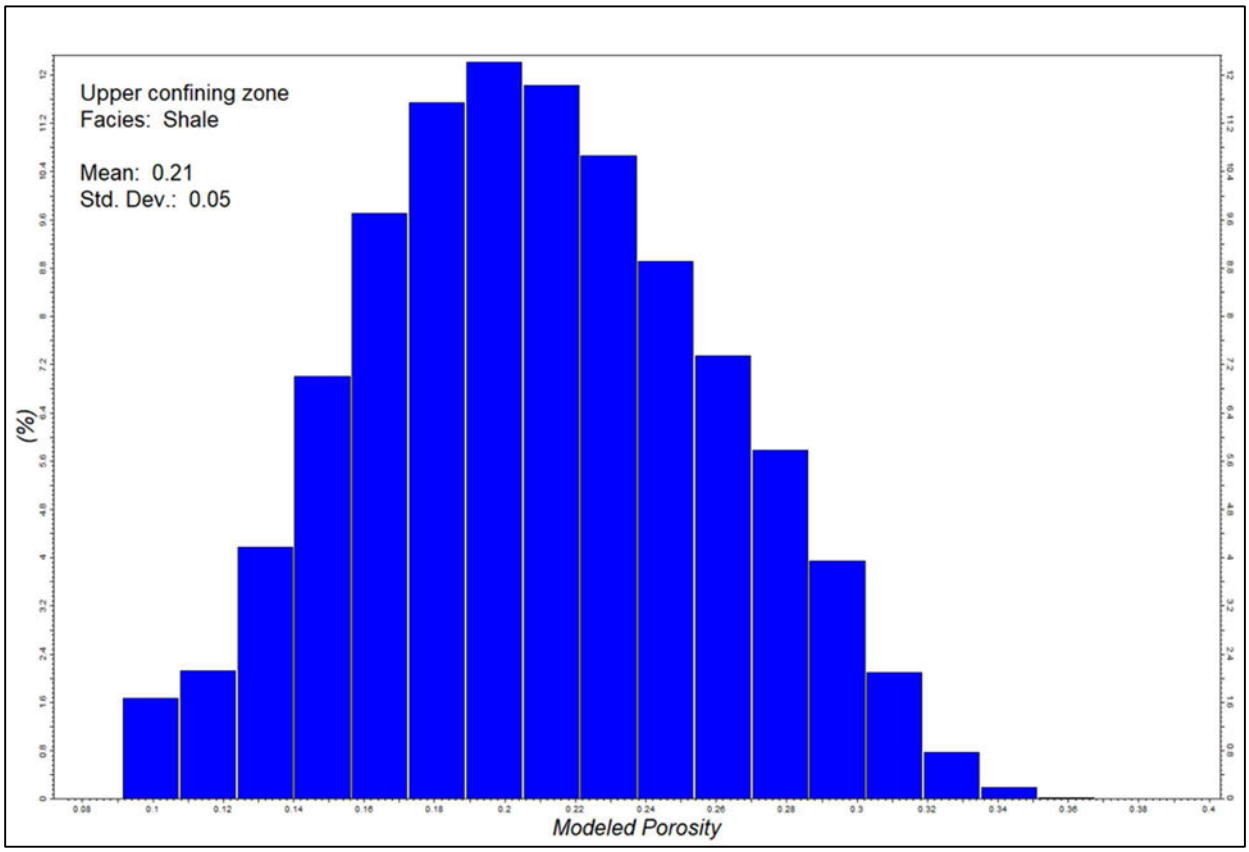

Figure 1-42. Distribution of modeled effective porosity for the shale facies of the upper confining zone.

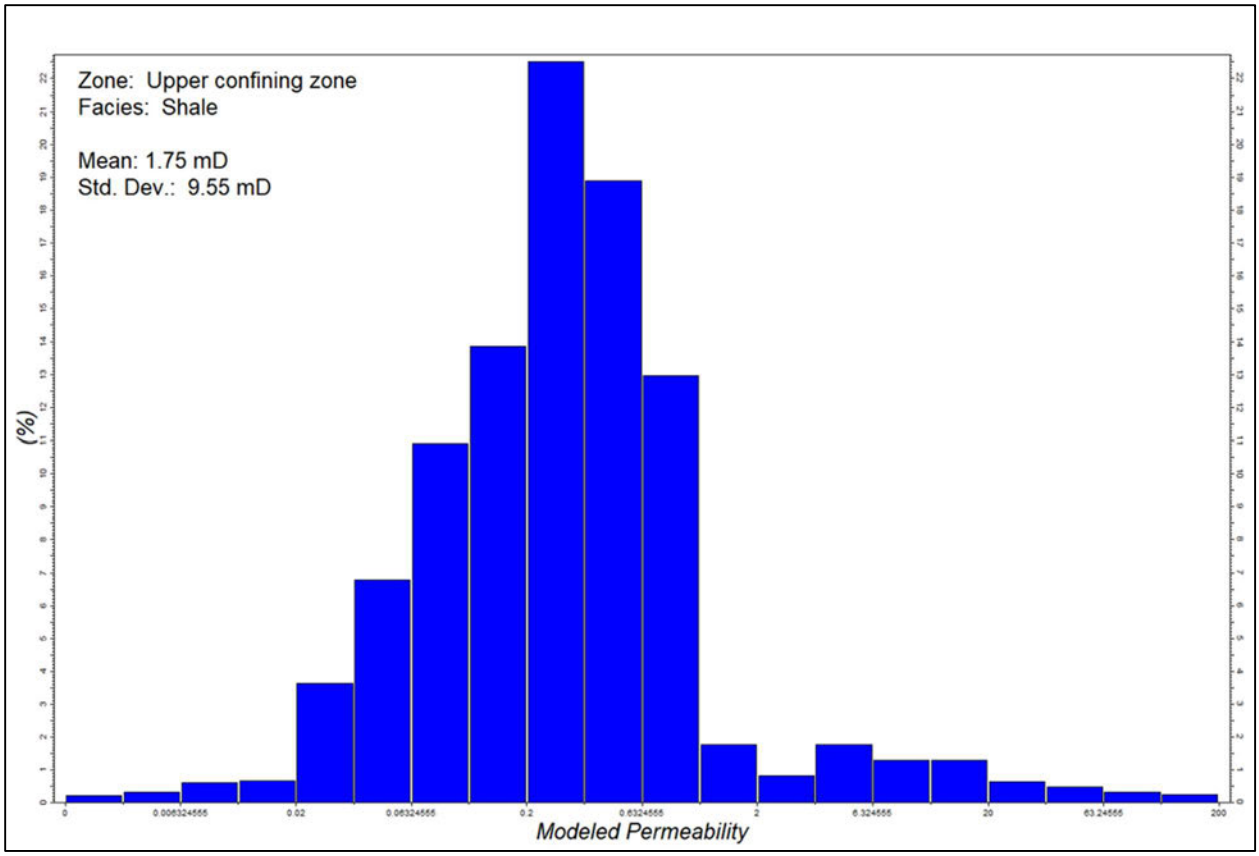

Figure 1-43. Histogram showing modeled permeability distribution for the shale facies of the upper confining zone.

Core is not available in the Upper Miocene near the Donaldsonville site. It will be collected as part of the site characterization well and provide measurements to calibrate the current petrophysical evaluation (porosity and permeability), mineralogy, and confining capacity from MICP.

The structure map of the top of the upper confining zone and the thickness map of the upper confining zone are shown in **Figure1-44** and **Figure 1-45**, respectively.

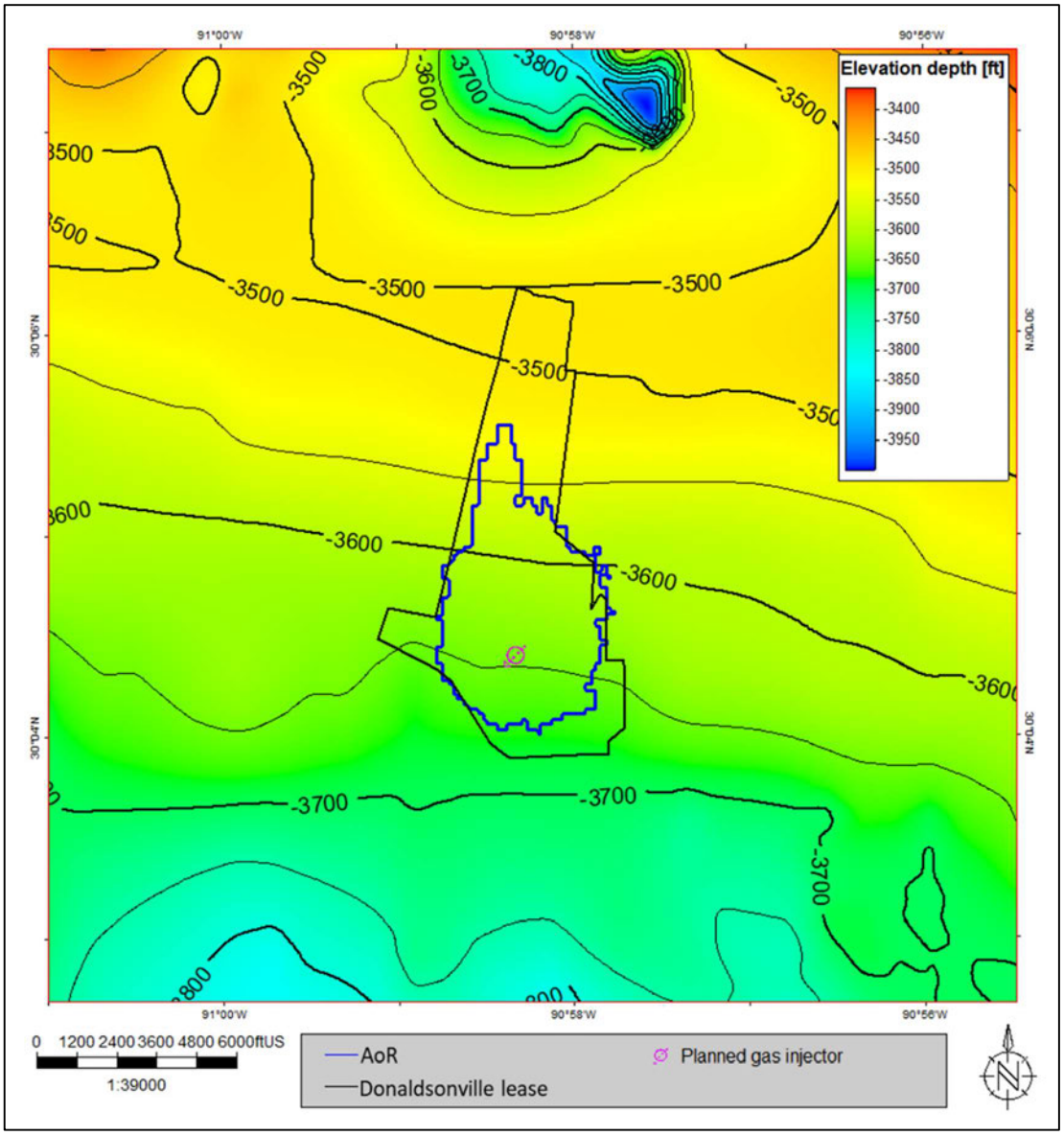

Figure 1-44. Structure map of the top of the upper confining zone.

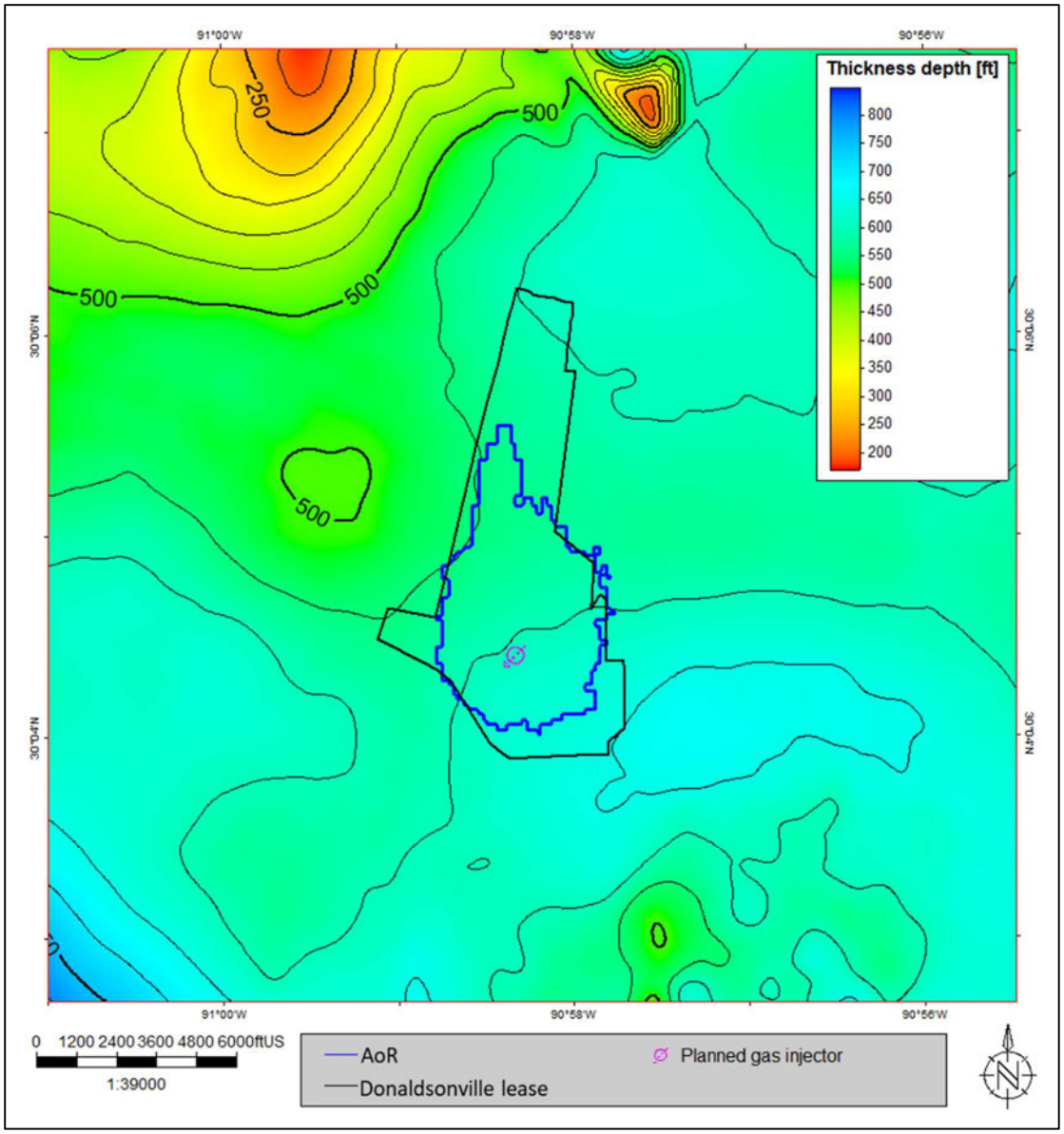

Figure 1-45. Thickness map of the upper confining zone.

Geomechanical and Petrophysical Information [40 CFR 146.82(a)(3)(iv)]

1.5.2 Petrophysics

Petrophysics is used to understand data from the field to evaluate geologic and reservoir components of the formations. Specifically in this study, petrophysics is used to understand the porosity and permeability of the zones of interest. The data used for this study are various wells logs that were acquired at the time of openhole logging, shortly after the well was drilled. These logs include, but are not limited to, spontaneous potential (SP), resistivity (ILD), gamma ray (GR), bulk density (RHOB), neutron porosity (NPHI), and compressional slowness (DT).

The first objective was to search the area for wells with digital logs of the correct depth and thickness and that had a minimum set of logs for evaluation. Initially, 10 wells were found to meet the criteria mentioned above, and the logs were loaded for processing. The log curves were edited and cleaned up for consistency. SPs were adjusted for drift, GRs were normalized, and all curves were edited for washouts and anomalies.

After the logs were edited for processing, a shale volume (VSH) was calculated using GR and SP to characterize the layering of sands and shales. VSH_GR and VSH_SP were used to make a combined VSH_FINAL. Rock classes were calculated through a neural network (a heterogeneous rock analysis, HRA, method) using VSH_FINAL to provide inputs for subsequent propagation of sand and shale facies throughout the geocellular model (**Figure 1-46**).

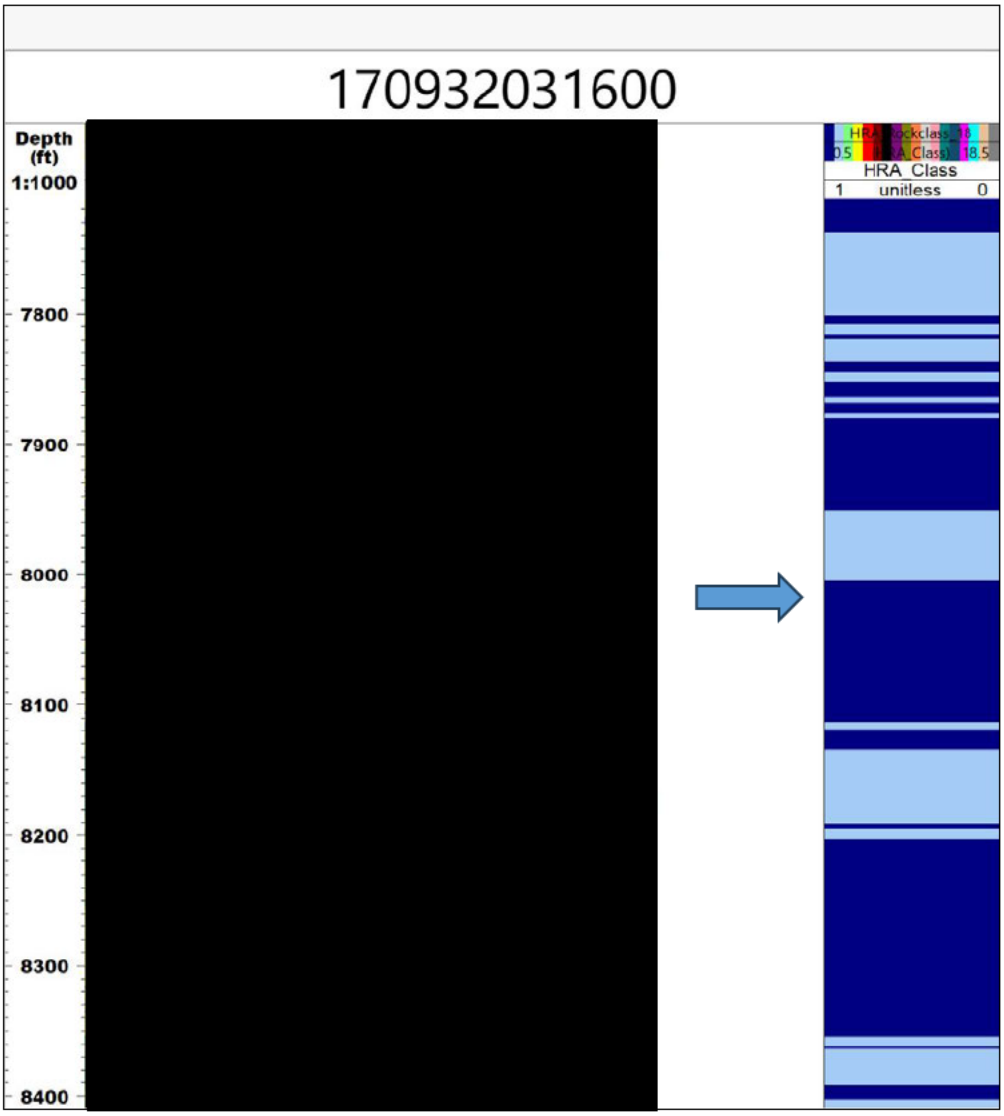

Figure 1-46. Schematic, showing the calculation of rock classes from GR volume of shale and SP volume of shale.

Porosity and permeability were processed, using eight of the ten logs, as the other two were not considered due to insufficient information in the wells. The Quanti.ELAN™ multicomponent inversion solver inside the Techlog™ software suite was used for processing porosity and permeability. The Techlog Quanti.Elan solver is a mineralogical inversion application that provides quantitative formation evaluation of openhole logs, level by level. The evaluation was accomplished by optimizing simultaneous equations describing one or more interpretation models. Input into these models were the digital logs for the area (RHOB, DT, NPHI, GR, ILD, etc.). With the inputs and defined endpoints for determining the chosen minerals, the Quanti.ELAN solver generated the outputs of porosities, permeabilities, and mineral volumes estimates (**Figure 1-47**).

Total and effective porosity were both calculated as part of the processing. Total porosity (PIGT_QE) is total pore space associated with the rock and includes all pore spaces. Effective porosity (PIGN_QE) is defined as the total pore space minus the pore space associated with the clay (clay-bound porosity). Permeability (KINT_GEO_QE) is derived from Herron's equation using total porosity and the calculated mineral volumes (Herron, 1987).

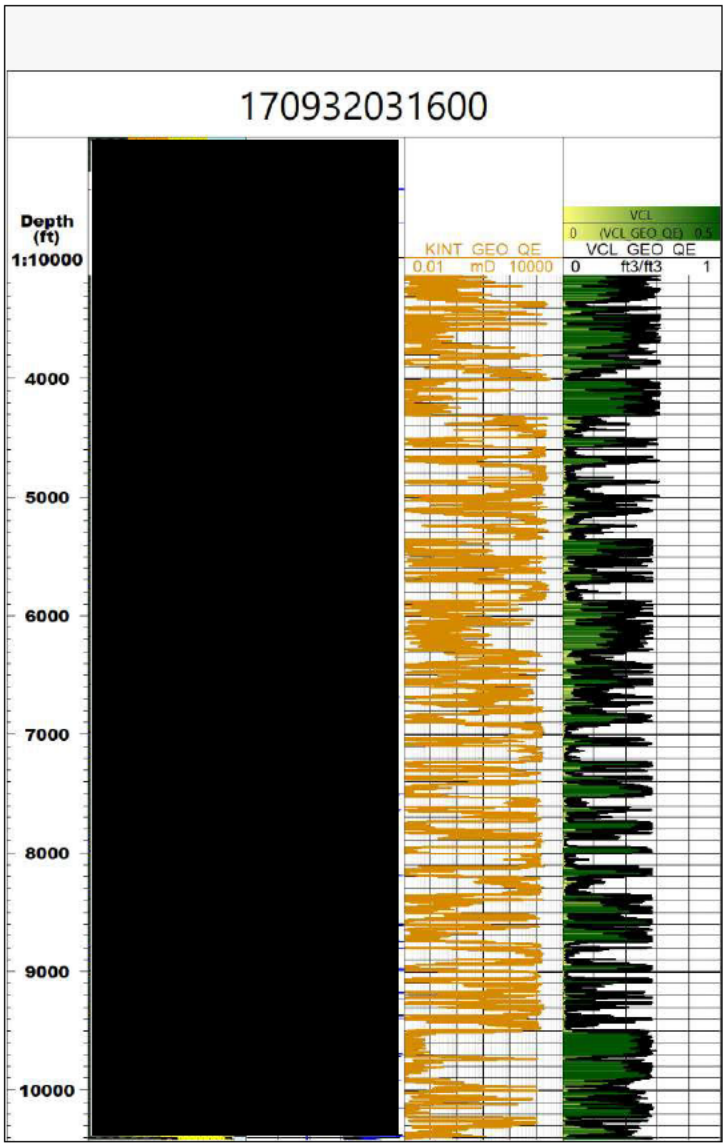

Figure 1-47. Outputs of mineralogy, porosity, permeability, and clay volume from the Quanti.ELAN solver.

1.5.3 Geomechanics

The method used to determine the geomechanics characteristics is through building a 1D mechanical earth model (MEM). A MEM provides information about mechanical behavior and strength by using relationships between rock properties, induced deformations, and subsurface

conditions. A MEM is a repository of data—models and measurements—representing the mechanical properties of rocks, stresses, pressures, and temperatures acting on them at depth. It may represent a snapshot at a time of interest, i.e., it may track how conditions evolve as the reservoir is being produced or undergoing injection. At this project stage, no rock geomechanics core analysis was conducted to determine the rock properties for the confining and injection zones, and no stress tests were performed. Therefore, the 1D MEM is based on empirical correlations founded on nearby offset well logs and data. The geomechanical model (MEM) will be fully updated with openhole logs and core data acquired from the Class V stratigraphic well, Soleil No.1.

Fracture Gradient

Class VI requirements are that injection pressure shall not exceed 90% of the fracture pressure of the injection interval. The fracture gradient can be derived by conducting fracturing tests such as a diagnostic formation integrity test (DFIT), extended leakoff test (XLOT) or minifrac test or it can be assessed with wellbore information such as downhole losses and leakoff tests (LOT). The available data to constrain the fracture gradient is a LOT performed in the confining zone (API 170052022000, well name Melancon William J) with a pressure of 2384.9 psi. The estimated fracture gradient is 2337.05 psi, 2% lower than the leakoff pressure. Usually, the LOT is higher than the minimum horizontal stress, which is referred to as the fracture gradient in this report.

Without direct measurements, an analytically based estimate of the fracture gradient was considered using a conservative approach for permitting purposes. Fundamentally, the Louisiana Gulf Coast is not a tectonically or seismically active region. Therefore, the simplified poroelastic equation (Thiercelin and Plumb, 1994) can estimate the fracture gradient in a tectonically relaxed area as part of the standard MEM procedures. This method is equivalent to Eaton's method (Eaton, 1969), assuming a Biot coefficient equal to 1 and no additional tectonic stress. Both equations are a function of the vertical stress, pore pressure, and Poisson's ratio. The estimated fracture gradient profile is consistent with the available LOT. The simplified poroelastic equation is defined below:

$$\sigma_h = \frac{\nu}{1-\nu}\sigma_V - \frac{\nu}{1-\nu}\alpha P_p + \alpha P_p \qquad \text{Equation 1.1}$$

where

ν = Poisson's ratio

σ_h = Minimum horizontal stress or fracture gradient

σ_v = Vertical stress (~ 0.93 psi/ft)

α = Biot coefficient (equal to 1)

P = pore pressure (0.465 psi/ft)

An average fracture gradient of 0.75 psi/ft is estimated in the injection interval and 0.77 psi/ft in the upper confining zone. These gradients are valid only in the normal pore pressure regime interval with an estimated formation pressure gradient of 0.465 psi/ft. Formations with higher pore pressure gradients may induce a higher fracture gradient. The fracture gradient uncertainty is approximately ±0.04 psi/ft in both formations.

Rock Strength Analysis of the Confining Zone

The rock strength is described based on the estimation of the unconfined compressive strength (UCS) that describes the amount of uniaxial stress that a rock can experience before shear failure occurs (i.e., the UCS is a reference to the resistance just prior to failure). In the absence of core analysis, the published correlation from Horsrud (2001) was used to calculate this parameter from rock deformation properties (compressional slowness measurements). The average rock strength in the confining and injection zones are 2,287 and 2,472 psi, with a standard deviation of 987 and 1,438 psi, respectively.

Ductility Analysis of the Confining Zone

The brittleness index (BRI) of the Donaldsonville sequestration site is the property used to describe the brittle-ductile behavior of the confining zone. Ductility refers to the rock's capacity to anneal any discontinuities and avoid open-dilatant fractures during subsurface deformation, thus representing a leak risk assessment. The ductility decreases as compressive strength increases. Within the studied area, four offset wells have compressional sonic data over the confining zone to calculate ductility and UCS.

Ductility calculations were performed based on the methodology from Ingram and Urai (1999) and the ductility of the confining layer(s) was calculated using the BRI. The BRI is determined by comparing the log-derived UCS against an empirically derived UCS_{NC} for a normally consolidated (NC) rock.

$$UCS_{NC} = 0.5\,\sigma_V - 0.5\,P_p \qquad \text{Equation 1.2}$$

$$BRI = \frac{UCS}{UCS_{NC}} \qquad \text{Equation 1.3}$$

where

UCS = Unconfined compressive strength

UCS_{NC} = Unconfined compressive strength of a normally consolidated rock in non-overpressure domain

σ_v = Vertical stress (~ 0.93 psi/ft)

P = pore pressure (0.465 psi/ft)

BRI = Brittleness index (unitless)

The UCS is computed based on compressional velocity (Horsrud, 2001). The UCS_{NC} is the UCS for a normally consolidated rock, defined by the equation above. BRI is the calculated brittleness from the rock's UCS used to identify the potential risk of fractures acting as conduits for fluid migration.

At the Donaldsonville site, the shale brittleness calculation drops to less than two. If the value of BRI is less than two, empirical observation shows that the risk of embrittlement is lessened, and the confining layer is sufficiently ductile to anneal discontinuities. BRI lower than two confirms that the confining zone is potentially a ductile confining layer. The average ductility of the upper confining zone based on data from four offset wells is 1.42, with a standard deviation of 0.458.

Due to the ductility analysis, there is a potential insignificant risk of fractures that will act directly as conduits for fluid migration from the multiple injection zones. This provisional interpretation can be validated with laboratory core data combined with historical fluid and pressure containment from the study area. A higher UCS may induce a lack of ductility.

Recommended Fracture Gradient Test and Geomechanics Core Analysis

Step-rate tests (SRT), XLOTs, DFITs, or minifrac tests can be used to calibrate the estimated stress profile. After a stress data assessment, a more accurate value of the fracture gradient will be obtained. The value will be the input into the computation of the maximum injection pressure as per Class VI requirements and used in the AoR modeling and delineation.

The geomechanical properties, including the elastic properties and rock strength, can be measured in the laboratory in oriented plugs/cores using the unconfined compression test, triaxial compressional test, multistage triaxial compression test, and Brazilian/indirect tensile strength test, combined with ultrasonic velocity measurement. Core will be acquired for this purpose in the characterization well. The log-derived geomechanical properties will be updated and calibrated when such data are available.

1.6 Seismic History [40 CFR 146.82(a)(3)(v)]

The Louisiana Gulf Coast is not a tectonically or seismically active region, which accounts for the rarity of earthquakes near the proposed Ciel No.1. Since 1900, only two seismic events have been detected within 40 miles of the Ciel No.1 location. The nearest documented seismic event occurred 5.3 miles south-southwest from the proposed Ciel No.1 location, at a magnitude of 4.2 in 1930. The other seismic event was a magnitude 3.0 event in 2005 located 3.12 miles (16,404.2 feet) below the surface. The map shown in **Figure 1-48** depicts the region's historical, recorded seismic events. Information on seismic events in the area is available from the USGS earthquake map (https://earthquake.usgs.gov/earthquakes/map).

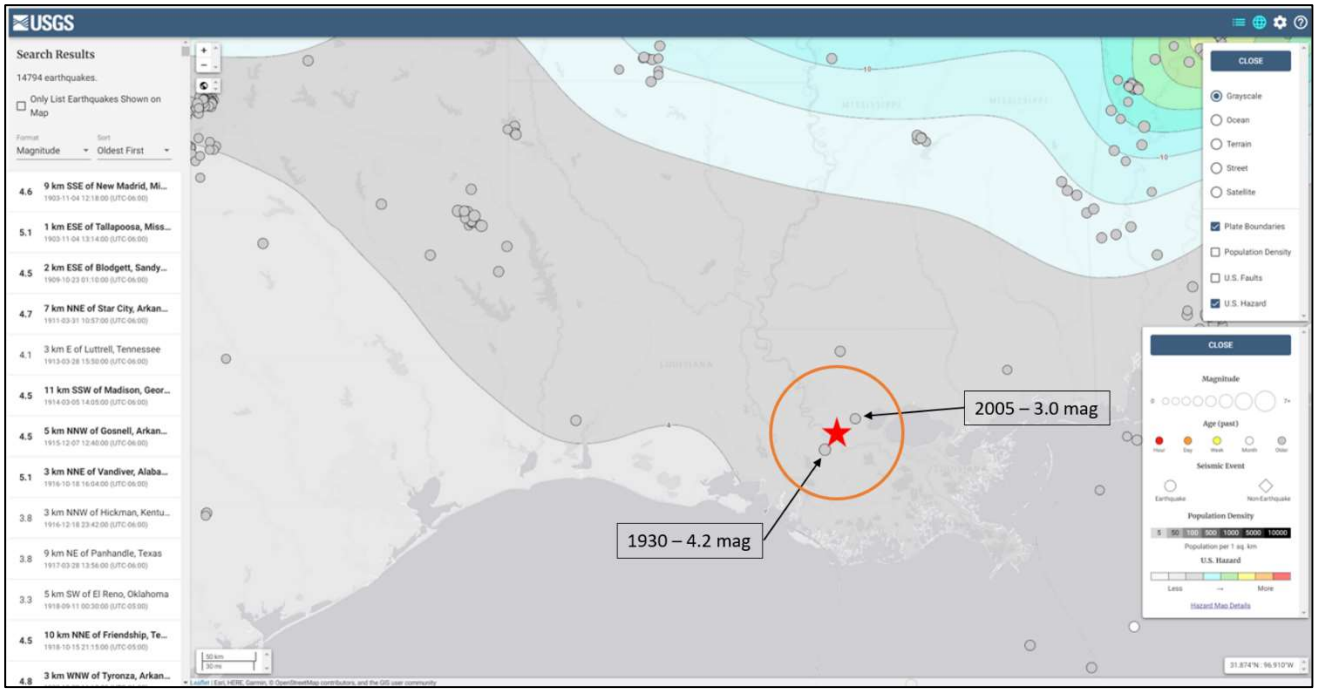

Figure 1-48. Map showing historical seismic event in the Louisiana Gulf Coast area. Map from the USGS shows two seismic events near Ciel No.1 (red star). The orange circle represents a 30-mile radius from Ciel No.1.

The USGS provides information on the location of the Gulf Coast monitoring stations (https://earthquake.usgs.gov/monitoring/operations/network.php?virtual_network=ANSS). The nearest seismic monitoring station (N4 545B) is approximately 29 miles to the southwest of the proposed Ciel No.1 (**Figure 1-49**). Additional detectors from the International Registry of Seismograph Stations (http:///www/isc.ac.uk/registries/) are located in the region for further data control.

As previously discussed, there is a low probability of induced seismicity during CO_2 injection in the Ciel No.1 as evidenced by historical seismicity and lack of faulting in the area. Furthermore, the nearest disposal well to the Ciel No.1 project site is more than 2.8 miles away, and there should be no risk of interference that would enhance the risk of induced seismicity.

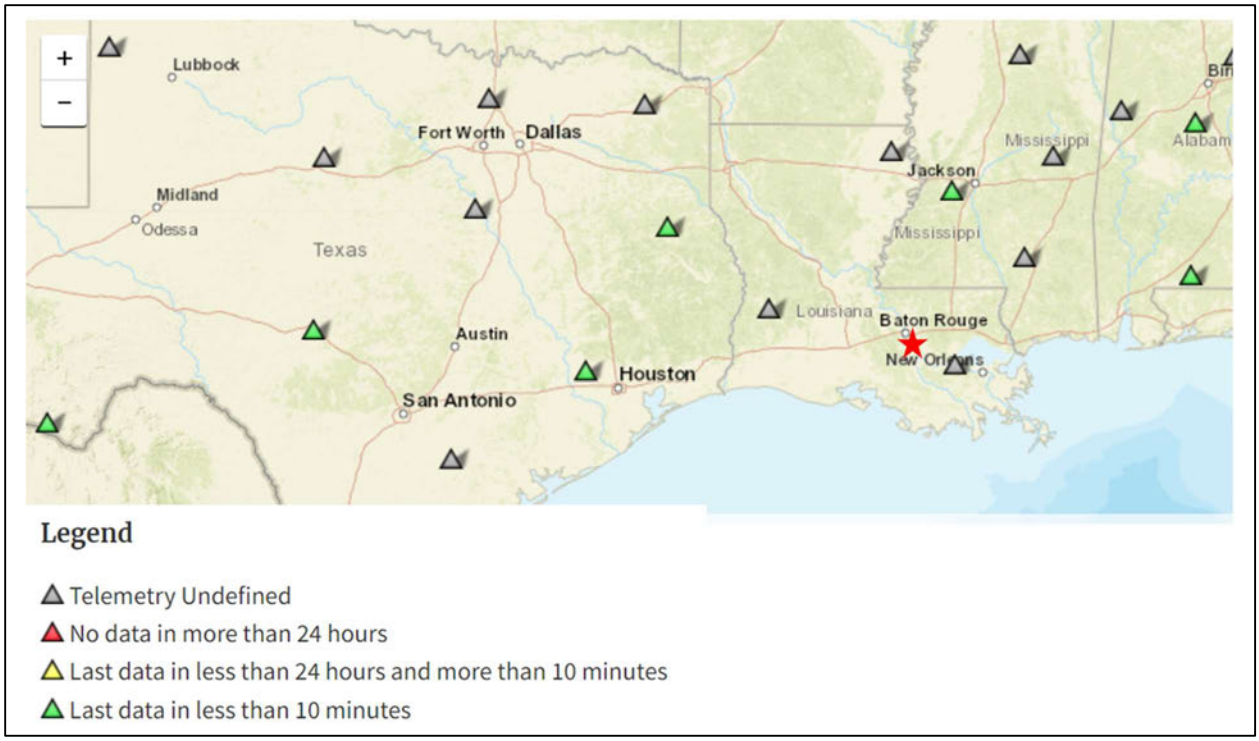

Figure 1-49. Location of the Gulf Coast monitoring stations. Map from the USGS shows closest monitoring station is 29 miles to the east-southeast of Ciel No.1 (located at the red star).

1.7 Hydrologic and Hydrogeologic Information [40 CFR 146.82(a)(3)(vi), 146.82(a)(5)]

The proposed Ciel No.1 injection well is located in Ascension Parish, which is wholly contained within the Mississippian River Alluvial Aquifer, as defined by the USGS and Department of Transportation and Development (DOTD) (**Figure 1-50**).

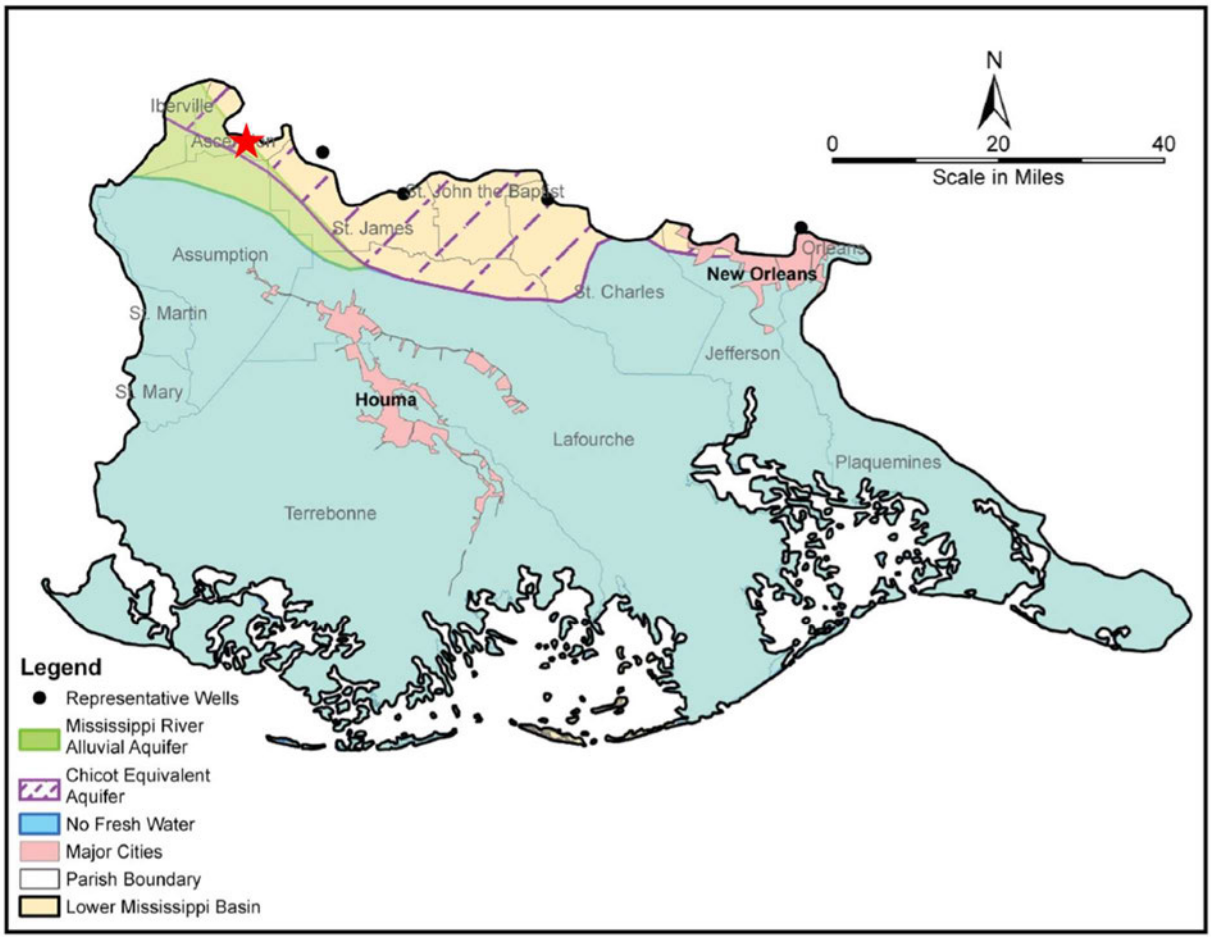

Figure 1-50. Map of the extents of major aquifers. The red star represents the location of the Donaldsonville injection site, which is located in the Mississippi River Alluvial Aquifer (Louisiana State Reservoir Priority and Development Program, 2009).

Figure 1-51 is a generalized cross section showing the hydrogeologic units present in the area. In descending stratigraphic order, these hydrogeologic units are the Mississippi River Alluvial Aquifer, and the Chicot Equivalent Aquifer. Water quality varies with depth and locality, though it is generally good in the northern part of the aquifer where total dissolved solids (TDS) are less than 500 mg/l. Areas of increased salinity along the Gulf Coast may be associated with saltwater intrusion in response to groundwater pumping intruding into the aquifer (Griffith, 2006).

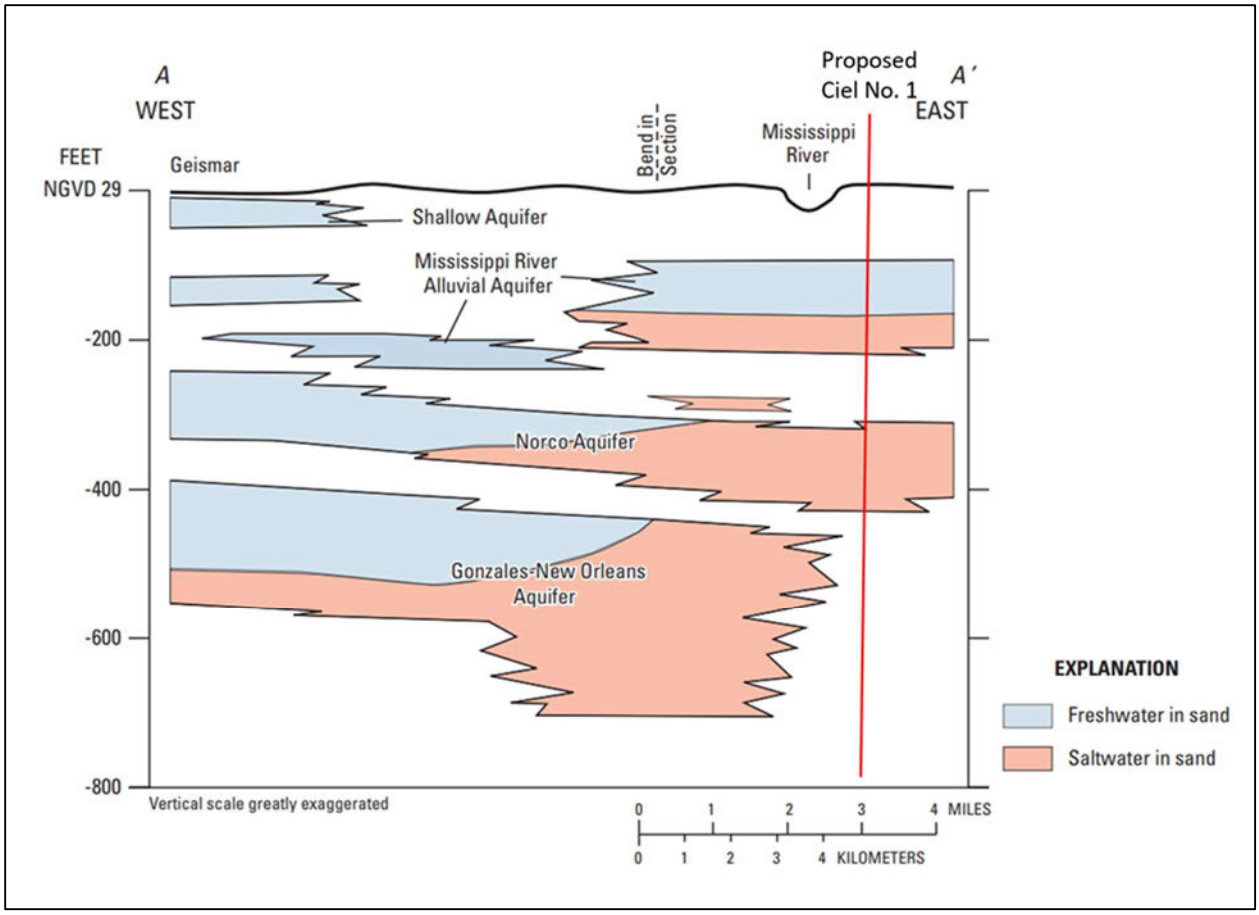

Figure 1-51. Map and cross section of the Ascension Parish aquifers with a red star and red line indicating the approximate location of the proposed Ciel No.1 (Griffith and Fendick, 2009).

Most of the groundwater in Ascension Parish is supplied by the Mississippi River Alluvial and Chicot-equivalent aquifers. The Quaternary-age Mississippi River Alluvial Aquifer consists of fining upward sequences of gravel, sand, silt, and clay (Mississippi River Alluvial Aquifer Summary Baseline Monitoring Project, FY 2002). The freshwater interval's thickness in the Mississippi River Alluvial Aquifer ranges from 50 to 500 feet and can be found 20 feet below sea level.

The Quaternary Chicot equivalent aquifer system is part of the Southern Hills Aquifer System. The Chicot equivalent aquifer system includes the Gramercy, Norco, and Gonzales-New Orleans aquifers and the 1,200-foot sand of the New Orleans aquifers (Louisiana Department of transportation and development, 2009).

Figure 1-52 illustrates the base of the USDW as identified by the Louisiana Department of Natural Resources UIC at a depth of 1,048 feet true vertical depth (TVD) at the Dugas-Leblanc No. 1 (API 170072027500). The well is 1.8 miles south-southwest of the proposed Ciel No.1.

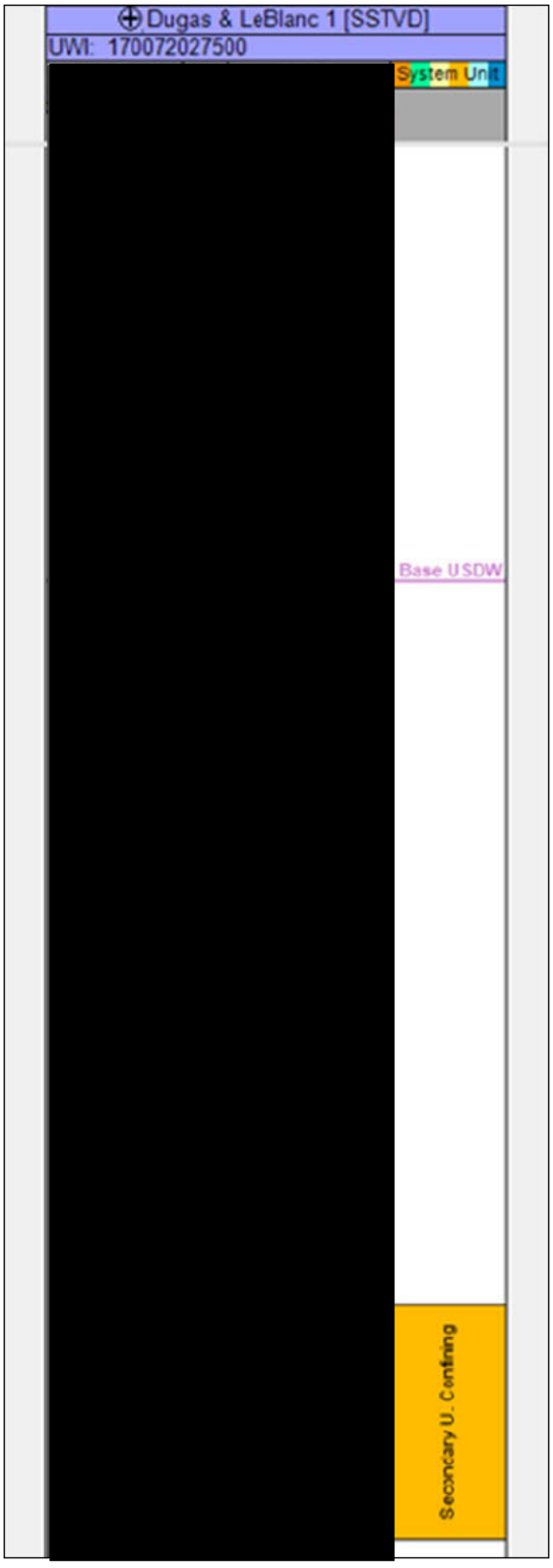

Figure 1-52. Well log for Dugas-Leblanc No. 1 (API 170072027500). The purple line represents base of USDW.

Geochemistry [40 CFR 146.82(a)(6)]

To estimate injection interval fluid conditions, seven Miocene-age sand fluid samples were identified within the USGS National Produced Waters Geochemical Database (Blondes et al., 2018). The locations of these selected wells are depicted on the map in **Figure 1-53**, along with their API and USGS ID numbers. The USGS ID number ties the wells from the map to the water chemistry data in **Table 1-3**.

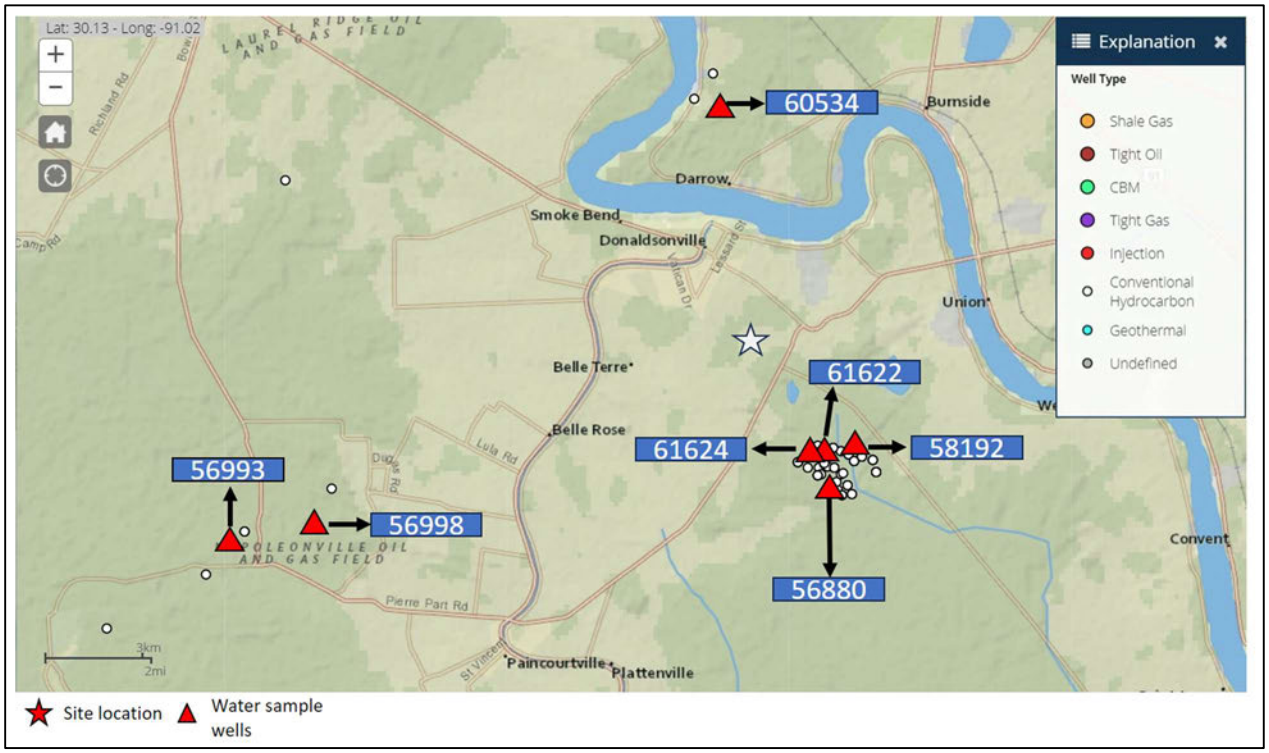

Figure 1-53. Map of selected wells from the USGS National Produced Waters Geochemical Database. Red triangles and associated USGS ID are wells close to the Ciel No.1 location (red star).

The closest sample to the proposed Ciel No.1 is from a well located approximately 2 miles southeast, and the farthest sample is just over 10 miles to the southwest. Sampling depths range from 3,453 feet to 10,894 feet. The TDS in these samples ranges from 119,886 to 189,385 milligrams per liter (mg/L) and averages 151,337 mg/L. According to these values, the anticipated salinity at the proposed injection interval depth for Ciel No.1 is greater than 100,000 mg/L. The remainder of the quantitative water chemistry data can be viewed **Table 1-3**.

These available water chemistry data show relatively consistent geochemical composition in the Miocene sands in this area. The formation waters are primarily Cl-Na type with moderate amounts of Ca, indicating a similar origin of the native pore waters, burial history, and diagenetic interactions with the formation rocks.

Table 1-3: Miocene water chemistry proximal to proposed Ciel No.1 injection well.

USGS ID	Perforation Interval (feet)	TDS	Ca	Cl	Fe Total (mg/L)	SO_4	Na	HCO_3	PH	SG	Distance from Injector Well	
		(mg/L)	(mg/L)	(mg/L)		(mg/L)	(mg/L)	(mg/L)			(feet)	(miles)
60534	3,453-3,456	165,424	2,897	87,854	-	1.09	51,341	136	6.1	1.09	47757	9.04489
61624	5,538-5,542	140,366	3,100	85,900	26	-	50,100	140	6.7	1.093	56528.2	10.7061
56993	6,755-6,758	136,625	2,814	83,627	26	44	48,813	117	7	1.098	24151.9	4.57422
58192	7,606-7,652	138,892	2,705	84,630	23	-	50,966	121	6.8	1.123	11005.4	2.08436
56880	8,531-8,543	189,385	332	78,246	6	98	50,130	204	6.9	1.095	10874	2.05947
56998	9,462-9,467	168,968	660	101,618	22	201	65,166	1,055	5.9	1.116	12498.3	2.3671
61622	10,882-10,894	119,886	5,530	72,900	300	442	40,200	139	5	1.081	14965.3	2.83434

1.8 Other Information (Including Surface Air and/or Soil Gas Data, if Applicable)

BKVerde will monitor surface air and soil gas per federal rule (40 CFR 146.9 (h)) and the Louisiana rule (LAC 43.XVII.3625.A.8, attached) to detect movement of CO_2 that could impact the USDW. If any CO_2 is emitted by surface leakage, BKVerde will report to the EPA. Further details about soil gas monitoring have been discussed in **Attachment D, Testing & Monitoring Plan.**

1.9 Site Suitability [40 CFR 146.83]

There are abundant shale streaks between the injection zones to limit the CO_2 migration into shallower injection zones. Most important is the fact that the CO_2 is contained in the injection interval. None rises to the confining zone because of the shale facies present at the top of the injection interval and the base of the confining zone.

The rock properties will be better classified after analyzing the data acquired during the characterization process. The injection zones will be selected to avoid high-permeability streaks and potential leakage pathways, preventing the injected CO_2 from entering thief zones that would direct carbon dioxide outside the injection zone.

The injected CO_2will remain in the proposed injection site due to the four trapping mechanisms expected in CO_2storage in aquifers: structural trapping of the CO_2, solubility of the CO_2in the saline aquifer, trapping of the CO_2as residual gas in the pore spaces, and trapping of CO_2in minerals by its reaction with the minerals in the reservoir rock. Simulation results show that 27.85% of the CO_2 will be dissolved in water, 12.61% will be mobile in gas phase, and 59.53% will be trapped in the gas phase, assuming minimal mineralization.

The reaction of injected CO_2 with the well materials and the rock in the injection and confining zone will be determined from geochemistry. The injection well will be completed with CO_2-resistant materials to ensure the long-term integrity of the well. The confining zone and injection interval rock fabric will be studied to understand the reaction of CO_2 with the different rock materials. The CO_2 will react with some minerals in the formation to create new rock materials ensuring permanent storage for the CO_2.

The storage capacity of saline aquifers is calculated from the equation below (DOE, 2015):

$$G_{CO2} = A_f H_g f_{total} \rho_{CO2} E_{saline} \qquad \text{Equation 1.2}$$

where

G_{CO2} = Mass of CO_2, in lbm

A_f = Area of formation, in ft^2

H_g = Thickness of formation, in ft

f_{total} = Total volume of pore space, fraction

ρ_{CO2} = CO_2 density, in lbm/ft^3

E_{saline}= Efficiency factor, taken as 0.51% for P10, 2% for P50, and 5.5% for P90.

The properties of CO_2 required to calculate the storage capacity are obtained from the results of the injection simulation carried out with the SLB ECLIPSE™ compositional simulator. The CO_2 density ranges from 44.99 lb/ft^3 in the shallowest injection zone (mid-perforation depth at 4,491 feet) to 52.23 lb/ft^3 in the deepest injection zone (mid-perforation depth at 10,878 feet).

These properties were used to calculate the storage capacity for each zone, with the area of the formation taken as the Donaldsonville lease extents. The P10, P50, and P90 mass of CO_2 that can be stored in the lease is 6,452 million metric tons, 25,300 million metric tons, and 69,576 million metric tons, respectively. There is sufficient capacity for the total proposed injectate volume. The estimated CO_2 storage capacity within the Donaldsonville lease is shown in **Table 1-5.**

Table 1-4. Properties of CO_2 in each of the 19 injection zones.

Injection Zone	Mid Perforation Depth	Average Pressure	Average Temperature	CO_2 Formation Volume Factor	CO_2 Density
	(feet)	(psi)	(F)	(rb/MSCF)	(lb/ft^3)
Injection Zone 19	4491	2086.45	110.26	0.458	44.99
Injection Zone 18	4916	2387.92	113.93	0.443	46.42
Injection Zone 17	5323	2562.75	116.93	0.436	46.93
Injection Zone 16	5609	2725	119.9	0.435	47.31
Injection Zone 15	6062	2910.83	123.79	0.432	47.63
Injection Zone 14	6667	3194.59	128.98	0.427	48.2
Injection Zone 13	7113	3464.48	132.85	0.421	48.86
Injection Zone 12	7246	3650	133.96	0.415	49.53

Injection Zone	Mid Perforation Depth	Average Pressure	Average Temperature	CO_2 Formation Volume Factor	CO_2 Density
	(feet)	(psi)	(F)	(rb/MSCF)	(lb/ft^3)
Injection Zone 11	7355	3659.2	134.9	0.416	49.43
Injection Zone 10	7541	3790.14	136.48	0.413	49.75
Injection Zone 9	8249	4105.21	142.57	0.41	50.11
Injection Zone 8	8454	4068.85	144.37	0.413	49.69
Injection Zone 7	8836	4369.18	147.65	0.407	50.4
Injection Zone 6	9326	4478.09	151.84	0.409	50.22
Injection Zone 5	9567	4616.79	153.91	0.407	50.45
Injection Zone 4	9785	4976.09	155.86	0.399	51.45
Injection Zone 3	10478	5406.98	161.74	0.394	52.09
Injection Zone 2	10723	5401.57	162.62	0.396	51.85
Injection Zone 1	10878	5590	165.19	0.393	52.23

Table 1-5. Storage capacity of the individual 19 zones within the Donaldsonville lease.

Injection Zone	Donaldsonville Lease Pore Volume (Million reservoir barrels)	Mass CO_2 (Million Metric Tons)			
		Total (No Efficiency Factor included)	P10 (0.51%)	P50 (2.0%)	P90 (5.5%)
Injection Zone 19	964	110.47	0.56	2.21	6.08
Injection Zone 18	587	69.40	0.35	1.39	3.82
Injection Zone 17	394	47.09	0.24	0.94	2.59
Injection Zone 16	517	62.30	0.32	1.25	3.43
Injection Zone 15	441	53.50	0.27	1.07	2.94
Injection Zone 14	557	68.37	0.35	1.37	3.76
Injection Zone 13	325	40.45	0.21	0.81	2.22
Injection Zone 12	140	17.66	0.09	0.35	0.97
Injection Zone 11	305	38.39	0.20	0.77	2.11
Injection Zone 10	329	41.68	0.21	0.83	2.29
Injection Zone 9	241	30.76	0.16	0.62	1.69
Injection Zone 8	348	44.04	0.22	0.88	2.42
Injection Zone 7	184	23.62	0.12	0.47	1.30
Injection Zone 6	371	47.45	0.24	0.95	2.61
Injection Zone 5	493	63.34	0.32	1.27	3.48

Injection Zone	Donaldsonville Lease Pore Volume (Million reservoir barrels)	Mass CO_2 (Million Metric Tons)			
		Total (No Efficiency Factor included)	P10 (0.51%)	P50 (2.0%)	P90 (5.5%)
Injection Zone 4	129	16.90	0.09	0.34	0.93
Injection Zone 3	173	22.95	0.12	0.46	1.26
Injection Zone 2	111	14.66	0.07	0.29	0.81
Injection Zone 1	119	15.83	0.08	0.32	0.87
Total	**6728**	**828.87**	**4.23**	**16.58**	**45.59**

2. AoR and Corrective Action

AoR and Corrective Action GSDT Submissions

GSDT Module: AoR and Corrective Action
Tab(s): All applicable tabs

Please use the checkbox(es) to verify the following information was submitted to the GSDT:
☒ Tabulation of all wells within AoR that penetrate confining zone ***[40 CFR 146.82(a)(4)]***
☒ AoR and Corrective Action Plan ***[40 CFR 146.82(a)(13) and 146.84(b)]***
☒ Computational modeling details ***[40 CFR 146.84(c)]***

Figure 1-54 presents the AoR based on the modeling results. The figure illustrates the combination of the maximum extent of the CO_2 plume and maximum pressure front (obtained during the injection into Zone 2 and that quickly dissipates at the stop of injection into that zone) along with the wells identified within the AoR. This AoR will be used for corrective actions on existing wells. Details of AOR and corrective actions are described in **Attachment C - AOR and Corrective Action Plan.**

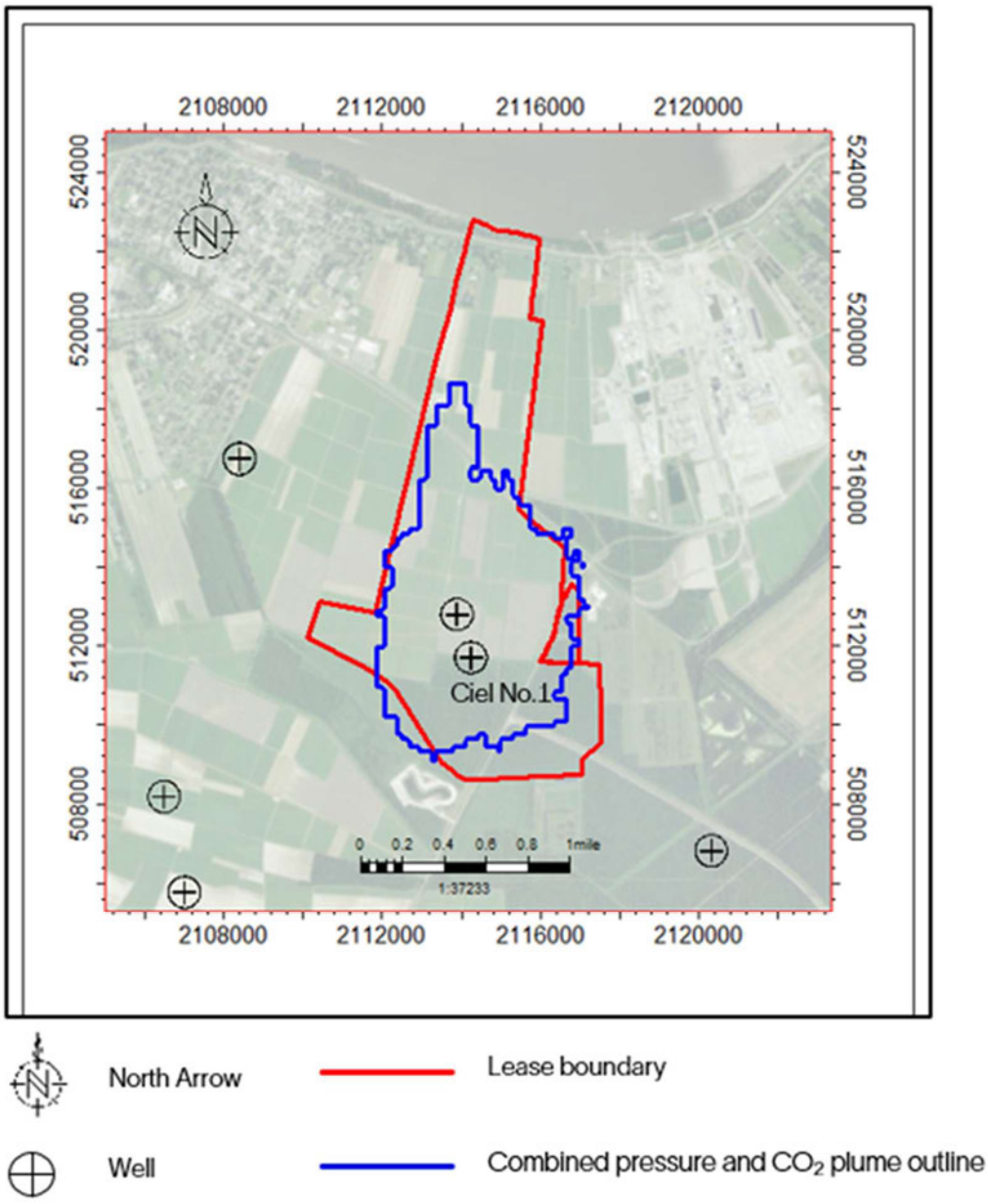

Figure 1-54. Map of the combined CO_2 and pressure plume AoR as delineated by the injection model simulation.

3. Financial Responsibility

Financial requirements have been discussed in detail in **Attachment No. I- Financial Assurance Demonstration**.

Financial Responsibility GSDT Submissions
GSDT Module: Financial Responsibility Demonstration ***Tab(s):*** Cost Estimate tab and all applicable financial instrument tabs Please use the checkbox(es) to verify the following information was submitted to the GSDT: ☒ Demonstration of financial responsibility ***[40 CFR 146.82(a)(14) and 146.85]***

4. Injection Well Construction

BKVerde plans to drill a newly constructed well (Ciel No,1) well to inject CO_2 at the Donaldsonville site.

In compliance with 40 CFR 146.82(a)(11), 146.82(a)(12), and 146.86, **Attachment H– Construction Details** contains well-specific construction details, procedures, design criteria, and a planned wellbore schematic for the Class VI CO_2 injection well.

The proposed injection well, Ciel No,1 (**Figure 1-55**), will be a new vertical well. In this description, all hole and casing depths reference ground level. The 30-inch 310-lb/ft conductor will be driven to ±150 feet or until refusal. A 26-inch-diameter hole will be drilled to a depth of 2,000 feet to cover the maximum USDW depth of 1,048 feet. The well will be logged to 2,000 feet and a 20-inch 133 lb/ft casing will be run into the hole and cemented to surface. A cased-hole cement evaluation logging suite will be run.

A 17 1/2-inch-diameter hole will be drilled to a depth of approximately 3,800 feet, which should be at the top of the upper confining zone (4,115 feet to 4,220 feet), which is the main seal of the injection interval. Well logs will provide formation properties and any needed formation sampling will be run from 3,800 feet to 2,000 feet. A 13 3/8-inch 68 lb/ft L-80 string of intermediate casing will be run into the hole and cemented to surface. Cement and casing evaluation logs will be run in addition to deviation surveys to ensure the wellbore is verticality sealed.

A 12 1/4-inch-diameter hole will be drilled to a depth of about 11,500 feet. The well will have extensive logging and sampling suites run from 3,800 feet to 11,500 feet fully evaluating the Miocene sands for injection and shales for seals. A 9 5/8-inch 53.5-lb/ft P-110 casing will be run from surface to 3,800 feet, and then a 9 5/8-inch 53.5-lb/ft 25CR-110 premium casing will be run from 3,800 feet to 4,300 feet and 9 5/8-inch 53.5 lb/ft 13CR-110 premium casing will be run from 4,300 feet to 11,500 feet. The longstring casing will be cemented using corrosion-resistant cement to the upper confining zone and conventional cement to surface. Casing and cement evaluation logs will be run along with baseline monitoring logs. After the cased-hole logs are run, the well will be perforated and completed with an injection packer and 5 ½-inch 20 lb/ft 13 Cr-MOD 110 tubing string. The perforation zones will be selected based on the log analysis but are anticipated to follow the predicted perforation zones as shown in **Table 1-2.**

The base of the USDW aquifers was calculated to extend to a depth of 1,048 feet true vertical depth (TVD). The surface casing planned depth is 2,000 feet in a generous 20-inch fully cemented hole to surface providing sufficient protection and coverage of the USDW aquifers.

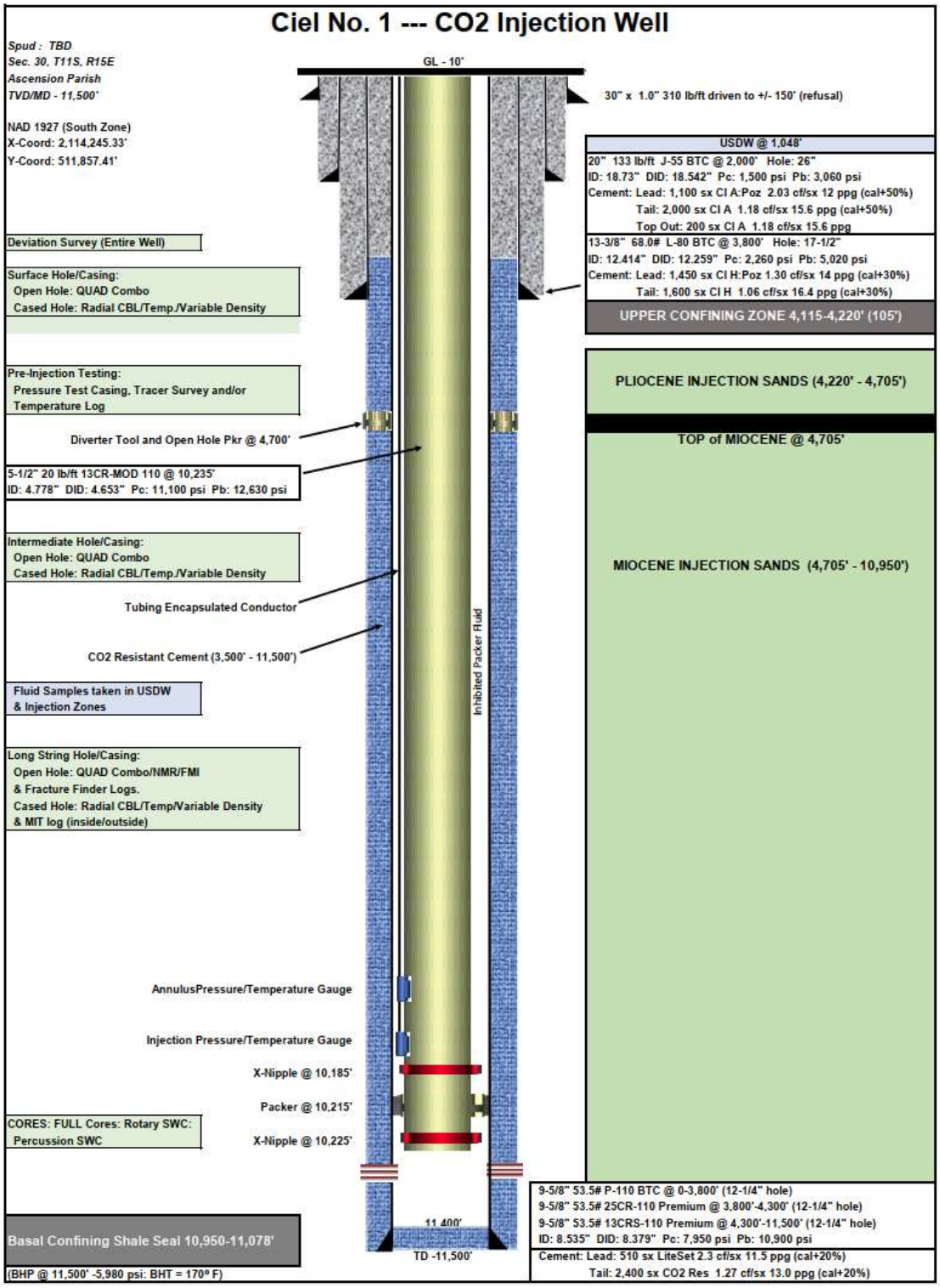

Figure 1-55. Ciel No.1 injection well construction.

Proposed Stimulation Program [40 CFR 146.82(a)(9)]

Stimulation Plans are discussed in **Attachment J-Stimulation Plans.**

4.1 Construction Procedures [40 CFR 146.82(a)(12)]

Construction plans of the Class VI injection well, Ciel No.1 is discussed in **Attachment H-Construction Details.**

Casing and Cementing

The well will be designed using carbon steel for the casing and tubulars that are not expected to be in contact with a mixture of the injectate (CO_2) and water. That is, the conductor, surface, and intermediate casing sections will all be carbon steel. The deep casing string will be constructed with corrosion-resistant alloy material across the injection interval and caprock to total depth (TD) and carbon steel from above the upper confining zone to surface.

The deepest underground source of drinking water (USDW) was confirmed at 1,048 feet where it will be covered by the surface casing, which will be set at 2,000 feet to protect the USDW.

The cemented casing strings of the Ciel No.1 well will all be cemented back to surface. The surface strings will be cemented using Class A cement. The injection string will be cemented using SLB EverCrete™ corrosion-resistant cement as the tail mix across the injection interval and caprock. Class A cement will be used as the lead above the caprock to surface. Casing details are shown in **Table 1-6** and a summary of cement types is presented in **Table 1-7**.

The injection interval temperature in the perforation zones ranges from 110.3 to 165.2 degrees Fahrenheit. These conditions are not extreme, and normal cementing and casing practices meet standards. The temperature differences between the CO_2 injectate and the injection interval are minimized to +/- 20 degrees Fahrenheit to minimize well integrity issues.

The surface and intermediate casings will be cemented using Class A cement to surface.

The longstring casing will be cemented in two stages utilizing diverter tools and openhole packer to set at 4,700 feet to ensure cement reach to surface. Corrosion-resistant cement will be utilized for cementing from the total depth to the top of the confining zone. The lead cement will be conventional Class A to surface. **Table 1-7** illustrates the cement program.

Table 1-6. Wellbore geometry.

Casing Interval	Depth Interval (feet)	Open Hole Diameter (inches)	Casing OD (inches)	Casing ID (inches)	Weight (lb/ft)	Grade (API)	Design Coupling (Short or Long Threaded)	Burst Strength (psi)	Collapse Strength (psi)
Conductor	0 – 150	Driven to refusal	30	28	310	X56	Welded	3,270	1,680
Surface	0 – 2,000	26 To bedrock	20	18.73	133	J55	Long or Buttress	3,060	1,500
Intermediate	0 – 3,800	17.5 To primary seal	13.375	12.415	68	L-80	Long or Buttress	5,020	2,260
Longstring	0 – 3,800		9.625	8.535	53.5	P-110		10,900	7,950
Longstring	3,800 – 4,300	12.25 To TD	9.625	8.535	53.5	25Cr-110	Special	10,900	7,950
Longstring	4,300 – 11,500		9.625	8.535	53.5	13Cr-110		10,900	7,950

Table 1-7. Cementing details for the Ciel No.1 well.

Casing	Depth interval (ft)	Cement Type	Cement Weight (ppg)
Surface	0 – 2,000	Class A	Lead: 12.0
			Tail: 15.6
Intermediate	0 – 3,800	Class H	Lead: 14.0
			Tail: 16.4
Long string	0 – 3500	LiteSet	Lead: 11.5
	3500 - 11,500	CO2 Resistant	Tail: 13.0

Tubing and Packer

The tubing and packer specifications in **Table 1-8** meet the minimum requirements at 40 CFR 146.86(c). BKVerde plans to use the tubing and packer described in the table, which will be made of corrosion-resistant materials and will update EPA as required.

Table 1-8. Tubing and packer details.

	Depth Interval	Outside Diameter	Inside Diameter	Weight	Grade	Design Coupling	Burst Strength	Collapse Strength
	(feet)	(inch)	(inch)	(lb/ft)	(API)	(Short or Long Thread)	(psi)	(psi)
Injection tubing	0 – 10,235	5.5	4.778	20	13Cr-MOD 110	Special	12,630	11,100

Packer	Casing Size (inch)	Casing Weight (lb/ft)	Gauge OD (inch)	Max OD (inch)	Tool ID (inch)
ASI-X	9.625	53.5	8.25	7.827	4
Packer	Casing Size (inch)	Casing Weight (lb/ft)	Gauge OD (inch)	Max OD (inch)	Tool ID (inch)
ASI-X	9.625	53.5	8.25	7.827	4

4.2 Contingency Plans

Lost Circulation while Drilling

Drilling in depleted oil and gas fields includes the risk of lost circulation when low-pressure production zones are penetrated. Drilling fluid loss rates range from minor to total loss. Minor losses can be managed by replenishing the supply of drilling fluid as needed and adding loss control material (LCM) to the fluid system to reduce or eliminate losses. Greater losses can be

mitigated by spotting fluid pills with high concentrations of LCM, waiting without pumping, and allowing the LCM pills to heal the loss zones. Severe to total losses can be treated with plugging materials that bridge and prevent losses. Cement plugs are an option and can be used to regain circulation. If these treatments are ineffective, techniques such as managed pressure drilling, aerated fluid, and drilling with foam are options that can be applied.

Responding to lost circulation while drilling is well understood in the industry, and materials, equipment, and procedures are readily available if needed.

Lost Circulation while Cementing

Cementing where lost circulation is occurring or is likely to occur is a more challenging problem. Methods to deal with lost circulation while cementing include reduced cement slurry density and modeling to determine if a given slurry design will likely be placed in the well without losing circulation resulting in a low cement top. Managed pressure cementing, staged cementing, foamed cement, and reverse cementing are technologies that can be implemented to reduce the risk of losing returns while cementing.

Drilling Contingencies

Deviation surveys will be taken while drilling the Ciel No.1 well. The surveys and well path will be monitored while drilling to demonstrate that the final bottomhole location satisfies the well's intended purpose. In the unlikely event the surveys show the borehole has unplanned excess deviation, the hole will be plugged back and redrilled.

If the drillstring parts and a fish are left in the well, fishing operations will commence to recover them. The risks of not recovering fish are low, and normal drilling operations will continue after the fish are recovered. In the unlikely event a fish cannot be recovered, appropriate steps will be taken to properly plug the open hole with cement to prevent migration of CO_2 and hydrocarbons to unauthorized zones.

Drilling fluid returns will be monitored while drilling to check for fluid gains or losses. If either is observed, the well will be monitored to determine the status, and steps will be taken to get the well back into a condition to resume drilling. If a fluid gain is detected, normal well control procedures will be conducted to circulate out the influx and the mud weight will be adjusted as required to resume safe operations. Fluid losses were discussed in the previous section.

5. Pre-Operational Logging and Testing

BKVerde provided operational and testing data to support the Donaldsonville project. Data and information provided meet the requirements pursuant to 40 CFR 146.82(a)(8) and 40 CFR 146.87. Details of these requirements are provided in **Attachment B – Pre operation Testing**.

Pre-Operational Logging and Testing GSDT Submissions
GSDT Module: Pre-Operational Testing

Tab(s): Welcome tab

Please use the checkbox(es) to verify the following information was submitted to the GSDT:
☐ Proposed pre-operational testing program ***[40 CFR 146.82(a)(8) and 146.87]***

6. Well Operation

6.1 Operational Procedures [40 CFR 146.82(a)(10)]

The Ciel No.1 injector well will be operated to inject the desired rate of super-critical phase CO_2.

The maximum injection bottomhole pressure entered as the limiting bottomhole pressure constraint into the reservoir simulator for each injection zone *i* is calculated as shown in **Equation 1.4**:

$$P_{BHP\ max,i} = D_{mp,i} * \text{FG} * \text{SF} \qquad \text{Equation 1.4}$$

where

$P_{BHP\ max,i}$ = Maximum bottomhole pressure for injection zone *i*, psi

$D_{mp,i}$ = Depth at mid-perforation for zone *i*, ft

FG = Fracture gradient (0.75 psi/ft)

SF = Safety Factor (0.9)

The calculated maximum injection bottomhole pressure for each zone is listed in **Table 1-9**.

The maximum injection surface pressure is calculated using **Equation 1.5**:

$$P_{SURF\ max,i} = P_{BHP\ max,i} - (\rho_{CO2,i} * 0.1337 * 0.052 * D_{mp,i}) \qquad \text{Equation 1.5}$$

where

$P_{SURF\ max,i}$ = Maximum injection surface pressure for injection zone *i*, psi

$P_{BHP\ max,i}$ = Maximum bottomhole pressure limit for injection zone *i*, psi

$\rho_{CO2,i}$ = Density of CO_2 at conditions in zone *i*, lb/ft^3

$D_{mp,i}$ = Depth at mid-perforation for zone *i*, ft

0.1337 = Conversion factor of lb/ft^3 to ppg

0.052 = Conversion factor of ppg to psi/ft

The average bottomhole pressure for each zone is taken as the average bottomhole pressure from the injection simulation results for the injection zone.

The average surface injection pressure, calculated using a flow assurance simulator, uses inputs for the average reservoir pressure, productivity index, and average reservoir temperature for the different zones from the injection simulation results. The calculated average surface injection pressure is listed in Table 1-9. Proposed operational procedures..

The annulus pressure for each zone *i*, is calculated as given in Equation 1.6:

$$P_{annulus,i} = P_{BHP\ max,i} + 100 - (\rho_{annulus\ fluid} * 0.052 * D_{packer,i}) \qquad \text{Equation 1.6}$$

where

$P_{annulus,i}$ = Annulus pressure for injection zone *i*, psi

$P_{BHP\ max,i}$ = Maximum bottomhole pressure for injection zone *i* obtained from Equation 1.2, psi

$\rho_{annulus\ fluid}$ = Annulus fluid density in pound per gallon (ppg)

$D_{packer,i}$ = Depth of packer for injection zone *i*

0.052 = Conversion factor of ppg to psi/ft

100 = Annulus pressure/differential tubing, psi

The calculated annular pressure for each injection zone is listed in **Table 1-9**.

The operational parameters will change throughout the lifetime of the project because the injection zones change through time. The injection starts from the deepest zone to the shallowest zone, and hence the surface injection pressure will change as the injection zone changes.

Table 1-9. Proposed operational procedures.

Parameters/Conditions	Limit or Permitted Value	Unit
Maximum Injection Pressure		
Surface		
Interval 1	3,393	Pound per Square inch
Interval 2	3,325	Pound per Square inch
Interval 3	3,279	Pound per Square inch
Interval 4	3,105	Pound per Square inch
Interval 5	3,103	Pound per Square inch
Interval 6	3,039	Pound per Square inch
Interval 7	2,868	Pound per Square inch

Parameters/Conditions	Limit or Permitted Value	Unit
Maximum Injection Pressure		
Interval 8	2,786	Pound per Square inch
Interval 9	2,694	Pound per Square inch
Interval 10	2,482	Pound per Square inch
Interval 11	2,438	Pound per Square inch
Interval 12	2,396	Pound per Square inch
Interval 13	2,385	Pound per Square inch
Interval 14	2,266	Pound per Square inch
Interval 15	2,085	Pound per Square inch
Interval 16	1,941	Pound per Square inch
Interval 17	1,857	Pound per Square inch
Interval 18	1,732	Pound per Square inch
Interval 19	1,627	Pound per Square inch
Downhole		
Interval 1	7,343	Pound per Square inch
Interval 2	7,190	Pound per Square inch
Interval 3	7,073	Pound per Square inch
Interval 4	6,605	Pound per Square inch
Interval 5	6,458	Pound per Square inch
Interval 6	6,295	Pound per Square inch
Interval 7	5,964	Pound per Square inch
Interval 8	5,707	Pound per Square inch
Interval 9	5,568	Pound per Square inch
Interval 10	5,090	Pound per Square inch
Interval 11	4,965	Pound per Square inch
Interval 12	4,891	Pound per Square inch
Interval 13	4,801	Pound per Square inch
Interval 14	4,500	Pound per Square inch
Interval 15	4,092	Pound per Square inch
Interval 16	3,786	Pound per Square inch
Interval 17	3,593	Pound per Square inch
Interval 18	3,319	Pound per Square inch
Interval 19	3,032	Pound per Square inch

Parameters/Conditions	Limit or Permitted Value	Unit
Average Injection Pressure		
Surface		
Interval 1	2,336	Pound per Square inch
Interval 2	2,183	Pound per Square inch
Interval 3	2,273	Pound per Square inch
Interval 4	2,135	Pound per Square inch
Interval 5	1,930	Pound per Square inch
Interval 6	1,891	Pound per Square inch
Interval 7	1,924	Pound per Square inch
Interval 8	1,818	Pound per Square inch
Interval 9	1,655	Pound per Square inch
Interval 10	1,659	Pound per Square inch
Interval 11	1,568	Pound per Square inch
Interval 12	1,606	Pound per Square inch
Interval 13	1,478	Pound per Square inch
Interval 14	1,407	Pound per Square inch
Interval 15	1,361	Pound per Square inch
Interval 16	1,199	Pound per Square inch
Interval 17	1,178	Pound per Square inch
Interval 18	1,146	Pound per Square inch
Interval 19	1,102	Pound per Square inch
Downhole		
Interval 1	5,838	Pound per Square inch
Interval 2	5,509	Pound per Square inch
Interval 3	5,602	Pound per Square inch
Interval 4	5,162	Pound per Square inch
Interval 5	4,716	Pound per Square inch
Interval 6	4,556	Pound per Square inch
Interval 7	4,493	Pound per Square inch
Interval 8	4,167	Pound per Square inch
Interval 9	4,234	Pound per Square inch
Interval 10	4,025	Pound per Square inch
Interval 11	3,804	Pound per Square inch
Interval 12	3,837	Pound per Square inch
Interval 13	3,561	Pound per Square inch
Interval 14	3,283	Pound per Square inch
Interval 15	3,028	Pound per Square inch

Parameters/Conditions	Limit or Permitted Value	Unit
Average Injection Pressure		
Interval 16	2,826	Pound per Square inch
Interval 17	2,694	Pound per Square inch
Interval 18	2,477	Pound per Square inch
Interval 19	2,147	Pound per Square inch
Maximum Injection Rate	**52,084.50**	**Mscf/day**
Average Injection Rate	**52,084.50**	**Mscf/day**
Maximum Injection Volume and/or Mass	**11.412**	**Million tonnes**
Average Injection Volume and/or Mass	**11.412**	**Million tonnes**

Parameters/Conditions	Limit or Permitted Value	Unit
Annulus Pressure		
Interval 1	2,544	Pound per Square inch
Interval 2	2,392	Pound per Square inch
Interval 3	2,465	Pound per Square inch
Interval 4	1,997	Pound per Square inch
Interval 5	1,850	Pound per Square inch
Interval 6	2,219	Pound per Square inch
Interval 7	1,888	Pound per Square inch
Interval 8	1,630	Pound per Square inch
Interval 9	1,980	Pound per Square inch
Interval 10	1,502	Pound per Square inch
Interval 11	1,377	Pound per Square inch
Interval 12	1,303	Pound per Square inch
Interval 13	1,736	Pound per Square inch
Interval 14	1,659	Pound per Square inch
Interval 15	1,515	Pound per Square inch
Interval 16	1,210	Pound per Square inch
Interval 17	1,017	Pound per Square inch
Interval 18	1,274	Pound per Square inch
Interval 19	1,204	Pound per Square inch

Annulus Pressure/Tubing Differential	**100**	**Pound per Square inch**

6.2 Proposed Carbon Dioxide Stream [40 CFR 146.82(a)(7)(iii) and (iv)]

The source of the CO_2 stream will be nearby. The volume of CO_2 expected from these emitters is 1,000,000 metric tons/year. The CO_2 will be composed of greater than 95% CO2. It will be compressed, delivered through a pipeline, and then sent through a 150-foot flowline to the injection wellhead. Details of the composition of the carbon dioxide is discussed in **Attachment D – Testing and Monitoring Plan.**

7. Testing and Monitoring

The BKVerde Testing and Monitoring plan pursuant to 40 CFR 146.82 (a)(15) and 40 CFR 146.90 describes the strategies for testing and monitoring to ensure protection of the USDW, injection well integrity, and plume monitoring. **Attachment D – Testing and Monitoring Plan** details the testing and monitoring plan.

Testing and Monitoring GSDT Submissions
GSDT Module: Project Plan Submissions ***Tab(s):*** Testing and Monitoring tab Please use the checkbox(es) to verify the following information was submitted to the GSDT: ☐ Testing and Monitoring Plan ***[40 CFR 146.82(a)(15) and 146.90]***

8. Injection Well Plugging

The BKVerde injection Well Plugging Plan pursuant to 40 CFR 146.92 describes the process, materials, and methodology for injection well plugging. The injection well plugging plan is detailed in **Attachment E – Plugging Plan**.***Injection Well Plugging GSDT Submissions***
GSDT Module: Project Plan Submissions ***Tab(s):*** Injection Well Plugging tab Please use the checkbox(es) to verify the following information was submitted to the GSDT: ☐ Injection Well Plugging Plan ***[40 CFR 146.82(a)(16) and 146.92(b)]***

9. Post-Injection Site Care (PISC) and Site Closure

BKVerde has developed a Post-Injection Site Care and Site Closure plan, **Attachment F**, pursuant to 40 CFR 146.93 (a) that defines post-injection testing and monitoring. Currently, BKVerde is not proposing an alternative PISC timeframe.

PISC and Site Closure GSDT Submissions
GSDT Module: Project Plan Submissions ***Tab(s):*** PISC and Site Closure tab Please use the checkbox(es) to verify the following information was submitted to the GSDT: ☐ PISC and Site Closure Plan ***[40 CFR 146.82(a)(17) and 146.93(a)]***
GSDT Module: Alternative PISC Timeframe Demonstration ***Tab(s):*** All tabs (only if an alternative PISC timeframe is requested) Please use the checkbox(es) to verify the following information was submitted to the GSDT: ☐ Alternative PISC timeframe demonstration ***[40 CFR 146.82(a)(18) and 146.93(c)]***

10. Emergency and Remedial Response

BKVerde Emergency and Remedial Response plan pursuant to 40 CFR 164.94 describes the process and response to emergencies to ensure USDW protection in **Attachment G**.

Emergency and Remedial Response GSDT Submissions
GSDT Module: Project Plan Submissions ***Tab(s):*** Emergency and Remedial Response tab Please use the checkbox(es) to verify the following information was submitted to the GSDT: ☒ Emergency and Remedial Response Plan ***[40 CFR 146.82(a)(19) and 146.94(a)]***

Injection Depth Waiver and Aquifer Exemption Expansion GSDT Submissions
GSDT Module: Injection Depth Waivers and Aquifer Exemption Expansions ***Tab(s):*** All applicable tabs Please use the checkbox(es) to verify the following information was submitted to the GSDT: ☐ Injection Depth Waiver supplemental report ***[40 CFR 146.82(d) and 146.95(a)]***

☐ Aquifer exemption expansion request and data ***[40 CFR 146.4(d) and 144.7(d)]***

References

Berggren, W. A., Kent, D. V., Swisher, C. C., III, and Aubry, M.-P. 1995. A revised Cenozoic geochronology and chronostratigraphy. In Berggren, W. A., Kent, D. V., Aubry, M. P., Hardenbol, J. eds., Geochronology, time scales and global stratigraphic correlation. Society for Sedimentary Geology, Special Publication 54, Tulsa, OK, pp. 129–212. https://doi.org/10.2110/pec.95.04.0129.

Blondes, M.S., Gans, K.D., Engle, M.A., Kharaka, Y.K., Reidy, M.E., Saraswathula, V., Thordsen, J.J., Rowan, E.L., and Morrissey, E.A. 2018. U.S. Geological Survey National Produced Waters Geochemical Database (ver. 2.3, January 2018). U.S. Geological Survey data release. https://doi.org/10.5066/F7J964W8.

Bump, A. P., Sahar B., Hailun N., Hovorka, S. D., Olariu, M. I., Dunlap, D., Hosseini, S. A., and Meckel, T. A. 2023. Composite confining systems: Rethinking geologic seals for permanent CO_2 sequestration. International Journal of Greenhouse Gas Control 126: 1–12. https://doi.org/10.1016/j.ijggc.2023.103908

Chen, Y., Chen, S., Li, D., and Jiang, X. 2023. Density-driven convection for CO_2 solubility trapping in saline aquifers: modeling and influencing factors. Geotechnics 3: 70–103. https://doi.org/10.3390/geotechnics3010006.

DOE. (2015). *Carbon Atlas - Fifth Edition.* NETL, Department of Energy. Retrieved from https://www.netl.doe.gov/coal/carbon-storage/strategic-program-support/natcarb-atlas

Dubiel, R.F., Coleman, J.L., Hackley, P.C., Hayba, D.O., Karlsen, A.W., Pearson, O.N., Pitman, J.K., Swanson, S.M., and Warwick, P.D. 2007. Assessment of undiscovered oil and gas resources in Tertiary strata of the Gulf Coast. U.S. Geological Survey Fact Sheet 2007–3066, 4 p.

Eaton, B. A. 1969. Fracture gradient prediction and its application in oilfield operations. Journal of Petroleum Technology 21(10): 1353–1360. https://doi.org/10.2118/2163-PA.

Fillon, R. H., Lawless, P. N., Lytton, R. G. et al. 1997, Gulf of Mexico Cenozoic biostratigraphic and cycle charts. In Lawless, P. N., Fillon, R. H., and Lytton, R. G. III, Gulf of Mexico Cenozoic biostratigraphic, lithostratigraphic and sequence stratigraphic event chronology. Gulf Coast Societies Transactions 42, p. 271: 282.

Galloway, W. E., P. E. Ganey-Curry, X. Li, and R. T. Buffler. 2000. Cenozoic depositional history of the Gulf of Mexico Basin: AAPG Bulletin 84(11): 1743–1774.

Galloway, W.E., 2008. Chapter 15 depositional evolution of the Gulf of Mexico sedimentary basin in Sedimentary Basins of the World. Elsevier, pp. 505–549. https://doi.org/10.1016/S1874-5997(08)00015-4.

Griffith, J.M. 2003. Hydrogeologic framework of southeastern Louisiana. Louisiana Department of Transportation and Development. Water Resources Technical Report 72, 21 pp.

Griffith, J.M., 2006, Hydrogeologic maps and sections of the "400-foot," "600-foot," and "800-foot" sands of the Baton Rouge area and adjacent aquifers in East and West Baton Rouge, East and West Feliciana, and Pointe Coupee Parishes, Louisiana: U.S. Geological Survey Scientific Investigations Report 2006-5072,15 p.

Griffith, J.M., and Fendick, R. B. 2009. Water resources of Ascension Parish. USGS Fact Sheet 2009-3063, 6 pp.

Herron, M. M. 1987. Estimating the intrinsic permeability of clastic sediments from geochemical data. Transactions, SPWLA 28th Annual Logging Symposium: 1–23.

Horsrud, P. 2001. Estimating mechanical properties of shale from empirical correlations. SPE Drilling and Completions 16: 68–73. https://doi.org/10.2118/56017-PA.

Hovorka, S.D., Holtz, M.H., Sakurai, S., Knox, P.R., Collins, D., Papadeas, P., and Stehli, D. 2003. Frio pilot in CO_2 sequestration in brine-bearing sandstones: The University of Texas at Austin, Bureau of Economic Geology, report to the Texas Commission on Environmental Quality to accompany a class V application for an experimental technology pilot injection well. GCCC Digital Publication Series #03-04.

Hulsey, J., 2016, Applying modern interpretation techniques to old hydrocarbon fields to find new reserves: A case study in the onshore Gulf of Mexico, U.S.A. University of New Orleans Theses and Dissertations, 52 p.

Ingram, G. M. and Urai, J. L. 1999. Top-seal leakage through faults and fractures: the role of mudrock properties. Geological Society of London 15: 125–135. https://doi.org/10.1144/gsl.sp.1999.158.01.10.

Louisiana Department of Transporation and Development. 2009. Louisiana State Reservoir Priority and Development Program (Mississippi River Delta Basin Characterization Report) http://wwwsp.dotd.la.gov/Inside_LaDOTD/Divisions/Engineering/Public_Works/Dam_Safety/RPDP_Reports/Mississippi%20Basin%20Report%20FINAL%204.pdf

Lu, J., Milliken, K., Reed, R.M., and Hovorka, S. 2011. Diagenesis and sealing capacity of the middle Tuscaloosa mudstone at the Cranfield carbon dioxide injection site, Mississippi, U.S.A. Environmental Geosciences, Vol. 18, No.1: 35–53.

Mancini, E.A., Obid, J., Badali, M., Liu, K., and Parcell, W.C. 2008. Sequence-stratigraphic analysis of Jurassic and Cretaceous strata and petroleum exploration in the central and eastern Gulf coastal plain, United States. AAPG Bulletin 92(12): 1655–1686. https://doi.org/10.1306/08130808046.

Roberts-Ashby, T.L., Brennan, S.T., Buursink, M.L., Covault, J.A., Craddock, W.H., Drake, R.M., II, Merrill, M.D., Slucher, E.R., Warwick, P.D., Blondes, M.S., Gosai, M.A., Freeman, P.A., Cahan, S.M., DeVera, C.A., and Lohr, C.D. 2014. Geologic framework for the national assessment of carbon dioxide storage resources—U.S. Gulf Coast. In Warwick, P.D., and Corum, M.D., eds., Geologic framework for the national assessment of carbon dioxide storage resources, Chapter 8.U.S. Geological Survey Open-File Report 2012–1024–H, 77 pp., https://doi.org/10.3133/ofr20121024h.

Sawyer, D.S, Buffler, R.T., and Pilger, Jr., R.H. 1991. The crust under the Gulf of Mexico Basin. In Salvador, A., ed., The geology of North America—The Gulf of Mexico Basin. Geological Society of America, Geology of North America J: 53–72.

Snedden, J., and Galloway, W. 2019. The Gulf of Mexico Sedimentary Basin: depositional evolution and petroleum applications. Cambridge: Cambridge University Press, 326 p.

Thiercelin, M. J., and Plumb, R. A. 1994. Core-based prediction of lithologic stress contrasts in East Texas formations. SPE Formation Evaluation 9(4): 251–258. https://doi.org/10.2118/21847-PA.

Treviño, R. H. and Rhatigan, J. L. T. 2017. Regional Geology of the Gulf of Mexico and the Miocene section of Texas near-offshore waters. In Treviño, R. H. and Meckel, T. A., eds. Geological CO_2 sequestration atlas of Miocene strata, offshore Texas State Waters, Chapter 1. Texas Bureau of Economic Geology Report of Investigations 283, 74 pp.

United States Geological Survey. 2004a. Estimated Thickness of the Lower Miocene 1 Sequence, Gulf Coast. U.S. Geological Survey data release. https://doi.org/10.5066/P944PUU7.

United States Geological Survey. 2004b. Estimated Thickness of the Lower Miocene 2 Sequence, Gulf Coast. U.S. Geological Survey data release. https://doi.org/10.5066/P9VU6W24.

United States Geological Survey. 2004c. Gulf Coast Estimated Thickness of the Middle Miocene Sequence. U.S. Geological Survey data release. https://doi.org/10.5066/P9CCL0B2.

United States Geological Survey. 2004d. Gulf Coast Estimated Thickness of the Upper Miocene Sequence. U.S. Geological Survey data release. https://doi.org/10.5066/P9EYQ3D3.

United States Geological Survey. 2004e. Structure Contour of the Top of the Upper Miocene Sequence, Gulf Coast. U.S. Geological Survey data release. https://doi.org/10.5066/P918NWU5.

United States Geological Survey, Earthquake map, https://earthquake.usgs.gov/earthquakes/map

United States Geological Survey, Monitoring stations map, https://earthquake.usgs.gov/monitoring/operations/network.php?virtual_network=ANSS

Warwick, P.D., Coleman, J.L., Hackley, P.C., Hayba, D.O., Karlsen, A.W., Rowan, E.L., and Swanson, S.M. 2007. USGS assessment of undiscovered oil and gas resources in Paleogene strata of the U.S. Gulf of Mexico coastal plain and State-waters. In Kennan, L., Pindell, J., and Rosen, N.C., eds., The Paleogene of the Gulf of Mexico and Caribbean Basins—Processes, events, and petroleum systems. Society of Economic Paleontologists and Mineralogists, Gulf Coast Section Foundation 27th Annual Research Conference, p. 2–44.